

Grace at one-loop:

Automatic calculation of 1-loop diagrams in the electroweak theory with
gauge parameter independence checks

G. Bélanger¹⁾, F. Boudjema¹⁾, J. Fujimoto²⁾, T. Ishikawa²⁾,
T. Kaneko²⁾, K. Kato³⁾, Y. Shimizu²⁾

1) LAPTH[†], B.P.110, Annecy-le-Vieux F-74941, France

2) KEK, Oho 1-1, Tsukuba, Ibaraki 305-0801, Japan

3) Kogakuin University, Nishi-Shinjuku 1-24, Shinjuku, Tokyo 163-8677, Japan

Abstract

A general non-linear gauge condition is implemented into GRACE, an automated system for the calculation of physical processes in high-energy physics. These new gauge-fixing conditions are used as a very efficient means to check the results of large scale automated computation in the standard model. We describe in detail the implementation of the general gauge condition and the renormalisation procedure at one-loop in the standard model. Explicit formulae for all two-point functions in a generalised non-linear gauge are given, together with the complete set of counterterms. We also show how infrared divergences are dealt with in the system. A new technique for the reduction of the tensor integrals is described. We give a comprehensive presentation of some systematic test-runs which have been performed at the one-loop level for a wide variety of two-to-two processes to show the validity of the gauge check. These cover fermion-fermion scattering, gauge boson scattering into fermions, gauge bosons and Higgs bosons scattering processes. Comparisons with existing results on some one-loop computation in the standard model show excellent agreement. These include $e^+e^- \rightarrow t\bar{t}, W^+W^-, ZH$; $\gamma\gamma \rightarrow t\bar{t}, W^+W^-$; $e\gamma \rightarrow eZ, \nu W$ and $W^+W^- \rightarrow W^+W^-$. All these tests confirm the reliability of the system to automatically perform one-loop radiative corrections in the standard model with the added possibility of conducting powerful checks on the result.

LAPTH-982/03
KEK-CP-138

[†]URA 14-36 du CNRS, associée à l'Université de Savoie.

1 Introduction

Much of the success of the \mathcal{SM} of electroweak interactions rests on the results of the various precision measurements, notably those of LEP and SLC. These precision measurements required the knowledge of higher order quantum corrections. Although the latter are rather involved, calculations are still under control since the bulk of the observables pertain to two-body final states. In fact due to the present available energy, the most precise predictions relate to fermion-pair production, a calculation which is far easier to handle than that for W pair production even if one leaves out the fact that for the latter one needs a full 4-fermion final state calculation. Next generation machines will involve much higher energies and luminosities opening up the thresholds for multiparticle production and/or the need to go beyond one and two-loop radiative corrections. On the other hand even when one *only* considers three particles in the final state, the complexity increases tremendously especially within the electroweak framework. So much so that even a process like $e^+e^- \rightarrow \nu_e \bar{\nu}_e H$ which would be the main production mechanism for the Higgs at the next linear collider and where the tree-level calculation receives a contribution from only a single (non-resonant) diagram, a full calculation has only now been completed[1, 2, 3]. For such processes, hand calculations become quickly intractable and very much prone to error. Moreover, a complete hand calculation for such processes is not possible, even for the tree-level cross sections, as one has to resort to numerical methods for the phase space integration. Especially for QCD processes, to alleviate some of the major hurdles in the calculation of matrix elements for physical observables beyond leading and next-to-leading order, one has devised some powerful alternatives to the standard diagrammatic Feynman approach[4]. However most of them, if not all, involve a single scale and a single parameter. Moreover the techniques work because of the exact gauge symmetry of QCD and thus apart from a handful processes, these methods can not be carried over to the electroweak theory where the computations involve a variety of masses and scales. Faced with these difficulties the need for computers is even more evident for the calculation of electroweak processes.

Ideally one would like to automatise the complete process of calculating radiative corrections and multi-particle production. Especially that most of the ingredients of perturbation theory are based on a well established algorithm. This has led to the implementation of a few softwares with varying degrees of automation and different domain of application[5]. With the increase in computer power and storage, together with possible parallelization, one could deal, in a relatively short time, with more and more complex projects thus bypassing the problem of huge output files being produced, at least in the intermediate stages. Another problem that has to be tackled is the reliability of the final result, most importantly the correctness of the matrix elements before phase space integration is carried out. Beside the ultraviolet and infrared finiteness of the result, the most powerful check is certainly that of gauge invariance and/or gauge-parameter independence of the physical observable, a check that can be also automated.

Many of these ingredients have now been implemented in **GRACE**[6], an automatic program for the calculation of physical processes that has been applied intensively to tree-level processes with up to 6 particles in the final state[7, 8] and some $2 \rightarrow 2$ processes at the loop level[9, 10]. Recently it has also been used for the calculation of the complete $\mathcal{O}(\alpha)$ radiative corrections to two important $2 \rightarrow 3$ processes: $e^+e^- \rightarrow \nu\bar{\nu}H$ [1, 2] and $e^+e^- \rightarrow t\bar{t}H$ [11]. The system covers both the standard model as well as the supersymmetric model[12]. From an input file that defines a specific model, the system outputs total cross sections and distributions as well as creating an event generator for the process. We will describe the system in more detail in the next section. Suffice to say here that for tree-level processes the gauge-parameter independence check has been applied successfully by comparing the results in the unitary gauge to those of the 't Hooft-Feynman gauge. An agreement up to ~ 15 (~ 30) digits in double (quadruple) precision has been reached confirming, at this stage, that the system works very well for tree-level processes.

A computation in a general R_ξ gauge or unitary gauge brings about unnecessary complications and sometimes troublesome numerical instabilities especially when one deals with several gauge bosons. These are due to the contribution of the longitudinal part of the gauge propagators. In the 't Hooft-Feynman gauge only the "transverse" part $g_{\mu\nu}$ contributes and leads to a straightforward contraction of neighbouring vertices. The longitudinal tensor structure considerably inflates the size of each intermediate result, for example with n intermediate heavy gauge bosons instead of performing n operations one performs 2^n operations. Moreover since the longitudinal expressions involve momenta, they can contribute terms that increase with energy and which require a subtle cancellation among various diagrams. A situation which is most acute in the unitary gauge. These problems are of course exacerbated in loop calculations and, as is known, calculations and renormalisability itself are arduous if not problematic in the unitary gauge[13]. Within **GRACE** one of the problems in these gauges (unitary, or general linear type gauges) is that the library containing the various loop integrals is designed assuming that the numerator for the propagator of the vector particles is $g^{\mu\nu}$. For instance, the library for the three-point vertex functions is implemented with only up-to the third-rank tensor and therefore the library applies equally well with fermion loops, gauge loops or a mixture of these if the calculation is performed in the 't Hooft-Feynman gauge. In any other gauge one would have, for the vertex functions alone, had to deal with a 9th rank tensor! Again this not only creates very large expressions but also introduces terms with large superficial divergences that eventually need to be canceled extremely precisely between many separate contributions.

Fortunately one can also work with a class of gauge-fixing conditions that maintain all the advantages of the usual 't Hooft-Feynman gauge with exactly the same simple structure for the gauge propagators. The new gauge parameters modify some vertices involving the gauge, scalar and ghost sector and at the same time introduce new vertices. In fact by judiciously choosing some of these parameters the structure of the vertices can get even simpler than with the usual linear gauge-fixing conditions. The class of gauges

we are referring to exploit non-linear gauge fixing conditions[14, 15]. Apart from the possible simplifications that these gauges bring, we have considered a generalised class of non-linear gauges so as to perform in an efficient way the gauge-parameter independence checks within the **GRACE** system. Actually the generalised gauge we choose depends on 5 parameters[15]. Therefore not only this allows for a wide range of checks but since the different parameters affect different parts of the bosonic sector one can check different classes of contributions to a single process and thus more easily track down any bug. There are other welcome features of these checks. They serve as powerful tools on every step of the automated computation, from the correct implementation of the model file which in fact can be checked mostly at tree-level to the correct implementation of the tensor integrals. The reduction of the latter to scalar integrals is most prone to error. We will show how the tensor reduction is carried out in **GRACE**. The gauge check allows therefore to test that the reduction of these integrals into the scalar integrals is implemented properly[2]. Additional tests like those of infrared finiteness further verify the scalar integrals. Another advantage of the non-linear gauge checks over those that may be attempted within a linear R_ξ gauge is that on a diagram by diagram basis, the gauge parameter dependence in our checks are polynomials in the non-linear gauge parameters whereas in the linear R_ξ gauge the dependence is buried within logarithms and rational functions. We will show how one can exploit this fact for a very powerful gauge check.

The aim of this paper is to describe the implementation of the non-linear gauge in **GRACE-loop**, which is the extension of **GRACE** to one-loop, and to show the power of fully automated one-loop radiative corrections in the electroweak theory. Although the present paper will mainly show results for $2 \rightarrow 2$ processes, it sets the basis for future computation involving multiparticle production. We will therefore in section 2 briefly describe the general set-up of **GRACE-loop** before introducing the non-linear gauge in section 3. Section 4 discusses the renormalisation program within these gauges. Section 5 is a description of the numerical implementation of the scalar loop integrals. In the same section we expose an algorithm for the reduction of the tensor integrals. In the present paper we do not go beyond the box. Section 6 presents in some detail the checks that we have performed on some 26 processes for $2 \rightarrow 2$ reactions. Section 7 compares the results of **GRACE-loop** for some selected $2 \rightarrow 2$ processes with those in the existing literature. The final section contains our conclusions. We provide some detailed appendices. In particular we provide the full set of Feynman rules within the generalised non-linear gauge as well as the library for the counterterms. Full results for all the self-energy diagrams of all the particles in the model including the Goldstone sector is relegated to an appendix.

2 The Grace System

GRACE can be used for a variety of models including supersymmetry. It has been used quite extensively at tree-level. The different components and steps that go in the cal-

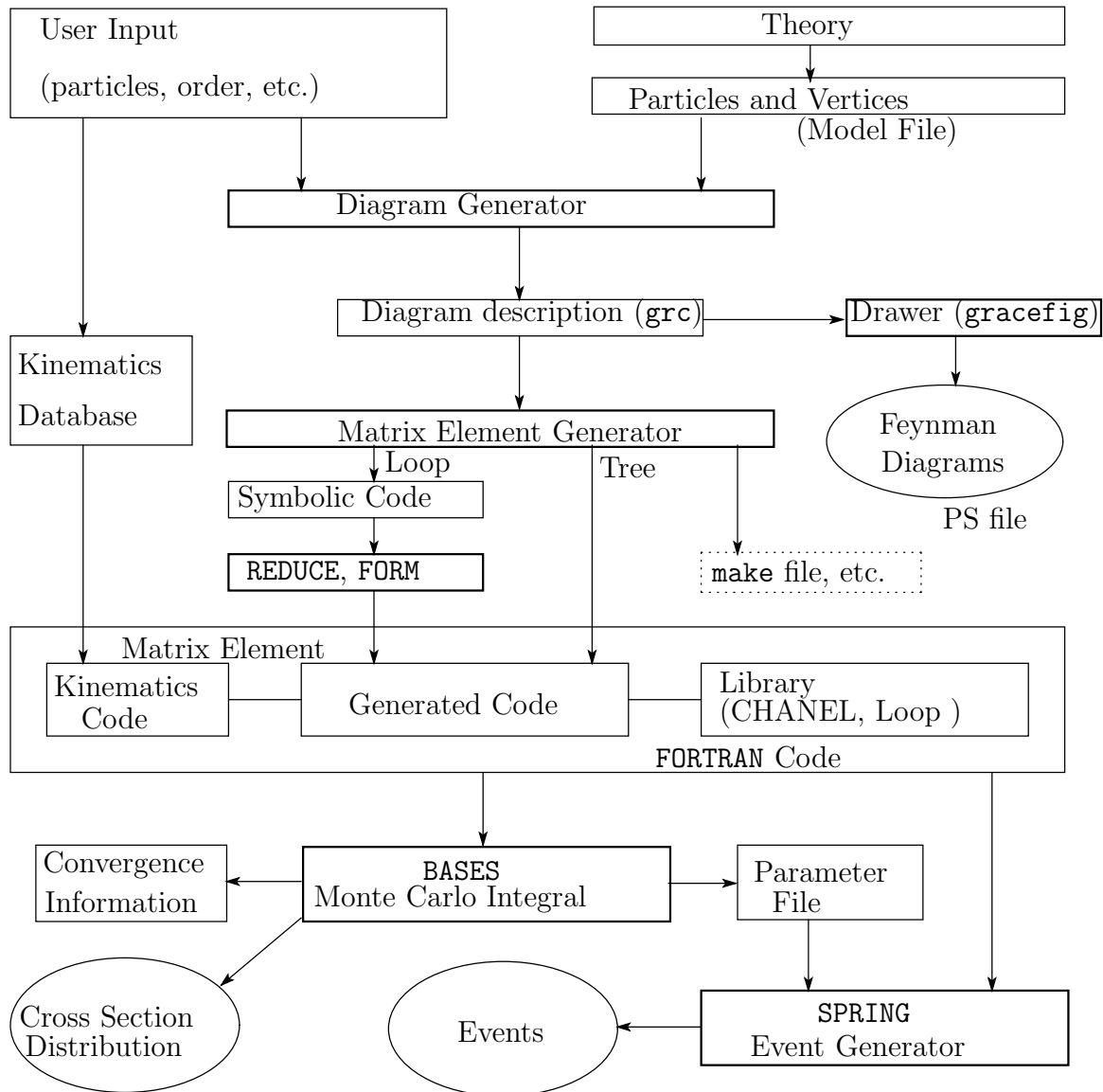


Figure 1: GRACE System Flow.

culation of a cross section or even the corresponding Monte-Carlo event generator are depicted in Fig. 1. The system first requires the implementation and definition of a model through a model file that gives the particle content, the parameters as well as the vertices as derived from the Lagrangian. The user sets as input the incoming particles and the final particles and specifies the order, in perturbation theory, at which the cross section is to be calculated. **GRACE** will first generate, through its own routine **grc** the full set of diagrams (tree and loop as well as counterterms for the latter) with the possibility of a **Postscript** output of the Feynman diagrams with the help of the utility diagram-drawer **gracefig**. The matrix element generator encodes all the information on the diagrams. For the tree-level process the system generates a **FORTRAN** code which describes the helicity amplitudes using the **CHANEL** library and routines[16]. For the computations at one-loop, one first generates a symbolic manipulation source code, based on **REDUCE**[17] or **FORM**[18] that writes, for each set of tree and loop diagram, the interference term $\mathcal{T}_i^{\text{loop}} \mathcal{T}_j^{\text{tree}\dagger}$. Only then the **FORTRAN** source code is generated and the cross section computed with the help of the loop library and the counterterm library that perform the integration over the Feynman parameters and takes into account the counterterm constants. The integration over phase space is carried *via* **BASES**[19] a Monte-Carlo integration package. The simulation and event generation is done through the package **SPRING**[19]. **GRACE** includes a number of kinematics routines for processes with up to 6 particles in the final state. The user can select the appropriate kinematics routine from the available library depending on the singular behaviour of the process. The symbolic manipulation for the loop calculation performs a number of important tasks, such as Dirac algebra (taking traces for fermion loops) and tensor manipulations in $n = 4 - 2\epsilon$ dimension¹, introducing Feynman parametric integrals, shifting loop momenta appropriately etc... Let us also mention that a *parallelised* version of **GRACE** has now been developed using the message passing libraries, **PVM** or **MPI**. This has been successfully tested on a Fujitsu AP3000 using up to 16 processors[20]. Having described the system and pointed to some technical issues related to computing, let us get back to the crucial issue of the gauge-parameter invariance checks that we perform exploiting the non-linear gauge.

3 The Standard Model in a general non-linear gauge

3.1 The classical Lagrangian

To help define our conventions and notations we first introduce the classical Lagrangian of the **SM** which is fully gauge invariant under $SU(2) \times U(1)$.

We denote the gauge fields of the theory of the $SU(2) \times U(1)$ group as $W_\mu^a (a = 0, 1, 2, 3)$. The weak isospin triplet refers to 1, 2, 3 and the hypercharge singlet to the 0

¹Dealing with the standard model processes, γ_5 is taken as fully anticommuting. Let us also point out that the cyclicity inside traces of gamma matrices is not used.

component. The corresponding gauge couplings are g^a . The gauge invariant field strength $F_{\mu\nu}^a$ writes in a compact form as

$$F_{\mu\nu}^a = \partial_\mu W_\nu^a - \partial_\nu W_\mu^a + g^a f^{abc} W_\mu^b W_\nu^c , \quad g^a = \begin{cases} g & (a = 1, 2, 3) \\ g' & (a = 0) \end{cases} , \quad f^{abc} = \begin{cases} \varepsilon^{abc} & (a, b, c \neq 0) \\ 0 & (\text{otherwise}) \end{cases} . \quad (3.1)$$

This leads to the pure gauge contribution \mathcal{L}_G

$$\mathcal{L}_G = -\frac{1}{4} F_{\mu\nu}^a F^{a\mu\nu} . \quad (3.2)$$

The gauge interaction of the matter fields is completely specified by their isospin and hypercharge (Y) quantum numbers, such that the electromagnetic charge is $Q = T^3 + Y$, and the covariant derivative, D_μ

$$D_\mu = \partial_\mu - ig \sum_{a=1}^3 W_\mu^a T^a - ig' Y W_\mu^0 . \quad (3.3)$$

with $T^a = \sigma^a/2$, where σ^a are the usual Pauli matrices. Left-handed fermions L of each generation belong to a doublet while right-handed fermions R are in $SU(2)$ singlet. The fermionic gauge Lagrangian is just

$$\mathcal{L}_F = i \sum \bar{L} \gamma^\mu D_\mu L + i \sum \bar{R} \gamma^\mu D_\mu R , \quad (3.4)$$

where the sum is assumed over all doublets and singlets of the three generations.

Mass terms for both the gauge bosons and fermions are generated in a gauge invariant way through the Higgs mechanism. To that effect one introduces a scalar doublet with hypercharge $Y = 1/2$ that spontaneously breaks the symmetry of the vacuum through a non-zero vacuum expectation value v

$$\phi = \frac{1}{\sqrt{2}} \begin{pmatrix} i\chi_1 + \chi_2 \\ v + H - i\chi_3 \end{pmatrix} = \begin{pmatrix} i\chi^+ \\ (v + H - i\chi_3)/\sqrt{2} \end{pmatrix} , \quad \langle 0|\phi|0 \rangle = v/\sqrt{2} . \quad (3.5)$$

The scalar Lagrangian writes

$$\mathcal{L}_S = (D_\mu \phi)^\dagger (D^\mu \phi) + \mathcal{L}_{\text{pot}} , \quad \mathcal{L}_{\text{pot}} = -V(\phi) = \mu^2 \phi^\dagger \phi - \lambda (\phi^\dagger \phi)^2 \equiv -\lambda \left(\phi^\dagger \phi - \frac{v^2}{2} \right)^2 + \frac{\mu^4}{4\lambda} . \quad (3.6)$$

The Nambu-Goldstone bosons χ^\pm, χ_3 in \mathcal{L}_S get absorbed by the Z and W^\pm to give the latter masses ($M_{Z,W}$), while the photon A remains massless. The physical fields W^\pm, A, Z relate to the original W quartet as

$$\begin{cases} A_\mu = \frac{g' W_\mu^3 + g W_\mu^0}{\sqrt{g^2 + g'^2}} = s_W W_\mu^3 + c_W W_\mu^0 \\ Z_\mu = \frac{g W_\mu^3 - g' W_\mu^0}{\sqrt{g^2 + g'^2}} = c_W W_\mu^3 - s_W W_\mu^0 \\ W_\mu^\pm = \frac{W_\mu^1 \mp i W_\mu^2}{\sqrt{2}}, \end{cases} \quad (3.7)$$

with

$$c_W = \frac{g}{\sqrt{g^2 + g'^2}}, \quad s_W = \frac{g'}{\sqrt{g^2 + g'^2}}, \quad (3.8)$$

the electromagnetic coupling e

$$e = \frac{g g'}{\sqrt{g^2 + g'^2}}, \quad g = \frac{e}{s_W}, \quad g' = \frac{e}{c_W}. \quad (3.9)$$

and the masses

$$M_W = \frac{ev}{2s_W}, \quad M_Z = \frac{ev}{2s_W c_W}. \quad (3.10)$$

\mathcal{L}_S also defines the mass of the Higgs

$$M_H^2 = 2\mu^2. \quad (3.11)$$

μ, λ and v are not all independent parameters. v is defined to be the minimum of the scalar potential. This is equivalent to requiring no tadpole in \mathcal{L}_S . In other words we require the coefficient, T ,

$$T = v(\mu^2 - \lambda v^2), \quad (3.12)$$

of the term linear in H in Eq. 3.6 to be zero, $T = 0$. We will impose this requirement to all orders.

Fermion masses require the introduction of a corresponding Yukawa coupling, f_U (f_D) for an up-type fermion f (for a down-type fermion)

$$\mathcal{L}_M = - \sum_{\text{up}} f_U \bar{L}_U \tilde{\phi} R_U - \sum_{\text{down}} f_D \bar{L}_D \phi R_D + (\text{h.c.}), \quad \tilde{\phi} = i\sigma^2 \phi^*, \quad m_{U,D} = \frac{f_{U,D} v}{\sqrt{2}}. \quad (3.13)$$

Instead of the original set of independent parameters $\{g, g', \lambda, \mu^2, f_{U,D}\}$, it is much more advantageous to revert to an equivalent set of physical parameters that is directly related to physical observables, namely $\{e, M_W, M_Z, M_H, m_U, m_D\}$. In this respect note that the weak mixing angle is just a book-keeping quantity that will be defined, at all orders of perturbation, in terms of the masses of the vector bosons:

$$c_W = \frac{M_W}{M_Z}. \quad (3.14)$$

If one allows v to be an independent parameter we will trade it for the tadpole, T , which we will add to the list of independent parameters that specify the theory.

3.2 Quantisation: Gauge-fixing and Ghost Lagrangian

As known because of the gauge freedom in the classical Lagrangian \mathcal{L}_C , $\mathcal{L}_C = \mathcal{L}_G + \mathcal{L}_F + \mathcal{L}_S + \mathcal{L}_M$, a Lorentz invariant quantisation requires a gauge fixing. We generalise the usual 't Hooft linear gauge condition to a more general non-linear gauge that involves five extra parameters[15], $\zeta = (\tilde{\alpha}, \tilde{\beta}, \tilde{\delta}, \tilde{\kappa}, \tilde{\epsilon})$.

$$\begin{aligned}\mathcal{L}_{GF} &= -\frac{1}{\xi_W} |(\partial_\mu - ie\tilde{\alpha}A_\mu - igc_W\tilde{\beta}Z_\mu)W^{\mu+} + \xi'_W \frac{g}{2}(v + \tilde{\delta}H + i\tilde{\kappa}\chi_3)\chi^+|^2 \\ &\quad - \frac{1}{2\xi_Z} (\partial_\mu Z + \xi'_Z \frac{g}{2c_W}(v + \tilde{\epsilon}H)\chi_3)^2 - \frac{1}{2\xi_A} (\partial_\mu A)^2 \\ &\equiv -\frac{1}{\xi_W} G^+G^- - \frac{1}{2\xi_Z} (G^Z)^2 - \frac{1}{2\xi_A} (G^A)^2\end{aligned}\tag{3.15}$$

Note that it is not essential for the Feynman parameters $\xi'_{W,Z}$ that appear within the functions $G^{\pm,Z}$ to be equal to those that appear as factors of G^+G^- (ξ_W) and $G_Z^2(\xi_Z)$. However in this case \mathcal{L}_{GF} does not cancel, at tree-level, the mixing terms $\chi\cdot W, \chi_3\cdot Z$. We will stick to $\xi'_{W,Z} = \xi_{W,Z}$.

To construct the ghost Lagrangian \mathcal{L}_{Gh} , we will require that the full effective Lagrangian, or rather the full action, be invariant under the BRS transformation (the measure being invariant). The required set of transformations needed to construct the ghost Lagrangian together with the definition of the ghost fields can be found in Appendix A. This is a much more appropriate procedure than the usual Fadeev-Popov approach especially when dealing with the quantum symmetries of the generalised non-linear gauges we are studying. This implies that the full quantum Lagrangian

$$\mathcal{L}_Q = \mathcal{L}_C + \mathcal{L}_{GF} + \mathcal{L}_{Gh},\tag{3.16}$$

be such that $\delta_{\text{BRS}}\mathcal{L}_Q = 0$ and therefore $\delta_{\text{BRS}}\mathcal{L}_{GF} = -\delta_{\text{BRS}}\mathcal{L}_{Gh}$.

Moreover we appeal to the auxiliary B -field formulation of the gauge-fixing Lagrangian \mathcal{L}_{GF} . We will see later that this formulation is also very useful to extract some Ward-Takahashi identities. Within this approach

$$\mathcal{L}_{GF} = \xi_W B^+B^- + \frac{\xi_Z}{2}|B^Z|^2 + \frac{\xi_A}{2}|B^A|^2 + B^-G^+ + B^+G^- + B^ZG^Z + B^AG^A.\tag{3.17}$$

From the equations of motion for the B -fields one recovers the usual \mathcal{L}_{GF} together with the condition $B^i = -\frac{G^i}{\xi_i}$ ($\xi = \{\xi_W, \xi_Z, \xi_A\}$).

Defining the anti-ghost, \bar{c}^i , from the gauge fixing functions, we write

$$\delta_{\text{BRS}}\bar{c}^i = iB^i.\tag{3.18}$$

Then by identification

$$\begin{aligned}\mathcal{L}_{Gh} &= i \left(\bar{c}^+ \delta_{\text{BRS}} G^+ + \bar{c}^- \delta_{\text{BRS}} G^- + \bar{c}^Z \delta_{\text{BRS}} G^Z + \bar{c}^A \delta_{\text{BRS}} G^A \right) + \delta_{\text{BRS}} \tilde{\mathcal{L}}_{Gh} \\ &\equiv \mathcal{L}_{FP} + \delta_{\text{BRS}} \tilde{\mathcal{L}}_{Gh}.\end{aligned}\quad (3.19)$$

That is, one recovers the Fadeev-Popov prescription, \mathcal{L}_{FP} , but only up to an overall function, $\delta_{\text{BRS}} \tilde{\mathcal{L}}_{Gh}$, which is BRS invariant. The complete Feynman rules we list assume $\tilde{\mathcal{L}}_{Gh} = 0$ which is sufficient for one-loop calculations. For higher orders a counterterm not of the Fadeev-Popov type, but which is BRS invariant on its own, may be required to renormalise a quartic ghost vertex, in this case one can take $\tilde{\mathcal{L}}_{Gh} = \lambda \epsilon_{ijk} \delta_{\text{BRS}} (\bar{c}^i \bar{c}^j c^k)$. The full set of Feynman rules derived from \mathcal{L}_Q is relegated to Appendix B. These Feynman rules are derived with an arbitrary set $\zeta = (\tilde{\alpha}, \beta, \tilde{\delta}, \tilde{\kappa}, \tilde{\epsilon})$, $\xi_i = (\xi_W, \xi_Z, \xi_A)$ although for one-loop applications and for all our tests we stick with the 't Hooft-Feynman gauge $\xi_W = \xi_Z = \xi_A = 1$ where the gauge boson propagators take a very simple form. Only their "transverse" part $g_{\mu\nu}$ contributes. This also greatly simplifies the calculations not only because the expressions get more compact but also because of the fact that the longitudinal parts introduce a high degree of (superficial) ultra-violet divergences. Although these greatly simplify when adding all diagrams the cancellations are very subtle and may be not efficiently handled when implemented numerically. In practical calculations one can also tune $\tilde{\alpha}, \tilde{\beta}, \dots$ so that one reduces the number of diagrams and simplify some of the vertices. For instance for photonic vertices $\tilde{\alpha} = 1$ is to be preferred since there is no $W^\pm \chi^\mp A$ vertex and also because the $WW\gamma$ simplifies considerably. One can also choose β so that $W^\pm \chi^\mp Z$ vanishes.

4 Renormalisation and counterterms

4.1 Renormalisation constants

The renormalisation procedure follows very closely the on-shell renormalisation scheme, carried in[21] in the case of the usual linear gauge. The set of physical input parameters includes all the masses of the model together with the value of the electromagnetic coupling as defined in the Thomson limit. As explained above we also add the tadpole, T , to this list. Renormalisation of these parameters would then lead to finite S-matrix elements. For the mass eigenstates and thus a proper identification of the physical particles that appear as external legs in our processes, field renormalisation is needed. S-matrix elements obtained from these rescaled Green's functions will lead to external legs with unit residue. Therefore one also needs wave function renormalisation of the fields. In the linear gauge with all $\xi = 1$ this also renders Green's functions finite. Especially for the unphysical sector of the theory, the precise choice of the fields redefinition is not essential if one is only interested in S-matrix elements of physical processes. We will therefore concentrate

essentially on the renormalisation of the physical parameters and physical fields, although we also introduce field renormalisation for the Goldstone bosons.

All fields and parameters introduced so far in section 3 are considered as bare parameters with the exception of the gauge fixing Lagrangian which we choose to write in terms of *renormalised fields*. Care should then be exercised when we split the tree-level contributions and the counterterms. In Appendix E we also present the alternative approach where the gauge-fixing term is also written in terms of bare parameters. Differences between the two approaches, of course, only affect the unphysical scalar sector. In Appendix D we derive some useful Ward identities that constrain the two-point functions in this sector.

For the renormalised quantity X , the corresponding bare value will be defined by an underlined $\underline{}$ symbol, \underline{X} and its counterterm by δX .

For the physical parameters, and the tadpole, we define

$$\begin{aligned}\underline{M}_W^2 &= M_W^2 + \delta M_W^2, \\ \underline{M}_Z^2 &= M_Z^2 + \delta M_Z^2, \\ \underline{m}_f &= m_f + \delta m_f, \\ \underline{M}_H^2 &= M_H^2 + \delta M_H^2, \\ \underline{e} &= Y e = (1 + \delta Y) e, \\ \underline{T} &= T + \delta T.\end{aligned}\tag{4.1}$$

We now turn to the fields and the wave function renormalisation constants.

1. Gauge fields

$$\begin{aligned}\underline{W}_\mu^\pm &= \sqrt{Z}_W W_\mu^\pm, \quad \sqrt{Z}_W = 1 + \delta Z_W^{1/2}, \\ \begin{pmatrix} \underline{Z}_\mu \\ \underline{A}_\mu \end{pmatrix} &= \begin{pmatrix} \sqrt{Z}_{ZZ} & \sqrt{Z}_{ZA} \\ \sqrt{Z}_{AZ} & \sqrt{Z}_{AA} \end{pmatrix} \begin{pmatrix} Z_\mu \\ A_\mu \end{pmatrix}, \\ \sqrt{Z}_{AA,ZZ} &= 1 + \delta Z_{AA,ZZ}^{1/2}, \quad \sqrt{Z}_{AZ,ZA} = \delta Z_{AZ,ZA}^{1/2}.\end{aligned}\tag{4.2}$$

2. Fermions

For simplicity we will assume no fermion mixing and therefore no \mathcal{CP} violation. In this case the wave functions renormalisation constants $\delta Z_{fL,fR}^{1/2}$ can be taken real as we will see later.

$$\underline{\overset{(-)}{f}}_{L,R} = \sqrt{Z}_{f_{L,R}} \overset{(-)}{f}_{L,R}, \quad \sqrt{Z}_{f_{L,R}} = 1 + \delta Z_{f_{L,R}}^{1/2}.\tag{4.3}$$

3. Scalars

$$\underline{S} = \sqrt{Z}_S S \ , \ \sqrt{Z}_S = 1 + \delta Z_S^{1/2} \ , \ S = H, \chi^\pm, \chi_3 . \quad (4.4)$$

Because we are only presenting an application to processes at one-loop, there is no need to be specific about the renormalisation of the ghost sector. This is sketched in Appendix C. Suffice to say that to generate the ghost Lagrangian including counterterms one needs to re-express \mathcal{L}_{GF} in terms of bare fields to first generate, through BRS transformations, \mathcal{L}_{Gh} with bare fields. This is because \mathcal{L}_{GF} is written in terms of renormalised fields and as such does not induce any counterterm. However the BRS transformations are defined for bare fields.

The generated counterterm library for all 3 and 4-point vertices is listed in Appendix F. The counterterms are fixed through renormalisation conditions that are set, with the exception of the eeA vertex, from the two-point functions to which we now turn.

4.2 Two-point functions at one-loop including counterterms

We work in the on-shell scheme closely following [21] for the determination of the renormalisation constants. The renormalisation conditions on the parameters are essentially derived by properly defining the masses of all the physical particles A, Z, W^\pm, f and the electromagnetic constant. They are all set from the propagator and the e^+e^-A vertex. Let us first turn to the propagators of the fields of the theory.

The counterterm contribution will be denoted by a caret while the full contribution (counterterm and one-loop diagrams contribution) is denoted by a tilde, so that for the vector boson we may write

$$\tilde{\Pi} = \Pi + \hat{\Pi} . \quad (4.5)$$

Moreover it is necessary to decompose these contributions according to their Lorentz structure. For our purpose we will only consider the case of no mixing (and hence no \mathcal{CP} violation) in the fermionic sector. The decomposition of two-point functions is as follows.

type	formula
vector-vector	$\Pi_{\mu\nu}(q^2) = \left(g_{\mu\nu} - \frac{q_\mu q_\nu}{q^2} \right) \Pi_T(q^2) + \frac{q_\mu q_\nu}{q^2} \Pi_L(q^2)$
scalar-scalar	$\Pi(q^2)$
vector-scalar	$iq_\mu \Pi(q^2)$ (q is the momentum of the incoming scalar)
fermion-fermion	$\Sigma(q^2) = K_1 I + K_5 \gamma_5 + K_\gamma \not{q} + K_{5\gamma} \not{q} \gamma_5$

Complete one-loop results for all two-point functions in the generalised non-linear gauge are collected in Appendix H.

The contribution of the counterterms to the two-point functions writes

1. Vector-Vector

$$\begin{array}{ll}
 \hline
 WW & \hat{\Pi}_T^W = \delta M_W^2 + 2(M_W^2 - q^2)\delta Z_W^{1/2} \\
 & \hat{\Pi}_L^W = \delta M_W^2 + 2M_W^2\delta Z_W^{1/2} \\
 \hline
 ZZ & \hat{\Pi}_T^{ZZ} = \delta M_Z^2 + 2(M_Z^2 - q^2)\delta Z_{ZZ}^{1/2} \\
 & \hat{\Pi}_L^{ZZ} = \delta M_Z^2 + 2M_Z^2\delta Z_{ZZ}^{1/2} \\
 \hline
 ZA & \hat{\Pi}_T^{ZA} = (M_Z^2 - q^2)\delta Z_{ZA}^{1/2} - q^2\delta Z_{AZ}^{1/2} \\
 & \hat{\Pi}_L^{ZA} = M_Z^2\delta Z_{ZA}^{1/2} \\
 \hline
 AA & \hat{\Pi}_T^{AA} = -2q^2\delta Z_{AA}^{1/2} \\
 & \hat{\Pi}_L^{AA} = 0 \\
 \hline
 \end{array}$$

2. Scalar-Scalar

$$\begin{array}{ll}
 \hline
 HH & \hat{\Pi}^H = 2(q^2 - M_H^2)\delta Z_H^{1/2} - \delta M_H^2 + \frac{3\delta T}{v} \\
 \hline
 \chi_3\chi_3 & \hat{\Pi}^{\chi_3} = 2q^2\delta Z_{\chi_3}^{1/2} + \frac{\delta T}{v} \\
 \hline
 \chi\chi & \hat{\Pi}^\chi = 2q^2\delta Z_\chi^{1/2} + \frac{\delta T}{v} \\
 \hline
 \end{array}$$

3. Vector-Scalar

$$\begin{array}{ll}
 \hline
 W\chi & \hat{\Pi}^{W\chi} = M_W(\delta M_W/M_W + \delta Z_W^{1/2} + \delta Z_\chi^{1/2}) \\
 \hline
 Z\chi_3 & \hat{\Pi}^{Z\chi_3} = M_Z(\delta M_Z/M_Z + \delta Z_{ZZ}^{1/2} + \delta Z_{\chi_3}^{1/2}) \\
 \hline
 A\chi_3 & \hat{\Pi}^{A\chi_3} = M_Z\delta Z_{ZA}^{1/2} \\
 \hline
 \end{array}$$

4. Fermion-Fermion

At one-loop, this sector is unaffected by the parameters of the non-linear gauge and thus all functions are as in the usual linear gauge case. As mentioned earlier, all wave functions constants are real since we do not consider mixing in the fermionic sector.

$$\begin{aligned}
 \hat{K}_1 &= -m_f \left(\delta Z_{fL}^{1/2} + \delta Z_{fR}^{1/2} \right) - \delta m_f, \\
 \hat{K}_5 &= 0, \\
 \hat{K}_\gamma &= \left(\delta Z_{fL}^{1/2} + \delta Z_{fR}^{1/2} \right), \\
 \hat{K}_{5\gamma} &= - \left(\delta Z_{fL}^{1/2} - \delta Z_{fR}^{1/2} \right). \tag{4.6}
 \end{aligned}$$

4.3 Renormalisation Conditions

Leaving aside the renormalisation of the electromagnetic charge, these two-point functions give all other renormalisation constants. Before deriving these let us first turn to the tadpole.

1. Tadpole

The counterterm for the tadpole contribution, δT , is defined such that the tadpole loop contribution T^{loop} and the counterterm δT combine such that the tadpole $\tilde{T} = T^{loop} + \delta T = 0$. Then

$$\delta T = -T^{loop}. \quad (4.7)$$

2. Charged vector

The conditions specify that the pole-position of the propagator is M_W^2 , and that the residue of the propagator at the pole is 1.

$$\Re e \tilde{\Pi}_T^W(M_W^2) = 0, \quad \frac{d}{dq^2} \Re e \tilde{\Pi}_T^W(q^2) \Big|_{q^2=M_W^2} = 0. \quad (4.8)$$

This gives the following relations.

$$\delta M_W^2 = -\Re e \Pi_T^W(M_W^2), \quad \delta Z_W^{1/2} = \frac{1}{2} \frac{d}{dq^2} \Re e \Pi_T^W(q^2) \Big|_{q^2=M_W^2}. \quad (4.9)$$

3. Neutral vector

The conditions to be imposed on the photon-photon and $Z - Z$ self-energies are the same as for the W - W transition. In addition we require that there should be no mixing between Z and the photon at the poles $q^2 = 0, M_Z^2$.

$$\Re e \tilde{\Pi}_T^{ZZ}(M_Z^2) = 0, \quad \frac{d}{dq^2} \Re e \tilde{\Pi}_T^{ZZ}(q^2) \Big|_{q^2=M_Z^2} = 0, \quad (4.10)$$

$$\tilde{\Pi}_T^{AA}(0) = 0, \quad \frac{d}{dq^2} \tilde{\Pi}_T^{AA}(q^2) \Big|_{q^2=0} = 0, \quad (4.11)$$

$$\tilde{\Pi}_T^{ZA}(0) = 0, \quad \Re e \tilde{\Pi}_T^{ZA}(M_Z^2) = 0. \quad (4.12)$$

Among these 6 conditions, $\tilde{\Pi}_T^{AA}(0) = 0$ produces nothing, except that it ensures that the loop calculation does indeed give $\Pi_T^{AA}(0) = 0$. One then derives,

$$\delta M_Z^2 = -\Re e \Pi_T^{ZZ}(M_Z^2), \quad \delta Z_{ZZ}^{1/2} = \frac{1}{2} \Re e \frac{d}{dq^2} \Pi_T^{ZZ}(q^2) \Big|_{q^2=M_Z^2}, \quad (4.13)$$

$$\delta Z_{AA}^{1/2} = \frac{1}{2} \frac{d}{dq^2} \Pi_T^{AA}(0) , \quad (4.14)$$

$$\delta Z_{ZA}^{1/2} = -\Pi_T^{ZA}(0)/M_Z^2, \quad \delta Z_{AZ}^{1/2} = \Re e \Pi_T^{ZA}(M_Z^2)/M_Z^2 . \quad (4.15)$$

4. Higgs

The conditions specify that the pole-position of the propagator is M_H^2 , and that the residue of the propagator at the pole is 1,

$$\Re e \tilde{\Pi}^H(M_H^2) = 0, \quad \frac{d}{dq^2} \Re e \tilde{\Pi}^H(q^2) \Big|_{q^2=M_H^2} = 0 . \quad (4.16)$$

This gives the following relations.

$$\delta M_H^2 = \Re e \Pi^H(M_H^2) + \frac{3\delta T}{v}, \quad \delta Z_H^{1/2} = -\frac{1}{2} \frac{d}{dq^2} \Re e \Pi^H(q^2) \Big|_{q^2=M_H^2} . \quad (4.17)$$

5. Fermion

The conditions for pole-positions and residues are the same as for the other physical particles. Also the vanishing of γ_5 and $\gamma^\mu \gamma_5$ terms at the pole is required. These conditions read

$$m_f \Re e \tilde{K}_\gamma(m_f^2) + \Re e \tilde{K}_1(m_f^2) = 0, \quad \frac{d}{dq^2} \Re e (\tilde{K}_\gamma(q^2) + \tilde{K}_1(q^2)) \Big|_{q^2=m_f^2} = 0, \quad (4.18)$$

$$\Re e \tilde{K}_5(m_f^2) = 0, \quad \Re e \tilde{K}_{5\gamma}(m_f^2) = 0. \quad (4.19)$$

\mathcal{CP} invariance leads to $K_5 = 0$. In this case, one can take both $\delta Z_{fL}^{1/2}$ and $\delta Z_{fR}^{1/2}$ to be real using the invariance under a phase rotation. We obtain the following relations.

$$\begin{aligned} \delta m_f &= \Re e (m_f K_\gamma(m_f^2) + K_1(m_f^2)) , \\ \delta Z_{fL}^{1/2} &= \frac{1}{2} \Re e (K_{5\gamma}(m_f^2) - K_\gamma(m_f^2)) - m_f \frac{d}{dq^2} (m_f \Re e K_\gamma(q^2) + \Re e K_1(q^2)) \Big|_{q^2=m_f^2} , \\ \delta Z_{fR}^{1/2} &= -\frac{1}{2} \Re e (K_{5\gamma}(m_f^2) + K_\gamma(m_f^2)) - m_f \frac{d}{dq^2} (m_f \Re e K_\gamma(q^2) + \Re e K_1(q^2)) \Big|_{q^2=m_f^2} . \end{aligned} \quad (4.20)$$

6. Charge

While there are many vertices in the theory, if the charge e is properly renormalised, we do not need any further renormalisation conditions. The condition can be imposed on any vertex. The most natural one is to fix the $e^+ e^- A$ vertex as is usually done in QED by relating it to the Thomson limit. The condition requests that

the coupling is $-e$ when q , the momentum of the photon, is 0, while the e^\pm with momentum p_\pm are one shell,

$$(e^+e^-A \text{ one loop term} + e^+e^-A \text{ counter term})\Big|_{q=0, p_\pm^2 = m_e^2} = 0. \quad (4.21)$$

The counterterm is defined in Appendix F. From this, we obtain δY . In fact we will see that due to a Ward identity, see for example [22], δY writes as a combination of $\delta Z_{AA}^{1/2}$ and $\delta Z_{ZA}^{1/2}$ which is valid in all gauges.

7. The unphysical sector

Because we are interested in applications to physical processes, the renormalisation of this sector is not adamant. Nonetheless one may choose to work, as far as possible, with finite Green's functions involving the Goldstones and the longitudinal modes of the vector bosons. With a linear gauge-fixing condition in the 't Hooft-Feynman gauge, and in the approach we are taking where the gauge-fixing Lagrangian is written in terms of renormalised fields from the outset, all divergences in this sector are taken care of by properly choosing Z_{χ_3, χ^\pm} . Therefore following [21] we define the wave-function renormalisation for $\chi = \chi_3, \chi^\pm$,

$$\delta Z_\chi^{1/2} = -\frac{1}{2} \frac{d}{dq^2} \left(\Pi^\chi(q^2) \right) \Big|_{C_{UV}-\text{part}}. \quad (4.22)$$

where $\Pi^\chi(q^2)|_{C_{UV}-\text{part}}$ is the divergent part of the Goldstone two-point functions. We extend the same definition in the case of the non-linear gauge, see for example Eq. E.10. In our approach, where the gauge fixing term is expressed in terms of renormalised quantities from the on-set, this is not sufficient to make all the unphysical scalar two-point functions and mixing finite in the non-linear gauge. In fact in our approach and with the non-linear gauge, even $\tilde{\Pi}_L^{W^\pm}$, which does not involve $\delta Z_{\chi^\pm}^{1/2}$, is not finite. However as shown in Appendix D, there is a strong constraint on the two-point functions of the unphysical scalars. For our purpose of using these kinds of gauge fixing to check the gauge parameter independence of the results, this also is a non trivial test on the finiteness and gauge independence of the results. In Appendix E we show explicitly how one may choose to have finite two-point functions in the Goldstone sector at the expense of renormalising the gauge parameters. This method could be followed but it introduces a few extra renormalisation constants, which may slow the code for the cross section evaluation. In any case, although we can calculate the cross sections in any gauge, the gauge-parameter independence check is systematically applied on some random points in phase space. When this is passed we generally calculate the cross section in the linear gauge, with all 't Hooft-Feynman parameters being equal to one. In this case, linear gauge condition with $\xi = 1$, both approaches are equivalent.

4.4 Some remarks on the explicit form of the renormalisation constants

The renormalisation procedure outlined above together with the exact and complete computation of all two-point functions permits to derive in a straightforward manner the explicit expressions for all parameters and wave function renormalisation constants. The complete expressions for all two-point functions are defined in Appendix H. From the conditions imposed in section 4.3 one immediately extracts all the necessary counterterms. Since the general expressions for these are lengthy and can be read off from Appendix H, we do not list all of them here, but just comment on some important general features.

4.4.1 Mass shifts and charge renormalisation

We first verify that all counterterms to the input parameter of the physical particles, namely the masses of all particles, $\delta M_{W,Z,H,f}$, are gauge-parameter independent. This also applies to the tadpole counterterm. This constitutes a strong check on our results.

The same holds for the charge renormalisation constant, δY . Although this may be derived from the knowledge of $\delta Z_{AA}^{1/2}$ and $\delta Z_{ZA}^{1/2}$ through a Ward identity, it is easy to compute it directly. This is done explicitly in Appendix I. We find the gauge parameter independent result

$$\delta Y = -\delta Z_{AA}^{1/2} + \frac{s_W}{c_W} \delta Z_{ZA}^{1/2}. \quad (4.23)$$

While both $\delta Z_{AA}^{1/2}$ and $\delta Z_{ZA}^{1/2}$ are gauge-parameter dependent, see Eqs. 4.26-4.27 below, the above combination is universal.

$$\delta Y = \frac{\alpha}{4\pi} \left\{ -\frac{7}{2}(C_{UV} - \log M_W^2) - \frac{1}{3} + \frac{2}{3} \sum_f Q_f^2 (C_{UV} - \log m_f^2) \right\}, \quad (4.24)$$

with

$$C_{UV} = 1/\varepsilon - \gamma_E + \log 4\pi, \quad n = 4 - 2\varepsilon, \quad (4.25)$$

n is the dimensionality of space-time in dimensional regularisation.

4.4.2 Wave function renormalisation constants

Since $\delta Z_{AA}^{1/2}$ and $\delta Z_{ZA}^{1/2}$ are crucial for charge renormalisation and since their expressions are rather simple we give them explicitly.

$$\underline{\delta Z_{AA}^{1/2}}$$

$$\delta Z_{AA}^{1/2} = \frac{\alpha}{4\pi} \left[\left(\frac{3}{2} + 2\tilde{\alpha} \right) (C_{UV} - \log M_W^2) + \frac{1}{3} - \frac{2}{3} \sum_f Q_f^2 (C_{UV} - \log m_f^2) \right]$$

$$\equiv \frac{\alpha}{4\pi} \left[\left(-2(1 - \tilde{\alpha}) + \frac{7}{2} \right) (C_{UV} - \log M_W^2) + \frac{1}{3} - \frac{2}{3} \sum_f Q_f^2 (C_{UV} - \log m_f^2) \right], \quad (4.26)$$

where a summation on all fermions of charge Q_f is performed.

$$\delta Z_{ZA}^{1/2} = -\frac{\alpha}{2\pi} \frac{c_W}{s_W} (1 - \tilde{\alpha}) (C_{UV} - \log M_W^2). \quad (4.27)$$

This shows that although both $\delta Z_{AA}^{1/2}$ and $\delta Z_{ZA}^{1/2}$ are gauge parameter dependent the combination that appears in the charge renormalisation is not. Moreover observe that the choice $\tilde{\alpha} = 1$ gives a vanishing Z - A transition at one-loop. This is due to the residual $U(1)$ gauge symmetry which remains after gauge fixing the charged sector, with this particular choice of the gauge parameter.

The remaining wave functions constants are not very illuminating and involve lengthy expressions that we can extract from Appendix H. Here we just list the gauge-parameter dependence of those of the physical particles which can be expressed in a rather compact form as

$$\begin{aligned} \delta Z_{AZ}^{1/2} &= \widetilde{\delta Z}_{AZ}^{1/2} + \frac{\alpha}{2\pi} \frac{c_W}{s_W} \tilde{\beta} (C_{UV} - \Re e F_0(W, W, Z)), \\ \delta Z_{ZZ}^{1/2} &= \widetilde{\delta Z}_{ZZ}^{1/2} + \frac{\alpha}{2\pi} \frac{c_W^2}{s_W^2} \tilde{\beta} (C_{UV} - \Re e F_0(W, W, Z)), \\ \delta Z_W^{1/2} &= \widetilde{\delta Z}_W^{1/2} - \frac{\alpha}{4\pi} \frac{1}{s_W^2} \left\{ s_W^2 \tilde{\alpha} (C_{UV} - \Re e F_0(A, W, W)) + c_W^2 \tilde{\beta} (C_{UV} - \Re e F_0(Z, W, W)) \right\}, \\ \delta Z_H^{1/2} &= \widetilde{\delta Z}_H^{1/2} + \frac{\alpha}{8\pi} \frac{1}{s_W^2} \left\{ \tilde{\delta} (C_{UV} - \Re e F_0(W, W, H)) + \frac{\tilde{\epsilon}}{2c_W^2} (C_{UV} - \Re e F_0(Z, Z, H)) \right\}. \end{aligned} \quad (4.28)$$

where the quantities with $\widetilde{}$ correspond to the linear gauge result with all Feynman parameters set to 1. The function F_0 is defined in Appendix G. As known[23] the requirement of having the residues of the renormalised propagators of all physical particles to be unity leads to a (very sharp) threshold singularity in the wave function of the Higgs at the thresholds corresponding to $M_H = 2M_W, 2M_Z$. This singularity is all contained in the explicit derivative term in $\delta Z_H^{1/2}$ and is therefore gauge-parameter independent. Solutions to smooth this behaviour[24], like the inclusion of the finite width of the W and Z , do exist but we have not implemented them yet in the present version of **GRACE-loop**. Therefore when scanning over M_H it is sufficient to avoid these regions within 1GeV around the thresholds.

5 Evaluation of the loop integrals

In the intermediate stage of the symbolic calculation dealing with loop integrals (in n -dimension), we extract the regulator constant C_{UV} defined in Eq. 4.25. We treat C_{UV} as a parameter in the subsequent (numerical) stages. We regularise any infrared divergence by giving the photon a fictitious mass, λ . By default we set this at $\lambda = 10^{-15}\text{GeV}$.

All tensor reductions of two, three and four-point functions are performed by solving a system of equations obtained by taking derivatives with respect to the Feynman parameters. All higher orders parametric integrals corresponding to the tensor integrals can then be recursively derived from the scalar integral, as will be described below. It is important to stress that this reduction is different to what is usually done through the Passarino-Veltman [25] or the Brown-Feynman[26] reductions. It is also different from the approach of Bern,Dixon and Kosower[27] who exploit differentiation of the scalar integral with respect to a set of kinematical variables. Since the computation of the scalar integrals is central let us first describe their implementation in **Grace-loop**.

5.1 Scalar integrals

The two-point integrals are implemented using simple analytical formulae and evaluated numerically. This allows to achieve a quite high precision. The scalar 3-point function and all but the infra-red divergent 4-point scalar functions are evaluated through a call to the FF package[28]. Although the FF package has been extensively used and checked by many authors, we have also tested its accuracy and implementation in **Grace-loop** by comparing its results against our own numerical approach to loop integrals[29].

For the infrared four-point function, see Fig. 2, we supply our own optimised routines. A purely numerical approach would lead to instabilities and would prevent a complete and satisfactory cancellation of infrared divergences between these loop functions and the infrared factors from the real soft bremsstrahlung part. Luckily some rather simple analytical results have been derived in this case [30, 31]. These can be further simplified when the box involves quite separate mass scales as often occurs in e^+e^- (smallness of the electron mass). In the example $e^+e^- \rightarrow F\bar{F}$ shown in Fig. 2, close to the Z resonance $s \simeq M_Z^2$ one needs to take into account the width of the Z circulating in the loop. This implementation ensures that, even close to the resonance, the infrared divergent part exactly cancels against the soft bremsstrahlung correction. The calculation of some of these photonic boxes is detailed in [30] and [31]. Let us also mention, although this article only deals with $2 \rightarrow 2$ process, that the treatment of the pentagon functions as implemented in **Grace-loop** has been described in [2].

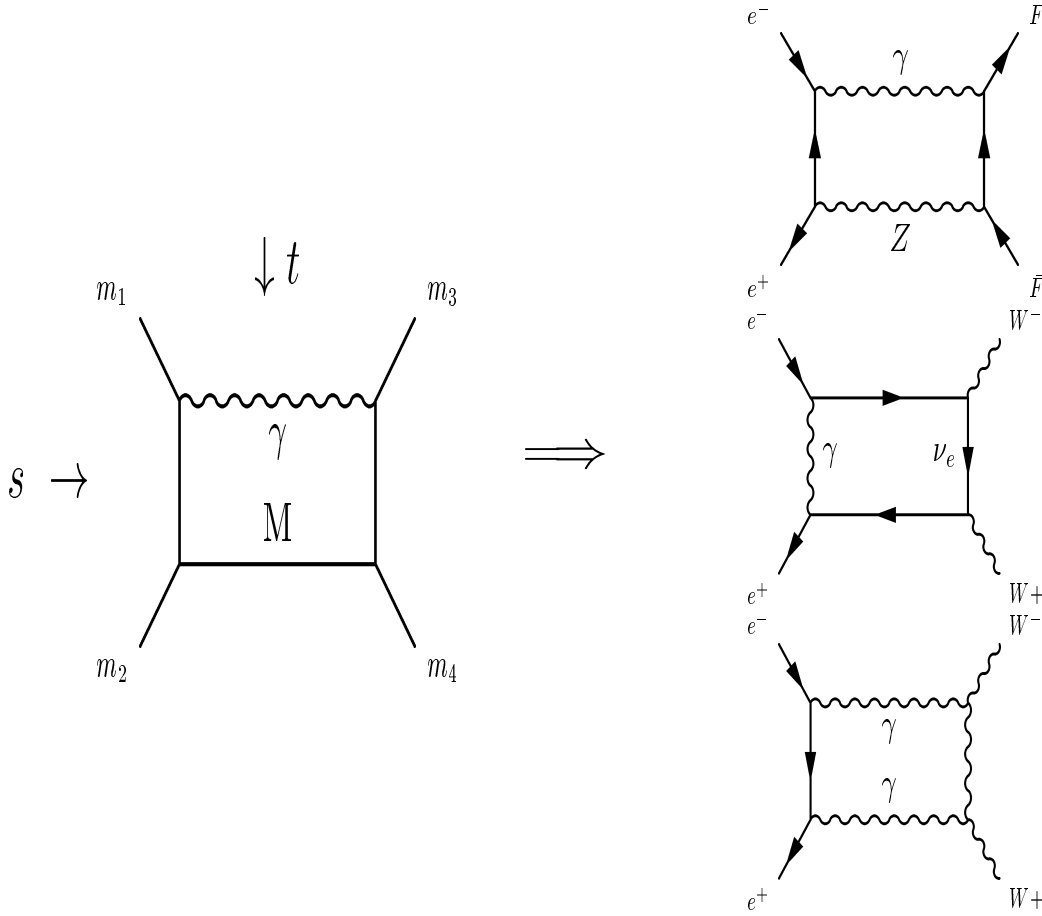


Figure 2: The left panel shows the general configuration of the infrared four-point functions of the scattering of incoming particles with masses m_1, m_2 to particles with masses m_3, m_4 . s, t are the usual Mandelstam variables. The right panel shows some examples that need to be treated carefully. In the first example, the Z can be close to the resonance.

5.2 Reduction of the tensor integrals

The tensor integral of rank M corresponding to a N -point graph that we encounter in the general non-linear gauge but with Feynman parameters $\xi = 1$ are such that $M \leq N$. They can all be deduced recursively from the knowledge of the N -point (and lower) scalar integrals. The object in question writes in dimensional regularisation as

$$\underbrace{T_{\mu\nu\cdots\rho}^{(N)}}_M = \int \frac{d^nl}{(2\pi)^n} \frac{l_\mu l_\nu \cdots l_\rho}{D_0 D_1 \cdots D_{N-1}}, \quad M \leq N, \quad (5.1)$$

where

$$D_i = (l + s_i)^2 - M_i^2, \quad s_i = \sum_{j=1}^i p_j, \quad s_0 = 0. \quad (5.2)$$

M_i are the internal masses, p_i the incoming momenta and l the loop momentum. We then use Feynman's parameterisation which combines all propagators such that

$$\begin{aligned} \frac{1}{D_0 D_1 \cdots D_{N-1}} &= \Gamma(N) \int [dx] \frac{1}{\left(D_1 x_1 + D_2 x_2 + \cdots + D_0 (1 - \sum_{i=1}^{N-1} x_i) \right)^N} \\ \int [dx] &= \int_0^1 dx_1 \int_0^{1-x_1} dx_2 \cdots \int_0^{1-\sum_{i=1}^{N-2} x_i} dx_{N-1}. \end{aligned} \quad (5.3)$$

Because the integrals are regulated we first deal with the loop momenta, before handling the integration over the parametric variables and write

$$\begin{aligned} \underbrace{T_{\mu\nu\cdots\rho}^{(N)}}_M &= \Gamma(N) \int [dx] \underbrace{\mathcal{T}_{\mu\nu\cdots\rho}^{(N)}}_M, \quad \text{with} \\ \mathcal{T}_{\mu\nu\cdots\rho}^{(N)} &= \int \frac{d^n l}{(2\pi)^n} \frac{l_\mu l_\nu \cdots l_\rho}{(l^2 - 2l \cdot P(x_i) - M^2(x_i))^N}, \quad M \leq N \end{aligned} \quad (5.4)$$

Integration over the loop momenta l is done trivially. We may write a compact formula that applies up to the boxes. Introducing

$$\begin{aligned} \Delta &= \sum_{i,j=1}^{N-1} Q_{ij} x_i x_j + \sum_{i=1}^{N-1} L_i x_i + \Delta_0, \quad Q_{ij} = s_i \cdot s_j, \quad L_i = -s_i^2 + (M_i^2 - M_0^2), \\ \Delta_0 &= M_0^2, \quad P = -\sum_{i=1}^{N-1} s_i x_i \end{aligned} \quad (5.5)$$

we can write

$$\begin{aligned} \mathcal{T}^{(N)} &= \tilde{\mathcal{T}}^{(N)} \Gamma(N - n/2) \quad \text{with} \quad \tilde{\mathcal{T}}^{(N)} = \frac{(-1)^N i \pi^{n/2}}{(2\pi)^n \Gamma(N)} \Delta^{-(N-n/2)}, \\ \mathcal{T}_\mu^{(N)} &= \mathcal{T}^{(N)} P_\mu, \\ \mathcal{T}_{\mu\nu}^{(N)} &= \tilde{\mathcal{T}}^{(N)} \left(\Gamma(N - n/2) P_\mu P_\nu - \frac{1}{2} g_{\mu\nu} \Delta \Gamma(N - 1 - n/2) \right), \\ \mathcal{T}_{\mu\nu\rho}^{(N)} &= \tilde{\mathcal{T}}^{(N)} \left(\Gamma(N - n/2) P_\mu P_\nu P_\rho - \frac{\Delta}{2} (g_{\mu\nu} P_\rho + g_{\mu\rho} P_\nu + g_{\nu\rho} P_\mu) \Gamma(N - 1 - n/2) \right), \end{aligned}$$

$$\begin{aligned}
\mathcal{T}_{\mu\nu\rho\sigma}^{(N)} &= \tilde{\mathcal{T}}^{(N)} \left(\Gamma(N-n/2) P_\mu P_\nu P_\rho P_\sigma + \frac{\Delta^2}{4} (g_{\mu\nu}g_{\rho\sigma} + g_{\mu\rho}g_{\nu\sigma} + g_{\mu\sigma}g_{\nu\rho}) \Gamma(N-2-n/2) \right. \\
&\quad \left. - \frac{\Delta}{2} (g_{\mu\nu}P_\rho P_\sigma + g_{\mu\rho}P_\nu P_\sigma + g_{\mu\sigma}P_\nu P_\rho + g_{\nu\rho}P_\mu P_\sigma + g_{\nu\sigma}P_\mu P_\rho + g_{\rho\sigma}P_\mu P_\nu) \Gamma(N-1-n/2) \right)
\end{aligned} \tag{5.6}$$

It now rests to integrate over the Feynman parameters contained in the momenta $P = P(\{x_i\})$. We show how this is done for the box ($N = 4$) and triangle ($N = 3$) integrals. As pointed out earlier the case $N = 2$ is straightforward and is implemented analytically, some examples are given in Appendix G. The problem now turns into finding solutions for the parametric integrals

$$I_{\underbrace{i \cdots k}_M}^{(N)} = \int [dx] \frac{x_i \cdots x_k}{\Delta^{(N-2)}} \quad \text{and} \tag{5.7}$$

$$J_{i;\alpha}^{(N)} = \int [dx] x_i^\alpha \log \Delta \quad \alpha = 0, 1. \tag{5.8}$$

solely in terms of the scalar integral $I^{(N)} = \int [dx] \Delta^{-(N-2)}$ (for which we use the FF package[28]). The appearance of the integrals $J_{i;\alpha}^{(N)}$ stems from expanding Eq. 5.6 around $n = 4 - 2\epsilon$ and originates from the ϵ independent terms in $\epsilon(1/\epsilon + \mathcal{O}(\epsilon^{0,1}))$. In fact one only needs $J^{(4)} = J_{i;0}^{(4)}$ and $J_{i;(0,1)}^{(3)}$. All these integrals are derived recursively. The integral in Eq. 5.7 will be referred to as the parametric integral of rank- M for the N -point function. It will then be expressed in terms of lower rank tensors and lower N integrals.

5.3 Reduction of the higher rank parametric box integrals

Let us first show how the tensor box integrals are implemented. Note that one needs 15 different integrals for the rank-4 box, 10 for the rank-3, 6 for the rank-2 and 3 for the rank-1. The trick is to use the fact that

$$\begin{aligned}
&\int [dx] \partial_i \left(\frac{x_k^\alpha x_l^\beta x_m^\gamma}{\Delta} \right), \\
&\text{with } \partial_i = \frac{\partial}{\partial x_i}, \quad 1 \leq \alpha + \beta + \gamma = M \leq N - 1
\end{aligned} \tag{5.9}$$

is a surface term that can be derived from the parametric integrals of the triangle. On the other hand expanding the partial derivative generates parametric integrals of order $M + 1$, beside parametric integrals of rank $M - 1$ and rank M . To wit,

$$\begin{aligned}
\partial_i \left(\frac{x_k^\alpha x_l^\beta x_m^\gamma}{\Delta} \right) &= -\frac{x_k^\alpha x_l^\beta x_m^\gamma}{\Delta^2} (L_i + 2 \sum_j Q_{ij} x_j) + \frac{1}{\Delta^2} \left(\Delta_0 + \sum_j L_j x_j + \sum_{jn} Q_{jn} x_j x_n \right) \times \\
&\quad (\alpha x_k^{\alpha-1} x_l^\beta x_m^\gamma \delta_{ki} + \beta x_l^{\beta-1} x_k^\alpha x_m^\gamma \delta_{li} + \gamma x_m^{\gamma-1} x_k^\alpha x_l^\beta \delta_{mi})
\end{aligned} \tag{5.10}$$

The term on the left-hand side can be trivially integrated and can be expressed in terms of the triangle integral of rank $M \leq 3$. The terms proportional to L_i on the right-hand side are box integrals of rank M whereas the term proportional to Δ_0 corresponds to boxes of rank $M - 1$. We combine all these terms into $C_{i;jkl}$, where the first index i shows that a derivative has been applied on the index i . The terms proportional to Q_{ij} are boxes of rank $M + 1$ that we want to derive. In particular, to generate the highest rank integrals for the box $M = 4$, we apply Eq. 5.10 with $\alpha = \beta = \gamma = 1$, ($M = 3$). This amounts to solving a system of equations for the integrals $I_{ijkl}^{(4)}$,

$$\begin{aligned} C_{i;klm} &= -2 \sum_j Q_{ij} I_{jklm}^{(4)} + \sum_{jn} Q_{jn} \left(\delta_{ki} I_{jnlm}^{(4)} + \delta_{li} I_{jnlm}^{(4)} + \delta_{mi} I_{jnkl}^{(4)} \right), \\ I_{ijkl}^{(4)} &= \int [dx] \frac{x_i x_j x_k x_l}{\Delta^2}. \end{aligned} \quad (5.11)$$

One can thus solve for a system of equations for the higher rank parametric integrals of order $M + 1$ in terms of (previously derived) integrals of rank $M - 1$ and M for the box and rank M for the triangle. One drawback of this approach is that one ends up with a larger set of equations than needed to solve the system, especially as the rank of the parametric integral increases. This however also shows that one can in principle carry consistency checks. To pick up a system of linearly independent equations we first construct

$$\sum_i C_{i;ikk} = 3 \sum_{jn} Q_{jn} I_{jnkk}^{(4)}, \quad (5.12)$$

in order to form the set²

$$\tilde{C}_{i;kkk} = -\frac{1}{2} \left(C_{i;kkk} - \delta_{ki} \sum_i C_{i;ikk} \right) = \sum_j Q_{ij} I_{jkkk}^{(4)}. \quad (5.13)$$

For the highest rank, $M = 4$, this provides 3 independent sets (one for each value of k) each consisting of three independent integrals $I_{jkkk}^{(4)}$ (for $j = 1, 2, 3$). Therefore one only

²This could have also been arrived at more directly had we used

$$\sum_j x_j \partial_j \Delta = 2\Delta - 2\Delta_0 - \sum_j L_j x_j.$$

This enables to re-express the second terms on the right-hand side of Eq. 5.10, involving the Kronecker symbols for the case $\alpha = \beta = \gamma = 1$, as lower rank terms and triangle integrals. Namely we can write

$$3 \frac{x_l x_m}{\Delta} = -2 \frac{\Delta_0}{\Delta^2} + \sum_j \left\{ \partial_j \left(\frac{x_j x_l x_m}{\Delta} \right) - L_j \left(\frac{x_j x_l x_m}{\Delta^2} \right) \right\}.$$

deals with 3 simple 3×3 matrices which help solve 9 out of 15 integrals. We may refer to this set as the diagonal integrals. The remaining integrals are provided by the set of the 6 independent equations $C_{i;jkk}$ where i, j, k are all different from each other,

$$C_{i;jkk} = -2 \sum_n Q_{in} I_{n j k k}^{(4)}, \quad i \neq j \neq k \quad (5.14)$$

It is obvious that the same trick applies to solving $I_{jkk}^{(4)}$ and provides 9 out of the 10 independent integrals. The remaining integral in this case is provided by any $C_{i;jk}$ where all indices are different. We also apply Eq. 5.13 to the set $I_{jk}^{(4)}$ and obtain $\tilde{C}_{i;k} = \sum_j Q_{ij} I_{jk}^{(4)}$.

This method shows that to solve for the 15 independent integrals of rank-4 one does not deal with a 15×15 matrix. Rather the previous formulation shows that this splits into simplified $3 \oplus 3 \oplus 3 \oplus 6$ systems of equations. The 6×6 matrix is also easy to deal with since each row consists of only 2 non-zero elements. For the rank-3 integrals the system of 10 equations decomposes into $3 \oplus 3 \oplus 3 \oplus 1$, while for the rank-2, the system of 6 equations decomposes into $3 \oplus 2 \oplus 1$.

5.4 $\log(\Delta)$ terms

To extract $J^{(4)}$ for the box and most of the results for the reduction of the higher rank integrals for the triangle, we start by giving a general representation for the logarithm. Take Δ_N where N is to just remind us that it comes from a N -point function. We can write

$$x_i^\alpha \log \Delta_N = \frac{1}{N + \alpha - 1} \sum_{j=1}^{N-1} \{ \partial_j (x_i^\alpha x_j \log \Delta_N) - x_i^\alpha x_j \partial_j (\log \Delta_N) \} \quad (5.15)$$

Specific formulae needed for the boxes and triangles are

$$x_i \log \Delta = \frac{1}{3} \sum_{j=1}^2 \left\{ \partial_j (x_i x_j \log \Delta) - x_i + \frac{x_i (L_j x_j + \Delta_0)}{\Delta} \right\}, \quad N = 3, \alpha = 1 \quad (5.16)$$

$$\log \Delta = \frac{1}{2} \sum_{j=1}^2 \left\{ \partial_j (x_j \log \Delta) - 1 + \frac{L_j x_j + \Delta_0}{\Delta} \right\}, \quad N = 3, \alpha = 0 \quad (5.17)$$

$$\log \Delta = \frac{1}{3} \sum_{j=1}^3 \left\{ \partial_j (x_j \log \Delta) - \frac{2}{3} + \frac{\Delta (L_j x_j + 2/3 \Delta_0)}{\Delta^2} \right\}, \quad N = 4, \alpha = 0 \quad (5.18)$$

Eq. 5.18 shows that $J^{(4)}$ can be expressed in terms of the “lower” integrals $J_{i;1}^{(3)}$ and $I_{M=0,1,2,3}^{(4)}$. In turn, all $J_{i;(0,1)}^{(3)}$ are expressed in terms of two-point functions and the integrals $I_{M=0,1,2}^{(3)}$.

5.5 Reduction of the higher rank parametric integrals for the triangle

To generate the triangle $I_{M=1,2,3}^{(3)}$, in analogy with Eq. 5.10, we use

$$\partial_i(x_k^\alpha x_l^\beta \log \Delta). \quad (5.19)$$

For example, for $M = 3$ exploiting Eq. 5.17 we get

$$\begin{aligned} \partial_i(x_k x_l \log \Delta) &= \frac{x_k x_l}{\Delta} \left(L_i + 2 \sum_j Q_{ij} x_j \right) \\ &+ \frac{1}{3} \left\{ \delta_{ki} \sum_j \left(\partial_j(x_l x_j \log \Delta) - x_l \left(1 - \frac{L_j x_j + \Delta_0}{\Delta} \right) \right) + (k \leftrightarrow l) \right\}. \end{aligned} \quad (5.20)$$

All terms with L_i, Δ_0 or partial derivatives are lower order terms (either in N or M). Grouping all these as $C_{i;kl}$ leads to the master equation

$$C_{i;kl} = \sum_j Q_{ij} I_{jkl}^{(3)}. \quad (5.21)$$

Following the same strategy as with the box, we choose the set $C_{i;kk}$ which furnishes 2 “orthogonal” systems of 2 equations each. Therefore instead of handling a 4×4 matrix we only deal with simple 2×2 matrices. Similar results are obtained for $I_{jk}^{(3)}$. The three needed integrals are arrived at by first solving for a reduced system of only two independent integrals and then deriving the third from a single equation.

Finally for $M = 1$, one solves a system with a 2×2 matrix. Note that the solution of all these equations involves the determinant of the same 2×2 matrix, namely Q_{ij} .

Note also that all the system of equations as described here leads to analytic solutions in terms of the scalar integrals. In **Grace-loop** we implement these analytical solutions.

6 Tests on the loop calculation

The results of the calculations are checked by performing three kinds of tests. This concerns the ultraviolet and infrared finiteness as well as the gauge parameter independence. These tests are performed at the level of the differential cross section before any phase space integration is performed for several points in phase space. These tests points are chosen at random. Usually for these tests one keeps all diagrams involving the couplings

of the Goldstones to the light fermions, such as $\chi_3 e^+ e^-$. For these tests to be passed one works in quadruple precision. After these tests have been passed one can switch off these very small couplings, involving the scalars and the light fermions, when calculating the total (integrated) cross section and hence speeding up the computation time. Results of these tests on a selection of the 26 processes for the $2 \rightarrow 2$ reactions displayed in Table. 1 are made available at this web location[32]. This list involves both purely vector bosons scattering, heavy as well as massless fermions scattering into gauge bosons as well as a few processes involving the Higgs. Therefore, as we will see, all the ingredients that enter the calculation of radiative corrections in the standard model are covered by this list.

6.1 Ultraviolet and infrared finiteness checks

6.1.1 Ultraviolet finiteness

We first check the ultraviolet finiteness of the results. This test applies to the whole set of the virtual one-loop diagrams. The ultraviolet finiteness test gives a result that is stable over 30 digits when one varies the dimensional regularisation parameter C_{UV} , that is kept in the code as a free parameter. This parameter could then be set to 0 in further computation. When conducting this test we regularise any infrared divergence by giving the photon a fictitious mass that we fix at $\lambda = 10^{-15}\text{GeV}$. The finiteness test, or C_{UV} independence test, is carried for a random series of the gauge fixing parameters that include the linear gauge as a special case.

6.1.2 Infrared finiteness and calculation of the soft-bremsstrahlung factor

When discussing the calculation and implementation of the loop integrals, diagrams involving photon exchange require special treatment. These diagrams can have an infrared divergence which is regulated by giving the photon a small mass λ . As known the dependence in this fictitious mass cancels against the one contained in the soft bremsstrahlung[33]. The second test that we perform relates to the infrared finiteness by checking that when the virtual loop correction and bremsstrahlung contributions are added there is no dependence on the fictitious photon mass λ . We indeed find results that are stable over 23 digits, or better, when varying λ .

The soft bremsstrahlung part consists of the tree-level process with an additional photon of very small energy, $E_\gamma < k_c$, and requires the introduction of the photon mass regulator, λ . The hard photon radiation with $E_\gamma > k_c$ is regular and will be discussed in section 6.3. The soft photon contribution is implemented in the system following an analytical result based on factorisation and which can be generalised to any process. The bremsstrahlung differential cross section factorises as

$$d\sigma_{\text{soft}}(\lambda, E_\gamma < k_c) = d\sigma_0 \times \delta_{\text{soft}}(\lambda, E_\gamma < k_c) . \quad (6.1)$$

k_c is assumed sufficiently small so that the tree-level $d\sigma_0$ does not change rapidly when the soft photon is emitted. In some cases, for instance around a resonance, special care must be exercised, see for example[30]. The factor δ_{soft} is completely determined from the classical (convection) current of a charged particle and does not involve the spin connection. Therefore this factor is universal and only depends on the charge Q_i and momentum p_i of the particles of the tree-level process,

$$\delta_{\text{soft}} = -e^2 \int_{|k| < k_c} \frac{d^3 k}{2E_\gamma (2\pi)^3} \sum_{ij} \varepsilon_i \varepsilon_i Q_i Q_j \frac{p_i \cdot p_j}{(k \cdot p_i)(k \cdot p_j)} = \sum_{ij} R_{ij}, \quad E_\gamma = \sqrt{k^2 + \lambda^2}. \quad (6.2)$$

where $\varepsilon_i = \pm 1$ depending on whether the particle is incoming (+1) or outgoing (-1). Very general expressions for R_{ij} have been derived most elegantly in [34]. Let us here just recall a few special cases and refer the reader to [30] for more details. For instance, for the diagonal term R_{ii} from a charged particle with $|Q| = 1$ of momentum $p = (E, \vec{p})$, $p^2 = m^2$ and $P = |\vec{p}|$, one gets the very simple result

$$R_{ii} = -e^2 \int_{|k| < k_c} \frac{d^3 k}{2E_\gamma (2\pi)^3} \frac{m^2}{(k \cdot p)^2} = -\frac{\alpha}{\pi} \left\{ \ln \left(\frac{2k_c}{\lambda} \right) + \frac{E}{P} \ln \left(\frac{m}{E + P} \right) \right\}. \quad (6.3)$$

Another quite useful result is the contribution, R_{pair} , from a pair of particle-antiparticle of mass m and charge ± 1 in their centre of mass system with total energy \sqrt{s} . The radiator function writes, with $\beta = \sqrt{1 - 4m^2/s}$

$$R_{\text{pair}} = \frac{2\alpha}{\pi} \left\{ \left(\frac{s - 2m^2}{s\beta} \ln \left(\frac{1 + \beta}{1 - \beta} \right) - 1 \right) \ln \left(\frac{2k_c}{\lambda} \right) + \frac{1}{2\beta} \ln \left(\frac{1 + \beta}{1 - \beta} \right) - \frac{s - 2m^2}{2s\beta} \left(\text{Sp} \left(\frac{2\beta}{1 + \beta} \right) - \text{Sp} \left(\frac{-2\beta}{1 - \beta} \right) \right) \right\}, \quad (6.4)$$

and

$$\text{Sp}(z) = - \int_0^z dt \frac{\ln(1-t)}{t}, \quad (6.5)$$

is the Spence function. This factor would represent the initial state bremsstrahlung part in e^+e^- processes and is usually written (for $s \gg m_e^2$) as

$$R_{\text{pair}}^{e^+e^-} = \frac{2\alpha}{\pi} \left\{ \left(\ln \left(\frac{s}{m_e^2} \right) - 1 \right) \ln \left(\frac{2k_c}{\lambda} \right) - \frac{1}{4} \ln^2 \left(\frac{s}{m_e^2} \right) + \frac{1}{2} \ln \left(\frac{s}{m_e^2} \right) - \frac{\pi^2}{6} \right\}. \quad (6.6)$$

The same factor in Eq. 6.4 can be used as the bremsstrahlung contribution for $\gamma\gamma \rightarrow W^+W^-$ ($m \rightarrow M_W$).

6.2 Gauge-parameter independence checks

For this check we set the value of the ultraviolet parameter C_{UV} to some fixed value. To tame the infrared divergence contained in the virtual corrections we give the photon a fictitious mass $\lambda = 10^{-15}\text{GeV}$. Moreover we also set all widths to zero so that no extra gauge breaking due to the introduction of a width is generated. We thus choose a non-singular point in phase space, away from any resonance, for this check on the differential cross section.

For each process we verify that it does not depend on any of the five non-linear gauge parameter of the set $\zeta = (\tilde{\alpha}, \tilde{\beta}, \tilde{\delta}, \tilde{\kappa}, \tilde{\epsilon})$. Let us remind the reader that we always work with $\xi_W = \xi_Z = \xi_A = 1$. The use of five parameters is not redundant as often these different parameters check complementary sets of diagrams. For example the parameter $\tilde{\beta}$ is involved in all diagrams containing the gauge WWZ coupling and their Goldstone counterpart, whereas $\tilde{\alpha}$ checks $WW\gamma$ and $\tilde{\delta}$ is implicitly present in WWH . For each parameter of the set, the first check is made while freezing all other four parameters to 0. In a second check we give, in turn, each of the remaining 4 parameters a non-zero value (we usually take the values (2, 3, 4, 5) for this set) so that we also check vertices and diagrams that involve cross terms (like $\tilde{\alpha} \times \tilde{\delta}$). In principle checking for 2 or 3 values of the gauge parameter should be convincing enough. We in fact go one step further and perform a comprehensive gauge parameter independence. To achieve this we generate for each non-linear gauge parameter ζ_i of the set ζ , the values of the loop correction to the total differential cross section as well as the individual contribution of each one-loop diagram g , $d\sigma_g$ for a sequence of values for ζ_i , while freezing the other parameters to a fixed value, not necessarily zero. The one-loop diagram contribution from each loop graph g to the fully differential cross section, is defined as

$$d\sigma_g \equiv d\sigma_g(\zeta) = \Re e \left(T_g^{loop} \cdot \mathcal{T}^{tree \dagger} \right) . \quad (6.7)$$

\mathcal{T}^{tree} is the tree-level amplitude summed over all tree-diagrams. Therefore the tree-level amplitude does not depend on any gauge parameter. Note that in many processes, some individual tree diagrams do depend on a gauge parameter, however after summing over all tree-level diagrams, the gauge parameter independence at tree-level for any process is exact within machine precision. T_g^{loop} is the one-loop amplitude contribution of a one-loop diagram g . It is not difficult to see, from the structure of the Feynman rules of the non-linear gauge, that for each $2 \rightarrow 2$ process the differential cross section is a polynomial of (at most) fourth degree in the gauge parameter. Therefore the contribution $d\sigma_g$ of diagram g to the one-loop differential cross section may be written as

$$d\sigma_g(\zeta) = d\sigma_g^{(0)} + \zeta d\sigma_g^{(1)} + \zeta^2 d\sigma_g^{(2)} + \zeta^3 d\sigma_g^{(3)} + \zeta^4 d\sigma_g^{(4)} . \quad (6.8)$$

We have therefore chosen the sequence of the five values $\zeta = 0, \pm 1, \pm 2$. For each contribution $d\sigma_g$, it is a straightforward matter, given the values of $d\sigma_g$ for the five input

Table 1: Accuracy measured by the number of digits for the gauge-parameter checks on the 26 processes for all five gauge parameters. The numbers that appear in the last five columns represent the number of digits which are stable when varying the corresponding gauge parameter. An empty entry means that the process does not depend on the gauge parameter. Only one parameter is varied at a time here. We also show the number of diagrams both at tree-level and at the one-loop level. The number of diagrams depends on the choice of the gauge parameter, for examples in some gauges some vertices are absent. The number of diagrams that we list corresponds to the gauge which leads to the maximum number of diagrams.

processes	# of graphs(Loop \times Tree)	$\tilde{\alpha}$	$\tilde{\beta}$	$\tilde{\delta}$	$\tilde{\epsilon}$	$\tilde{\kappa}$
$\nu_e \bar{\nu}_e \rightarrow \nu_e \bar{\nu}_e$	46×2	–	30	–	–	–
$e^+ e^- \rightarrow \nu_e \bar{\nu}_e$	112×3	31	31	31	–	32
$e^+ e^- \rightarrow t\bar{t}$	150×4	32	31	31	31	31
$e^+ e^- \rightarrow e^+ e^-$	288×4	32	30	30	31	31
$e^+ e^- \rightarrow W^+ W^-$	334×4	27	27	30	31	–
$e^+ e^- \rightarrow Z^0 Z^0$	336×3	33	29	31	31	–
$e^+ e^- \rightarrow H^0 Z^0$	341×3	30	30	31	31	30
$\mu \bar{\nu}_\mu \rightarrow W^- \gamma$	162×3	27	27	28	–	28
$\mu \bar{\nu}_\mu \rightarrow W^- Z^0$	213×4	31	29	30	–	30
$\mu \bar{\nu}_\mu \rightarrow W^- H^0$	196×3	30	29	31	31	31
$t\bar{b} \rightarrow W^+ \gamma$	239×4	22	25	29	–	29
$t\bar{b} \rightarrow W^+ Z^0$	284×4	31	22	31	–	32
$t\bar{b} \rightarrow W^+ H^0$	285×4	29	28	21	26	30
$\gamma\gamma \rightarrow t\bar{t}$	267×2	24	34	30	–	–
$Z^0 Z^0 \rightarrow t\bar{t}$	338×3	30	29	31	31	–
$W^+ W^- \rightarrow t\bar{t}$	354×4	30	26	31	31	–
$Z^0 H^0 \rightarrow t\bar{t}$	355×4	30	28	29	29	31
$\gamma\gamma \rightarrow W^+ W^-$	619×5	22	24	32	–	31
$Z^0 Z^0 \rightarrow Z^0 Z^0$	657×3	–	24	31	31	–
$Z^0 \gamma \rightarrow W^+ W^-$	680×5	28	28	31	–	31
$Z^0 W^- \rightarrow Z^0 W^-$	840×6	26	24	29	30	29
$W^+ W^- \rightarrow W^+ W^-$	925×7	27	26	30	31	–
$Z^0 H^0 \rightarrow W^+ W^-$	823×5	29	25	29	26	31
$Z^0 H^0 \rightarrow Z^0 H^0$	830×6	–	23	24	20	31
$H^0 W^- \rightarrow H^0 W^-$	827×6	29	23	22	23	30
$H^0 H^0 \rightarrow H^0 H^0$	805×4	–	–	29	27	–

$\zeta = 0, \pm 1, \pm 2$, to reconstruct $d\sigma_g^{(0,1,2,3,4)}$. For each set of parameters we automatically pick up all those diagrams that involve a dependence on the gauge parameter. The number of diagrams in this set depends on the parameter chosen. Different parameters involve different (often) complementary sets. In some cases a very large number of diagrams is involved. An example is $ZW^+ \rightarrow ZW^+$ with $\tilde{\beta} \neq 0, \tilde{\kappa} = 1$ where the set involves 601 one-loop diagrams out of a total of 840. We then numerically verify that the (physical) differential cross section is independent of ζ

$$d\sigma = \sum_g d\sigma_g = \sum_g d\sigma_g^{(0)} , \quad (6.9)$$

and therefore that

$$\text{sum}_i = \frac{\sum_g d\sigma_g^{(i)}}{\text{Max}(|d\sigma_g^{(i)}|)} = 0 , \quad i = 1, 2, 3, 4 . \quad (6.10)$$

As summarised in Table 1, we find a precision of at least 21 digits on all sum_i for all the checks we have done. We usually get a much better precision when the number of diagrams involved in the check is smaller.

To appreciate how this level of accuracy is arrived at after summing on all diagrams, we show here, see Table 2, in some detail the result for $W^+W^- \rightarrow W^+W^-$ for the check on the $\tilde{\alpha}$ gauge parameter independence (all other parameters set to zero). This is extracted from the web-page where we have made these checks public[32]. This process involves some 925 one-loop diagrams (and 7 at tree-level). Even for this particular example it is not possible to list all the entries of the table (that is the numerical contributions for all the diagrams) since they would not fit into a single page (the check on $\tilde{\alpha}$ involves some 336 diagrams), thus the skip (skip) on some of the data. For each graph, labeled by its graph number in Table 2, we give all $d\sigma_g^{(i)}$. We see that although individual contributions can be of the order of 10^2 , when summed up they give a total of the order of 10^{-27} . We also show, at the bottom of the table, $\sum_g d\sigma_g$ for the input values $\tilde{\alpha} = 0, \pm 1, \pm 2$ and compare these results to the result obtained by setting $\tilde{\alpha} = 5$ in Eq. 6.8 after $d\sigma_g^{(0,1,2,3,4)}$ have been reconstructed. In this example concerning $\tilde{\alpha}$ we have set the values of the other gauge parameters, $\tilde{\beta}, \tilde{\delta}, \tilde{\kappa}, \tilde{\epsilon}$ to zero. We have also made a similar test on $\tilde{\alpha}$ allowing all other parameters non-zero. The same tests done on $\tilde{\alpha}$ are in turn made for all other parameters. These tests are made on 26 processes. More information on the check concerning $W^+W^- \rightarrow W^+W^-$ and all those listed in Table 1 are to be found at [32].

One more note concerning the checks on the non-linear gauge parameter compared to a check one would do through the Feynman gauge parameter $\xi_{W,A,Z}$ in the usual linear gauge. Having more parameters that clearly affect different sectors differently helps in detecting any possible bug. Within the linear gauge, the usual gauge parameter dependence is not a polynomial, it also involves $\log \xi$ and other functions of ξ . It is therefore almost impossible to fit the exact ξ dependence of each graph. Moreover as pointed out earlier

Table 2: Non-linear gauge parameter checks on $\tilde{\alpha}$ (all other parameters set to zero), for the differential cross section $W^+W^- \rightarrow W^+W^-$. For details see text.

Graph number	$d\sigma_g^{(4)}$	$d\sigma_g^{(3)}$	$d\sigma_g^{(2)}$	$d\sigma_g^{(1)}$	$d\sigma_g^{(0)}$
2			.2335514E+03	.7789374E+03	.5615925E+03
5			-.1721616E+01	-.1171640E+01	.2893256E+01
10			-.4324751E+01	.8649502E+01	-.4324751E+01
13			-.1721616E+01	-.1171640E+01	.2893256E+01
33				.1048909E+01	-.1048909E+01
35				.1048909E+01	-.1048909E+01
			\mathcal{N}		
			\mathcal{N}		
321	-.3606596E+02	.1243056E+03	.6056929E+03	-.1534141E+04	-.4615316E+04
322			-.7411780E-02	.2758337E+00	-.2984030E+01
323			-.2864131E+01	-.2648726E+02	.2935139E+02
324	.2999432E+02	-.1197862E+03	-.1886059E+03	.6165932E+03	-.3381954E+03
325			.7411780E-02	-.1453286E+00	.1379168E+00
326			.7411780E-02	-.1453286E+00	.1379168E+00
327			-.2864131E+01	-.2648726E+02	.2935139E+02
			\mathcal{N}		
			\mathcal{N}		
493		-.1798684E+03	.4305188E+03	-.2277636E+03	-.8935366E+03
494		.8331849E+02	-.2608640E+03	.2717725E+03	-.9422699E+02
495		.8331849E+02	-.2608640E+03	.2717725E+03	-.9422699E+02
496			.1666370E+03	-.3332740E+03	.1666370E+03
498				-.2274438E-01	.2274438E-01
499				-.2274438E-01	.2274438E-01
			\mathcal{N}		
			\mathcal{N}		
741	.3286920E-31	-.6573841E-31	-.2380925E+01	.2380925E+01	.0000000E+00
743				.3853975E+01	-.8927045E+01
749		.6445007E+00	.4734479E+00	.1060865E+01	-.2457305E+01
755				.2853713E+00	-.2853713E+00
758				-.4247529E+01	.4261065E+02
764		.6615728E+01	-.2526752E+02	-.7116714E+01	.7139393E+02
			\mathcal{N}		
			\mathcal{N}		
923				-.1479291E+01	-.1127685E+02
924				-.8424135E+00	.4331788E+03
<hr/>					
Results for $\sum_g d\sigma_g$					
$\tilde{\alpha} = 0$			928.43820021286338928513117418831577		(input)
$\tilde{\alpha} = 1$			928.43820021286338928513117432490231		(input)
$\tilde{\alpha} = -1$			928.43820021286338928513117410983989		(input)
$\tilde{\alpha} = 2$			928.43820021286338928513117455347002		(input)
$\tilde{\alpha} = -2$			928.43820021286338928513117411023117		(input)
$\tilde{\alpha} = 5$			928.43820021286338928513117695043335		(derived)

one needs to prepare new libraries for handling (very) high rank tensor integrals that are not necessary in the Feynman gauges.

6.3 Inclusion of hard bremsstrahlung, k_c stability

A complete $\mathcal{O}(\alpha)$ correction necessitates the inclusion of the contribution from hard photon bremsstrahlung. Although this is a tree-level process, in most cases the total cross section can not be derived analytically. There is no difficulty in computing the matrix elements. In **GRACE** this is done automatically keeping all particle masses. The integration over phase space can get tricky in many cases. In fact in most cases of interest like for e^+e^- processes some care must be exercised. The reason is that though there is no infrared problem one still needs to very carefully control the k_c dependence and also the collinear mass singularity. This k_c dependence when combined with the one in the soft bremsstrahlung part (based on a analytical implementation), see section 6.1.2, should cancel leaving no dependence on the cut-off k_c . This would constitute another test on the $\mathcal{O}(\alpha)$ calculation of **GRACE-loop**.

The collinear mass singularity is most acute when the mass of the charged particle is very small compared to the typical energy scale of the problem, as in e^+e^- at high energies. All these problems are due to the integration over the propagators encountered in Eq. 6.2. For example, take the emission from the positron with momentum, p . This propagator is defined from

$$k.p = E_\gamma(E - P \cos \theta_\gamma) = E_\gamma P \left[\frac{m_e^2}{P(E + P)} + (1 - \cos \theta_\gamma) \right] \quad (6.11)$$

This becomes extremely peaked in the forward direction, $\cos \theta_\gamma = 1$. For instance, while the term in square bracket is of order one for $\cos \theta_\gamma = -1$ it is of order $\sim 10^{-13}$ for linear collider energies of 500GeV. In **GRACE**, integration is done with **BASES**[19] which is an adaptive Monte-Carlo program. For these particular cases one adapts the integration variables so that one fully picks up the singularities brought about by the hard photon collinear mass singularities. This step is therefore not as automatic as the previous ones in the calculation of the radiative corrections since one needs to judiciously choose the integration variables. For more details see[30].

Stability of the result as concerns the cut-off k_c is tested by varying the value of the cut-off k_c . One finds agreement within the precision of the Monte-Carlo which is at least better than 4 digits.

In e^+e^- processes where corrections from initial state radiation can be large it is possible to sum up the effect of multiple emission of photons, either through a structure function approach (see for instance [30]) or more sophisticated approaches that even takes into account the p_T of the photon like that of the **QEDPS** approach[35].

7 Checks on selected cross sections

The previous sections have shown that the system passes highly non trivial checks for the calculation of the one-loop radiative corrections to standard model processes. All those tests are *internal* tests within the system. To further establish the reliability of the system we have also performed comparisons with a number of one-loop electroweak calculations that have appeared in the literature. For all the comparisons we tune our input parameters to those given by the authors. Therefore one should remember that some of the results in the following tables are outdated due to the use of by now obsolete input parameters. All results refer to integrated cross sections with, in some cases, cuts on the scattering angle so as to avoid singularities in the forward direction. Apart from $e^+e^- \rightarrow t\bar{t}$ where a complete fully tuned comparison was conducted with high precision and includes the effect of hard photon radiation at $\mathcal{O}(\alpha)$, we compare the results of the virtual electroweak and soft photon bremsstrahlung ($V+S$), taking the same cut-off, k_c , on the soft photon as specified in those references. We note in passing that since the **GRACE** system is adapted to multi-particle production, we can, contrary to some calculations, treat both the loop corrections and the bremsstrahlung correction within the same system. Let us also note that for all the processes we will consider below, we have taken the widths of all particles to zero since we never hit a pole.

7.1 $e^+e^- \rightarrow t\bar{t}$

Table 3: *Comparison of the total cross section $e^+e^- \rightarrow t\bar{t}$ between **GRACE**-loop and [36]. The corrections refer to the full one-loop electroweak corrections including hard photon radiation.*

$e^+e^- \rightarrow t\bar{t}$	GRACE-loop	[36]
$\sqrt{s} = 500\text{GeV}$		
tree-level(in pb)	0.5122751	0.5122744
$\mathcal{O}(\alpha)$ (in pb)	0.526371	0.526337
δ (in %)	2.75163	2.74513
$\sqrt{s} = 1\text{TeV}$		
tree-level(in pb)	0.1559187	0.1559185
$\mathcal{O}(\alpha)$ (in pb)	0.171931	0.171916
δ (in %)	10.2696	10.2602

This process is an extension of the 2-fermion production program that has been successfully carried at LEP/SLC. The radiative corrections to this process first appeared in[37]

and then in[38]. A new computation has appeared very recently [36]. A dedicated tuned comparison between **GRACE-loop** and the program **topfit**[36] has recently been conducted at some depth including hard photon radiation and with the active participation of the authors of[36]. Details of the comparison are to be found in [39]. Here we only show the excellent quality of the agreement for the total cross section including hard photons and we refer the reader to [39] for other comparisons concerning differential cross sections and forward-backward asymmetries. Let us point out however that the comparisons at the level of the differential cross sections agree within 8 digits before inclusion of the hard photon correction and to 7 digits when the latter are included. For the totally integrated cross section including hard photons this quality of agreement is somehow degraded but stays nonetheless excellent even at high energies. As Table 3 shows, the agreement is still better than 0.1permil.

The authors of [36] have also conducted a tuned comparison with another independent calculation based on[38]. Practically similar conclusions to the ones presented here are reached, see[40].

7.2 $e^+e^- \rightarrow W^+W^-$

Table 4: *Comparison of the total cross section $e^+e^- \rightarrow W^+W^-$ between **GRACE-loop** and [41]. The calculation includes full one-loop electroweak corrections, but no hard photon radiation.*

$e^+e^- \rightarrow W^+W^-$	GRACE-loop	[41]
$\sqrt{s} = 190\text{GeV}$ tree-level(in pb) δ (in %)	17.8623 -9.4923	17.863 -9.489
$\sqrt{s} = 500\text{GeV}$ tree-level(in pb) δ (in %)	6.5989 -12.743	6.599 -12.74
$\sqrt{s} = 1\text{TeV}$ tree-level(in pb) δ (in %)	2.4649 -15.379	2.465 -15.375

This process is the most important electroweak process at LEP2 and constitutes one of the most important reactions for the linear collider. A few independent calculations[42] exist and the most recent ones agree better than the per-mil. To check the results given by

GRACE-loop , we have set our parameters to those appearing in Table 2 of the review [41]. The results refer to the total cross section but without the inclusion of the hard photon bremsstrahlung. As we see the agreement for energies ranging from LEP2 to 1TeV are about at least 0.1permil.

7.3 $e^+e^- \rightarrow ZH$

Table 5: *Comparison of percentage correction to the total cross section $e^+e^- \rightarrow ZH$ between **GRACE-loop** and [43].*

$e^+e^- \rightarrow ZH$	GRACE-loop	[43]
$\sqrt{s} = 500\text{GeV}$ $M_H = 100\text{GeV}$	4.15239	4.1524
$\sqrt{s} = 500\text{GeV}$ $M_H = 300\text{GeV}$	6.90166	6.9017
$\sqrt{s} = 1000\text{GeV}$ $M_H = 100\text{GeV}$	-2.16561	-2.1656
$\sqrt{s} = 1000\text{GeV}$ $M_H = 300\text{GeV}$	-2.49949	-2.4995
$\sqrt{s} = 1000\text{GeV}$ $M_H = 800\text{GeV}$	26.10942	26.1094
$\sqrt{s} = 2000\text{GeV}$ $M_H = 100\text{GeV}$	-11.54131	-11.5414
$\sqrt{s} = 2000\text{GeV}$ $M_H = 300\text{GeV}$	-12.82256	-12.8226
$\sqrt{s} = 2000\text{GeV}$ $M_H = 800\text{GeV}$	11.24680	11.2468

This process is an important discovery channel for an intermediate mass Higgs at a moderate energy linear collider and could permit to study the properties of the Higgs. Three independent one-loop calculations exist[23] which all agree beyond the precision of any future linear collider. A comparison was conducted against the first calculation in[23] where one of the authors has provided us with more precise numbers than those appearing in Table 1 of [43]³. Table 5 shows that the results given by our system **GRACE-loop** and

³We thank A. Denner for providing us with the correct M_W masses used in this table. Beside the input given in [43], M_W is crucial for a precise comparison. The following M_W masses have been used: $M_W = 80.231815\text{GeV}$ ($M_H = 100\text{GeV}$), $M_W = 80.159313\text{GeV}$ ($M_H = 300\text{GeV}$), $M_W = 80.081409\text{GeV}$ ($M_H = 800\text{GeV}$).

those of [43] agree on all digits. This means that the radiatively corrected cross sections at different energies for a Higgs mass ranging from the light to the heavy agree within at least 6 digits. The corrections refer to the full one-loop electroweak corrections but without hard photon radiation.

7.4 $\gamma\gamma \rightarrow t\bar{t}$

Table 6: *Comparison of the total cross section $\gamma\gamma \rightarrow t\bar{t}$ between GRACE-loop and [44] include full one-loop electroweak corrections at one-loop, but no hard (final) photon radiation.*

$\gamma\gamma \rightarrow t\bar{t}$	GRACE-loop	[44]
$\sqrt{s} = 350\text{GeV}$ tree-level (in pb) δ (in %)	0.332477 −6.889	0.33248 −6.88
$\sqrt{s} = 500\text{GeV}$ tree-level (in pb) δ (in %)	0.904371 −4.824	0.90439 −4.82
$\sqrt{s}=1\text{TeV}$ tree-level (in pb) δ (in %)	0.434459 −5.633	0.43447 −5.63

The comparison has been made with Table 1 of [44] without any convolution over any photon spectra. $M_H = 150\text{GeV}$ so as to avoid the Higgs resonance. As we see the agreement is very good, it is just limited by the precision of the numbers provided in [44].

7.5 $\gamma\gamma \rightarrow W^+W^-$

The first complete calculation of the electroweak radiative corrections to $\gamma\gamma \rightarrow W^+W^-$ has been performed in [45]. Jikia has performed a full $\mathcal{O}(\alpha)$ calculation, including hard photon radiation [46]. Comparison has been made on the one hand with Table 1 of [45] without convolution over any photon spectra as well as with Table 2 of [46]. In both comparisons we considered the total integrated cross section but with no inclusion of the hard photon radiation which in any case is not treated in [45]. Because the fermionic contribution is extremely small compared to the bosonic contribution in the radiative correction to the

Table 7: Comparison for $\gamma\gamma \rightarrow W^+W^-$ between GRACE-loop and [45] and GRACE-loop and [46]. No hard (final) photon radiation is included. When not stated the cross sections and corrections refer to the total cross section with no angular cut.

$\gamma\gamma \rightarrow W^+W^-, M_W = 80.36\text{GeV} M_H = 300\text{GeV}$	GRACE-loop	[46]
$\sqrt{s} = 500\text{GeV}$ tree-level(in pb) δ (in %)	77.497 -10.06	77.50 -10.1
$\sqrt{s} = 1\text{TeV}$ tree-level(in pb) δ (in %)	79.995 -18.73	79.99 -18.7
$\sqrt{s} = 2\text{TeV}$ tree-level(in pb) δ (in %)	80.531 -27.25	80.53 -27.2
$\sqrt{s} = 2\text{TeV} 60^\circ < \theta < 120^\circ$ tree-level(in pb) δ (in %)	0.39356 -75.6827	0.3936 -75.6
$M_W = 80.333\text{GeV} M_H = 250\text{GeV}$	GRACE-loop	[45]
$\sqrt{s} = 500\text{GeV}$ tree-level(in pb) δ (in %)	77.552 -3.376	77.55 -3.38
$\sqrt{s} = 1\text{TeV}$ tree-level(in pb) δ (in %)	80.049 -7.087	80.05 -7.08

total cross section, we also looked at the correction with an angular cut on the outgoing W as check on the fermionic correction. As can be seen from Table 7 the agreement is just limited by the precision of the numbers provided in [45] and [46]. Note that in [46], the correction is split between the bosonic corrections and the fermionic corrections. When considering the total cross section the latter are much too small and are below the precision with which the bosonic corrections are displayed in [46]. Therefore given the precision of the data in [46] the corrections are essentially given by the bosonic part for the total cross section. For the entry with the angular cut, the fermionic corrections are not negligible.

7.6 $e\gamma \rightarrow W\nu_e$

Table 8: *Comparison of the total cross section $e\gamma \rightarrow W\nu_e$ between GRACE-loop and [47]*

$e\gamma \rightarrow W\nu_e$	GRACE-loop	[47]
$\sqrt{s} = 500\text{GeV}$ tree-level(in pb) δ (in %)	36.5873 -12.2803	36.587 -12.281
$\sqrt{s} = 2\text{TeV}$ tree-level(in pb) δ (in %)	43.9368 -19.0917	43.937 -19.092

The comparison shown in Table. 8 is made on the total cross section ($0^\circ \leq \theta \leq 180^\circ$) based on Table 5.1 of [47]. No convolution on the photon spectra is applied nor is the hard photon bremsstrahlung included. The agreement is rather excellent.

7.7 $e\gamma \rightarrow eZ$

The comparison shown in Table. 9 is made with Table 5.3 of [48]. No convolution on the photon spectra is applied nor is the hard photon bremsstrahlung included. The agreement is excellent.

7.8 $W^+W^- \rightarrow W^-W^+$

This is one of the most difficult $2 \rightarrow 2$ processes in the \mathcal{SM} ever to be calculated. As discussed previously the number of diagrams at one-loop is of the order 1000. Moreover

Table 9: *Comparison of the total cross section $e\gamma \rightarrow eZ$ between GRACE-loop and [48].*

$e\gamma \rightarrow eZ$	GRACE-loop	[48]
$\sqrt{s} = 500\text{GeV}$, tree-level(in pb) δ (in %)	0.70515 -25.689	0.7051 -25.69
$\sqrt{s} = 500\text{GeV}$, $1^\circ \leq \theta \leq 179^\circ$ tree-level(in pb) δ (in %)	1.7696 -22.313	1.770 -22.31
$\sqrt{s} = 2\text{TeV}$, $20^\circ \leq \theta \leq 160^\circ$ tree-level(in pb) δ (in %)	0.046201 -39.529	0.04620 -39.53
$\sqrt{s} = 2\text{TeV}$, $1^\circ \leq \theta \leq 179^\circ$ tree-level(in pb) δ (in %)	0.1170 -30.845	0.117 -30.84

very subtle gauge cancellations take place especially as the energy of the participating W 's increases. The most complete calculation has been performed in [49] and the code is freely available at www.hep-processes.de. However, hard photon radiation is not included. Following [49] we have compared our results with those of the code by requiring a cut on the forward-backward direction such that integration over the scattering angle is over $10^\circ \leq \theta \leq 170^\circ$. Moreover we have considered two cuts on the photon energy (for the bremsstrahlung part), $k_c = .05\sqrt{s}$ and $k_c = .5\sqrt{s}$. The Higgs in this comparison is light, see [49] for a justification on this issue. Having at our disposal the code, a tuned comparison could be performed. We can see from Table 10 that at centre of mass energy of the W pair of 2TeV one reaches agreement over 6 digits, 4-5 digits for $\sqrt{s} = 5\text{TeV}$ but “only” 3 digits agreement for $\sqrt{s} = 10\text{TeV}$. Note that even in this case this means that the radiative corrections are known to about 0.1permil. This very high energy for the WW would probably never be reached. Moreover as the authors of[49] warn, for this kind of energy an integration in quadruple precision is probably already mandatory. Therefore it is fair to conclude that one has for this reaction an excellent agreement. Note that GRACE-loop automatic calculation is the first confirmation of the result of [49].

Table 10: *Comparison of the total (unpolarised) cross section $W^+W^- \rightarrow W^-W^+$ between GRACE-loop and [49]. $M_H = 100\text{GeV}$. For the cuts see the text.*

$W^+W^- \rightarrow W^-W^+$	GRACE-loop	[49]
$k_c = .05\sqrt{s}$		
$\sqrt{s} = 2\text{TeV}$		
tree-level(in pb)	77.17067	77.17067
δ (in %)	-21.0135	-21.0135
$\sqrt{s} = 5\text{TeV}$		
tree-level(in pb)	14.2443	14.2443
δ (in %)	-57.1567	-57.1556
$\sqrt{s} = 10\text{TeV}$		
tree-level(in pb)	3.644573	3.644573
δ (in %)	-93.9942	-94.0272
$k_c = .5\sqrt{s}$		
$\sqrt{s} = 2\text{TeV}$		
tree-level(in pb)	77.17067	77.17067
δ (in %)	-17.23988	-17.23989
$\sqrt{s} = 5\text{TeV}$		
tree-level(in pb)	14.24434	14.24434
δ (in %)	-49.9736	-49.9724
$\sqrt{s} = 10\text{TeV}$		
tree-level(in pb)	3.644574	3.644573
δ (in %)	-83.9247	-83.9577

8 Conclusions

We have given a detailed implementation of the non-linear gauge in **GRACE-loop** , the electroweak one-loop extension of **GRACE** for the calculation of one-loop processes in the \mathcal{SM} . These gauges are ideally suited for a numerical implementation of loop calculations and checks on these computations. The non-linear gauge that we exploit introduces 5 gauge parameters. This gauge fixing modifies a large number of vertices in the bosonic sector but can be chosen so as to leave the propagators of all gauge bosons as simple as in the standard linear 't Hooft-Feynman gauge. Technically this means that the structure of any one-loop n -point function is not more involved than what it is with fermionic loops and therefore that many libraries for these functions need not be extended. We have extensively described the quantisation as well as the renormalisation in this type of gauges. We have given a complete list of all Feynman rules including the inclusion of counter-terms and have given an exhaustive set of all the self-energy corrections. We have also described how the system handles the loop integration. Moreover, we believe the system to be unique, in that it handles in the same environment the effect of photon radiation since the system is well adapted to multi-particle production. Hard photon radiation is therefore part of the system and can be separated from the rest of the calculation through the imposition of an energy cut-off on the additional photon. A very thorough check of the finiteness, both infrared and ultraviolet, and the gauge parameter independence of the results pertaining to some 26 processes for $2 \rightarrow 2$ reactions have been performed. These checks are verified with a precision that attains at least 20 digits. We have also used the new system to carry further comparison on radiative corrections to a few processes that have appeared in the literature. This selection includes heavy fermion production, vector boson and Higgs boson production in both e^+e^- , $\gamma\gamma$ and $e\gamma$ machines as well as the very challenging WW scattering process. For the latter we provide the first check to the complete calculation that has appeared in the literature. In all cases we find excellent agreement. This shows that the automatic system of calculating radiative corrections numerically has now all the ingredients to perform all $2 \rightarrow 2$ processes confidently. Note that the system already successfully tackled the calculation of many body final states which means that the phase space integration should not pose undue difficulties. We have exploited this feature to calculate[1, 2] the full $\mathcal{O}(\alpha)$ corrections to the important process $e^+e^- \rightarrow \nu_e \bar{\nu}_e H$ which is the dominant Higgs production mechanism at the next linear collider. This computation constitutes the first full calculation of such $2 \rightarrow 3$ process in the electroweak theory and opens the way to further applications. We recently have also performed a full order $\mathcal{O}(\alpha)$ calculation of $e^+e^- \rightarrow t\bar{t}H$ [11]. These $2 \rightarrow 3$ process have now been confirmed by an independent calculation[3, 50]

To improve the efficiency of the system for applications to one-loop corrections for processes with more than 2 particles in the final state, one should seek a derivation based on helicity amplitudes. At tree-level this has been nicely implemented in **GRACE** and applied to processes up to 6 particles in the final state. Moreover a derivation based on

helicity amplitudes allows the implementation of full spin-correlation, for processes when the final particle is unstable. At the one-loop level, another advantage is that it would allow the calculation by the system of processes that are not generated at tree-level, such as $\gamma\gamma \rightarrow \gamma\gamma$, $\gamma\gamma \rightarrow ZZ$, $Z \rightarrow 3\gamma$, $H \rightarrow \gamma\gamma$. The working version of **GRACE-loop** can not handle such processes since the one-loop correction are calculated as products of tree-level and one-loop matrix elements. A version of **GRACE-loop** which is being developed is based on helicity amplitudes. Preliminary results are encouraging. This new version will also be used as an additional test on the results given by the traditional method of squaring matrix elements.

Acknowledgment

This work is part of a collaboration between the **GRACE** project in the Minami-Tateya group and LAPTH. D. Perret-Gallix and Y. Kurihara deserve special thanks for their contribution. We also thank M. Kuroda for reading part of the manuscript. This work was supported in part by Japan Society for Promotion of Science under the Grant-in-Aid for scientific Research B(N°. 14340081) and PICS 397 of the French National Centre for Scientific Research.

Appendices

A Specific form of the BRS transformations

The action of the BRS transformations is derived as a generalisation of the usual gauge transformations. The ghost fields corresponding to the four gauge bosons write in terms of the ghosts of the $SU(2) \times U(1)$ fields as:

$$\begin{aligned} c^\pm &= \frac{1}{\sqrt{2}}(c^1 \mp i c^2) \\ c^A &= s_W c^3 + c_W c^B \\ c^Z &= c_W c^3 - s_W c^B . \end{aligned} \quad (\text{A.1})$$

One obtains

$$\begin{aligned} \delta_{\text{BRS}} W_\mu^\pm &= \partial_\mu c^\pm \mp ie \left[\left((A_\mu + \frac{c_W}{s_W} Z_\mu) c^\pm - \left(c^A + \frac{c_W}{s_W} c^Z \right) W_\mu^\pm \right) \right] \\ \delta_{\text{BRS}} Z_\mu &= \partial_\mu c^Z - ig c_W \left(W_\mu^+ c^- - W_\mu^- c^+ \right) \\ \delta_{\text{BRS}} A_\mu &= \partial_\mu c^A - ie \left(W_\mu^+ c^- - W_\mu^- c^+ \right) . \end{aligned} \quad (\text{A.2})$$

Likewise by considering the gauge transformation on the Higgs doublet one gets

$$\begin{aligned} \delta_{\text{BRS}} H &= -\frac{g}{2} (c^- \chi^+ + c^+ \chi^-) - \frac{e}{2s_W c_W} c^Z \chi_3 , \\ \delta_{\text{BRS}} \chi_3 &= -\frac{ig}{2} (-c^+ \chi^- + c^- \chi^+) + \frac{e}{2s_W c_W} c^Z (v + H) , \\ \delta_{\text{BRS}} \chi^\pm &= \frac{g}{2} (v + H \mp i \chi_3) c^\pm \pm ie \chi^\pm \left(c^A + \frac{c_W^2 - s_W^2}{2s_W c_W} c^Z \right) . \end{aligned} \quad (\text{A.3})$$

To find the transformation for the ghost fields, notice that the BRS transformation is nilpotent. For instance from $(\delta_{\text{BRS}})^2 W_\mu^i = 0$ one gets $\delta_{\text{BRS}} c^i$. Indeed more generally one has, for any group,

$$\delta_{\text{BRS}} A_\mu^i = D_\mu c^i = \partial_\mu c^i + g[A_\mu, c]^i \rightarrow \delta_{\text{BRS}} c^i = -g \frac{1}{2} [c, c]^i \quad (\text{A.4})$$

Care should be taken that δ_{BRS} being a fermion operator the graded Leibnitz rule applies: $\delta_{\text{BRS}}(XY) = (\delta_{\text{BRS}} X)Y \pm X(\delta_{\text{BRS}} Y)$ where the minus sign applies if X has an odd number of ghosts or antighosts, note also that $(c^i)^2 = 0$.

In our case this implies

$$\delta_{\text{BRS}} c^B = 0 \quad \delta_{\text{BRS}} c^i = -\frac{1}{2} g \epsilon_{ijk} c^j c^k \quad (\text{A.5})$$

and thus

$$\begin{aligned}
 \delta_{\text{BRS}} c^\pm &= \mp i g c^\pm (s_W c^A + c_W c^Z) \\
 \delta_{\text{BRS}} c^A &= +i e c^+ c^- \\
 \delta_{\text{BRS}} c^Z &= +i g c_W c^+ c^- \tag{A.6}
 \end{aligned}$$

The transformation for the anti-ghost field is defined through the auxiliary B field of the gauge functions,

$$\delta_{\text{BRS}} \bar{c}^i = i B^i. \tag{A.7}$$

B Feynman Rules

The basic Feynman rules follow the so-called Kyoto convention[21]. A particle at the endpoint *enters* the vertex. For instance, if a line is denoted as W^+ , then the line shows either the incoming W^+ or the outgoing W^- . The momentum assigned to a particle is defined as *inward* except for the case of a ghost particle for which the momentum is defined *along the flow of its ghost number*, as will be shown in the figures.

B.1 Propagators

W^\pm	$\frac{1}{k^2 - M_W^2} \left(g_{\mu\nu} - (1 - \xi_W) \frac{k_\mu k_\nu}{k^2 - \xi_W M_W^2} \right)$
Z	$\frac{1}{k^2 - M_Z^2} \left(g_{\mu\nu} - (1 - \xi_Z) \frac{k_\mu k_\nu}{k^2 - \xi_Z M_Z^2} \right)$
A	$\frac{1}{k^2} \left(g_{\mu\nu} - (1 - \xi_A) \frac{k_\mu k_\nu}{k^2} \right)$
f	$\frac{-1}{k - m_f}$
H	$\frac{-1}{k^2 - M_H^2}$
χ^\pm	$\frac{-1}{k^2 - \xi_W M_W^2}$
χ_3	$\frac{-1}{k^2 - \xi_Z M_Z^2}$
c^\pm	$\frac{-1}{k^2 - \xi_W M_W^2}$
c^Z	$\frac{-1}{k^2 - \xi_Z M_Z^2}$
c^A	$\frac{-1}{k^2}$

B.2 Vector-Vector-Vector

p_1, μ	p_2, ν	p_3, ρ	
			$W^- \quad W^+ \quad A \quad e \left[g^{\mu\nu} (p_1 - p_2)^\rho + (1 + \tilde{\alpha}/\xi_W) (p_3^\nu g^{\mu\rho} - p_3^\mu g^{\nu\rho}) + (1 - \tilde{\alpha}/\xi_W) (p_2^\mu g^{\nu\rho} - p_1^\nu g^{\mu\rho}) \right]$
			$W^- \quad W^+ \quad Z \quad e \frac{c_W}{s_W} \left[g^{\mu\nu} (p_1 - p_2)^\rho + (1 + \tilde{\beta}/\xi_W) (p_3^\nu g^{\mu\rho} - p_3^\mu g^{\nu\rho}) + (1 - \tilde{\beta}/\xi_W) (p_2^\mu g^{\nu\rho} - p_1^\nu g^{\mu\rho}) \right]$

B.3 Vector-Vector-Scalar

$p_1 (\mu)$	$p_2 (\nu)$	p_3	
W^\pm	A	χ^\mp	$\mp ieM_W(1 - \tilde{\alpha})g^{\mu\nu}$
W^\pm	Z	χ^\mp	$\pm ie\frac{1}{s_W c_W}M_W(1 - c_W^2(1 - \tilde{\beta}))g^{\mu\nu}$
W^-	W^+	H	$e\frac{1}{s_W}M_W g^{\mu\nu}$
Z	Z	H	$e\frac{1}{s_W c_W^2}M_W g^{\mu\nu}$

B.4 Scalar-Scalar-Vector

p_1	p_2	$p_3 (\mu)$	
H	χ^\mp	W^\pm	$ie\frac{1}{2s_W}[(1 - \tilde{\delta})p_2^\mu - (1 + \tilde{\delta})p_1^\mu]$
χ_3	χ^\mp	W^\pm	$\pm e\frac{1}{2s_W}[(1 - \tilde{\kappa})p_2^\mu - (1 + \tilde{\kappa})p_1^\mu]$
χ^-	χ^+	A	$e(p_2 - p_1)^\mu$
χ^-	χ^+	Z	$e\frac{c_W^2 - s_W^2}{2s_W c_W}(p_2 - p_1)^\mu$
H	χ_3	Z	$ie\frac{1}{2s_W c_W}[(1 - \tilde{\varepsilon})p_2^\mu - (1 + \tilde{\varepsilon})p_1^\mu]$

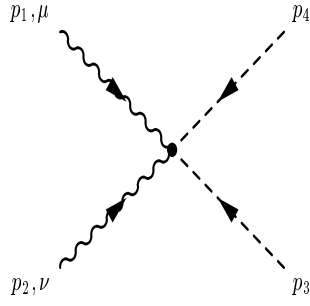
B.5 Scalar-Scalar-Scalar

p_1	p_2	p_3	
			$H \quad H \quad H \quad -e \frac{3}{2s_W M_W} M_H^2$
p_1		p_3	
p_2			$H \quad \chi^- \quad \chi^+ \quad -e \frac{1}{2s_W M_W} (M_H^2 + 2\tilde{\delta} M_W^2 \cdot \xi_W)$
			$H \quad \chi_3 \quad \chi_3 \quad -e \frac{1}{2s_W M_W} (M_H^2 + 2\tilde{\varepsilon} M_Z^2 \cdot \xi_Z)$

B.6 Vector-Vector-Vector-Vector

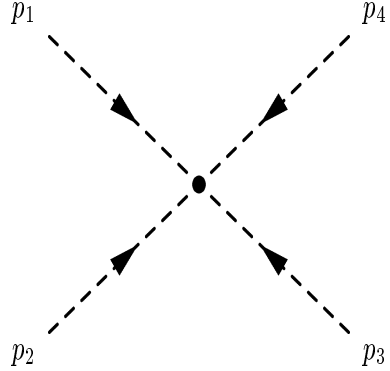
$p_1 \ (\mu)$	$p_2 \ (\nu)$	$p_3 \ (\rho)$	$p_4 \ (\sigma)$
W^+	W^-	A	A
p_1, μ	p_2, ν	p_3, ρ	p_4, σ
W^+	W^-	A	Z
$e^2 \frac{c_W}{s_W} [-2g^{\mu\nu}g^{\rho\sigma} + (1 - \tilde{\alpha}^2/\xi_W)(g^{\mu\rho}g^{\nu\sigma} + g^{\mu\sigma}g^{\nu\rho})]$			
W^+	W^-	Z	Z
p_1, μ	p_2, ν	p_3, ρ	p_4, σ
W^+	W^-	Z	Z
$e^2 \frac{c_W^2}{s_W^2} [-2g^{\mu\nu}g^{\rho\sigma} + (1 - \tilde{\alpha}\tilde{\beta}/\xi_W)(g^{\mu\rho}g^{\nu\sigma} + g^{\mu\sigma}g^{\nu\rho})]$			
W^+	W^-	W^-	W^+
p_1, μ	p_2, ν	p_3, ρ	p_4, σ
W^+	W^-	W^-	W^+
$e^2 \frac{c_W^2}{s_W^2} [-2g^{\mu\nu}g^{\rho\sigma} + (1 - \tilde{\beta}^2/\xi_W)(g^{\mu\rho}g^{\nu\sigma} + g^{\mu\sigma}g^{\nu\rho})]$			
W^+	W^-	W^-	W^+
p_1, μ	p_2, ν	p_3, ρ	p_4, σ
W^+	W^-	W^-	W^+
$-e^2 \frac{1}{s_W^2} [-2g^{\mu\sigma}g^{\nu\rho} + (g^{\mu\rho}g^{\nu\sigma} + g^{\mu\nu}g^{\rho\sigma})]$			

B.7 Vector-Vector-Scalar-Scalar



p_1	(μ)	p_2	(ν)	p_3	p_4	
A		W^\pm		H	χ^\mp	$\mp ie^2 \frac{1}{2s_W} (1 - \tilde{\alpha}\tilde{\delta}) g^{\mu\nu}$
A		W^\pm		χ_3	χ^\mp	$-e^2 \frac{1}{2s_W} (1 - \tilde{\alpha}\tilde{\kappa}) g^{\mu\nu}$
Z		W^\pm		H	χ^\mp	$\pm ie^2 \frac{1}{2s_W^2 c_W} (1 - c_W^2 (1 - \tilde{\beta}\tilde{\delta})) g^{\mu\nu}$
Z		W^\pm		χ_3	χ^\mp	$e^2 \frac{1}{2s_W^2 c_W} (1 - c_W^2 (1 - \tilde{\beta}\tilde{\kappa})) g^{\mu\nu}$
A		A		χ^+	χ^-	$2e^2 g^{\mu\nu}$
Z		A		χ^+	χ^-	$2e^2 \frac{c_W^2 - s_W^2}{2s_W c_W} g^{\mu\nu}$
Z		Z		χ^+	χ^-	$2e^2 \left(\frac{c_W^2 - s_W^2}{2s_W c_W} \right)^2 g^{\mu\nu}$
W^+		W^-		H	H	$e^2 \frac{1}{2s_W^2} g^{\mu\nu}$
W^+		W^-		χ_3	χ_3	$e^2 \frac{1}{2s_W^2} g^{\mu\nu}$
W^+		W^-		χ^-	χ^+	$e^2 \frac{1}{2s_W^2} g^{\mu\nu}$
Z		Z		H	H	$e^2 \frac{1}{2s_W^2 c_W^2} g^{\mu\nu}$
Z		Z		χ_3	χ_3	$e^2 \frac{1}{2s_W^2 c_W^2} g^{\mu\nu}$

B.8 Scalar-Scalar-Scalar-Scalar

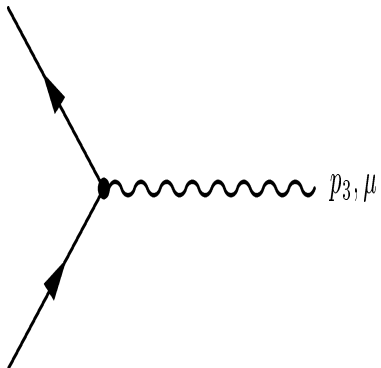


p_1	p_2	p_3	p_4	
H	H	H	H	$-e^2 \frac{3M_H^2}{4s_W^2 M_W^2}$
χ_3	χ_3	χ_3	χ_3	$-e^2 \frac{3M_H^2}{4s_W^2 M_W^2}$
χ^\pm	χ^\mp	χ^\mp	χ^\pm	$-e^2 \frac{M_H^2}{2s_W^2 M_W^2}$
H	H	χ_3	χ_3	$-e^2 \frac{M_H^2 + 2\tilde{\varepsilon}^2 M_Z^2 \cdot \xi_Z}{4s_W^2 M_W^2}$
H	H	χ^+	χ^-	$-e^2 \frac{M_H^2 + 2\tilde{\delta}^2 M_W^2 \cdot \xi_W}{4s_W^2 M_W^2}$
χ^+	χ^-	χ_3	χ_3	$-e^2 \frac{M_H^2 + 2\tilde{\kappa}^2 M_W^2 \cdot \xi_W}{4s_W^2 M_W^2}$

B.9 Fermion-Fermion-Vector

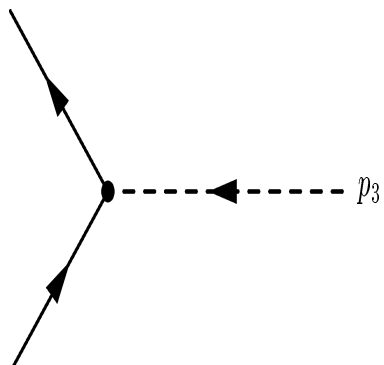
Fermion mixing is not shown here. Colour for quarks is also not explicit and should be taken into account when appropriate.

f		I_3	Q_f		I_3	Q_f
U	u, c, t	$\frac{1}{2}$	$\frac{2}{3}$	ν_e, ν_μ, ν_τ	$\frac{1}{2}$	0
D	d, s, b	$-\frac{1}{2}$	$-\frac{1}{3}$	e, μ, τ	$-\frac{1}{2}$	-1



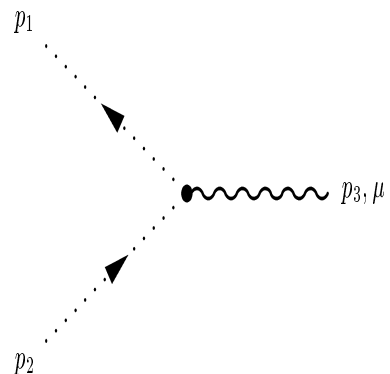
p_1	p_2	$p_3 (\mu)$	
\bar{f}	f	A	$eQ_f \gamma^\mu$
\bar{f}	f	Z	$e \frac{1}{2s_W c_W} \gamma^\mu (I_3(1 - \gamma_5) - 2s_W^2 Q_f)$
\bar{U}/\bar{D}	D/U	W^+/W^-	$e \frac{1}{2\sqrt{2}s_W} \gamma^\mu (1 - \gamma_5)$

B.10 Fermion-Fermion-Scalar



p_1	p_2	p_3	
\bar{f}	f	H	$-e \frac{1}{2s_W} \frac{m_f}{M_W}$
\bar{U}/\bar{D}	U/D	χ_3	$(-/+)(-/-)ie \frac{1}{2s_W} \frac{m_f}{M_W} \gamma_5$
\bar{U}	D	χ^+	$-ie \frac{1}{2\sqrt{2}s_W} \frac{1}{M_W} [(m_D - m_U) + (m_D + m_U)\gamma_5]$
\bar{D}	U	χ^-	$-ie \frac{1}{2\sqrt{2}s_W} \frac{1}{M_W} [(m_U - m_D) + (m_U + m_D)\gamma_5]$

B.11 Ghost-Ghost-Vector

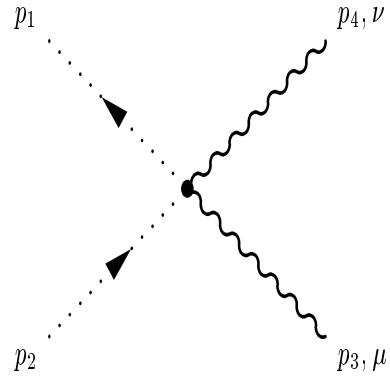


p_1	p_2	p_3 (μ)	
\bar{c}^A	c^\mp	W^\pm	$\pm e p_1^\mu$
\bar{c}^Z	c^\mp	W^\pm	$\pm e \frac{c_W}{s_W} p_1^\mu$
\bar{c}^\mp	c^A	W^\pm	$\mp e(p_1^\mu - \tilde{\alpha} p_2^\mu)$
\bar{c}^\mp	c^Z	W^\pm	$\mp e \frac{c_W}{s_W} (p_1^\mu - \tilde{\beta} p_2^\mu)$
\bar{c}^\mp	c^\pm	A	$\pm e(p_1^\mu + \tilde{\alpha} p_2^\mu)$
\bar{c}^\mp	c^\pm	Z	$\pm e \frac{c_W}{s_W} (p_1^\mu + \tilde{\beta} p_2^\mu)$

B.12 Ghost-Ghost-Scalar

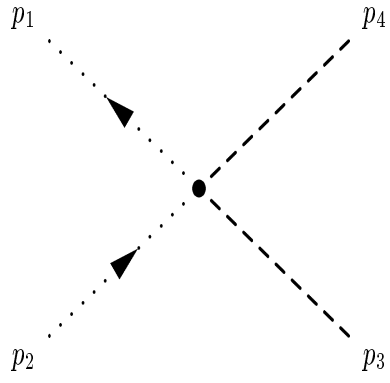
p_1	p_2	p_3	
\bar{c}^Z	c^Z	H	$-e \frac{1}{2s_W c_W^2} (1 + \tilde{\varepsilon}) M_W \cdot \xi_Z$
\bar{c}^Z	c^\mp	χ^\pm	$\pm ie \frac{1}{2s_W c_W} M_W \cdot \xi_Z$
\bar{c}^\mp	c^A	χ^\pm	$\mp ie M_W \cdot \xi_W$
\bar{c}^\mp	c^Z	χ^\pm	$\mp ie \frac{1}{2s_W c_W} (c_W^2 - s_W^2 + \tilde{\kappa}) M_W \cdot \xi_W$
\bar{c}^\mp	c^\pm	H	$-e \frac{1}{2s_W} (1 + \tilde{\delta}) M_W \cdot \xi_W$
\bar{c}^\mp	c^\pm	χ_3	$\pm ie \frac{1}{2s_W} (1 - \tilde{\kappa}) M_W \cdot \xi_W$

B.13 Ghost-Ghost-Vector-Vector



p_1	p_2	$p_3 (\mu)$	$p_4 (\nu)$	
\bar{c}^\mp	c^A	A	W^\pm	$-e^2 \tilde{\alpha} g^{\mu\nu}$
\bar{c}^\mp	c^A	Z	W^\pm	$-e^2 \frac{c_W}{s_W} \tilde{\beta} g^{\mu\nu}$
\bar{c}^\mp	c^Z	A	W^\pm	$-e^2 \frac{c_W}{s_W} \tilde{\alpha} g^{\mu\nu}$
\bar{c}^\mp	c^Z	Z	W^\pm	$-e^2 \frac{c_W^2}{s_W^2} \tilde{\beta} g^{\mu\nu}$
\bar{c}^\mp	c^\pm	W^\mp	W^\pm	$-e^2 \left(\tilde{\alpha} + \frac{c_W^2}{s_W^2} \tilde{\beta} \right) g^{\mu\nu}$
\bar{c}^\mp	c^\mp	W^\pm	W^\pm	$2e^2 \left(\tilde{\alpha} + \frac{c_W^2}{s_W^2} \tilde{\beta} \right) g^{\mu\nu}$
\bar{c}^\mp	c^\pm	A	A	$2e^2 \tilde{\alpha} g^{\mu\nu}$
\bar{c}^\mp	c^\pm	Z	A	$e^2 \frac{c_W}{s_W} (\tilde{\alpha} + \tilde{\beta}) g^{\mu\nu}$
\bar{c}^\mp	c^\pm	Z	Z	$2e^2 \frac{c_W^2}{s_W^2} \tilde{\beta} g^{\mu\nu}$

B.14 Ghost-Ghost-Scalar-Scalar



p_1	p_2	p_3	(μ)	p_4	(ν)
\bar{c}^Z	c^Z	H	H	$-e^2 \frac{1}{2s_W^2 c_W^2} \tilde{\varepsilon} \cdot \xi_Z$	
\bar{c}^Z	c^Z	χ_3	χ_3	$e^2 \frac{1}{2s_W^2 c_W^2} \tilde{\varepsilon} \cdot \xi_Z$	
\bar{c}^Z	c^\pm	χ^\mp	H	$\mp ie^2 \frac{1}{4s_W^2 c_W} \tilde{\varepsilon} \cdot \xi_Z$	
\bar{c}^Z	c^\pm	χ^\mp	χ_3	$e^2 \frac{1}{4s_W^2 c_W} \tilde{\varepsilon} \cdot \xi_Z$	
\bar{c}^\mp	c^A	χ^\pm	H	$\mp ie^2 \frac{1}{2s_W} \tilde{\delta} \cdot \xi_W$	
\bar{c}^\mp	c^A	χ^\pm	χ_3	$e^2 \frac{1}{2s_W} \tilde{\kappa} \cdot \xi_W$	
\bar{c}^\mp	c^Z	χ^\pm	H	$\mp ie^2 \frac{1}{4s_W^2 c_W} (\tilde{\kappa} + \tilde{\delta}(c_W^2 - s_W^2)) \cdot \xi_W$	
\bar{c}^\mp	c^Z	χ^\pm	χ_3	$e^2 \frac{1}{4s_W^2 c_W} (\tilde{\delta} + \tilde{\kappa}(c_W^2 - s_W^2)) \cdot \xi_W$	
\bar{c}^\mp	c^\pm	H	H	$-e^2 \frac{1}{2s_W^2} \tilde{\delta} \cdot \xi_W$	
\bar{c}^\mp	c^\pm	χ_3	χ_3	$-e^2 \frac{1}{2s_W^2} \tilde{\kappa} \cdot \xi_W$	
\bar{c}^\mp	c^\pm	χ_3	H	$\mp ie^2 \frac{1}{4s_W^2} (\tilde{\kappa} - \tilde{\delta}) \cdot \xi_W$	
\bar{c}^\mp	c^\pm	χ^-	χ^+	$e^2 \frac{1}{4s_W^2} (\tilde{\delta} + \tilde{\kappa}) \cdot \xi_W$	
\bar{c}^\mp	c^\mp	χ^\pm	χ^\pm	$-e^2 \frac{1}{2s_W^2} (\tilde{\kappa} - \tilde{\delta}) \cdot \xi_W$	

C Counterterms in the ghost sector

Since we deal specifically with processes at one-loop, there is no need to dwell on the renormalisation of the ghost sector. We only briefly sketch the procedure without giving explicit formulae for the various counterterms and the renormalisation constants.

There is some freedom for the introduction of renormalisation constants for the ghost fields. We use the following convention.

$$\begin{aligned} \underline{c}^\pm &= \tilde{Z}_3 c^\pm \\ \begin{pmatrix} \underline{c}^Z \\ \underline{c}^A \end{pmatrix} &= \begin{pmatrix} \tilde{Z}_{ZZ} & \tilde{Z}_{ZA} \\ \tilde{Z}_{AZ} & \tilde{Z}_{AA} \end{pmatrix} \begin{pmatrix} c^Z \\ c_A \end{pmatrix} \\ \underline{\bar{c}}^\pm &= \bar{c}^\pm \\ \underline{\bar{c}}^Z &= \bar{c}^Z \\ \underline{\bar{c}}^A &= \bar{c}^A \end{aligned} \tag{C.1}$$

To derive the full counterterm Lagrangian for the ghost we appeal to the auxiliary B -field formulation of the gauge-fixing Lagrangian \mathcal{L}_{GF} , see Eq. 3.17 in section 3.2. As stressed previously \mathcal{L}_{GF} is written in terms of renormalised fields and as such does not induce any counterterm. However the BRS transformation are defined for bare fields. Therefore in order to generate the ghost Lagrangian including counterterms one needs to re-express \mathcal{L}_{GF} in terms of bare fields to first generate \mathcal{L}_{Gh} with bare fields. From there one can then derive the counterterm ghost Lagrangian. One exploits the freedom in the renormalisation of the B -fields so that the combination of the B fields and gauge fields shows no explicit dependence on wave function renormalisation. We therefore define

$$\underline{B}^\pm = \sqrt{Z_W}^{-1} B^\pm, \quad \begin{pmatrix} \underline{B}^Z \\ \underline{B}^A \end{pmatrix} = \begin{pmatrix} \sqrt{Z}_{ZZ} & \sqrt{Z}_{ZA} \\ \sqrt{Z}_{AZ} & \sqrt{Z}_{AA} \end{pmatrix}^{-1} \begin{pmatrix} B^Z \\ B^A \end{pmatrix} \tag{C.2}$$

The relation is just the inverse of that for gauge fields.

Then Eq. 3.17 is

$$\begin{aligned} \mathcal{L}_{GF} = & \underline{B}^+ \partial^\mu \underline{W}_\mu^- + B^+ \xi_W M_W \chi^- + (h.c.) \\ & + \underline{B}^Z \partial^\mu \underline{Z}_\mu + B^Z \xi_Z M_Z \chi_3 + \underline{B}^A \partial \underline{A}_\mu \\ & + \text{non-linear gauge terms}(\tilde{\alpha}, \tilde{\beta}, \tilde{\delta}, \tilde{\epsilon}, \tilde{\kappa}) \\ & + \underline{B}\text{-linear terms.} \end{aligned} \tag{C.3}$$

One then makes the identifications

$$B^+ \xi_W M_W \chi^- = \underline{B}^+ \underline{\xi}_W \underline{M}_W \underline{\chi}^-, \tag{C.4}$$

$$B^Z \xi_Z M_Z \chi_3 = \underline{B}^Z \underline{\xi}_Z \underline{M}_Z \underline{\chi}_3 + \underline{B}^A \underline{\xi}_A \underline{M}_Z \underline{\chi}_3 \tag{C.5}$$

where we defined the renormalisation of the gauge parameters as

$$\begin{aligned}\underline{\xi}_W &= \xi_W (M_W / \underline{M}_W) \sqrt{Z}_W \sqrt{Z}_\chi^{-1} \\ \underline{\xi}_Z &= \xi_Z (M_Z / \underline{M}_Z) \sqrt{Z}_{ZZ} \sqrt{Z}_{\chi_3}^{-1} \\ \underline{\xi}_{ZA} &= \xi_Z (M_Z / \underline{M}_Z) \sqrt{Z}_{ZA} \sqrt{Z}_{\chi_3}^{-1}\end{aligned}\tag{C.6}$$

$\underline{\xi}_{ZA}$ is not an independent parameter but the short-hand notation given by Eq. C.6. Non-linear gauge terms can be transformed in a similar way by the renormalisation of $(\tilde{\alpha}, \tilde{\beta}, \tilde{\delta}, \tilde{\epsilon}, \tilde{\kappa})$. Note that the terms bilinear in the B fields would get extra factors. However this does not affect the renormalisation program since $\delta_{\text{BRS}} B = 0$. This helps define the bare G functions.

We obtain bare G terms by the above equations.

$$\begin{aligned}\underline{G}^\mp &= \partial^\mu \underline{W}_\mu^\mp + \underline{\xi}_W \underline{M}_W \underline{\chi}^\mp + \text{non-linear gauge terms} \\ \underline{G}^Z &= \partial^\mu \underline{Z}_\mu + \underline{\xi}_Z \underline{M}_Z \underline{\chi}_3 + \text{non-linear gauge terms} \\ \underline{G}^A &= \partial^\mu \underline{A}_\mu + \underline{\xi}_{ZA} \underline{M}_Z \underline{\chi}_3 + \text{non-linear gauge terms}\end{aligned}\tag{C.7}$$

Except for G^A , these are the same as those in 3.15 assuming that quantities are bare ones. With these, one defines the bare ghost Lagrangian, that contains extra terms than those obtained at tree-level due to the induced mixing ξ_{ZA} . One then readily obtains the renormalised ghost Lagrangian.

D Auxiliary Fields and Generalised Ward-Takahashi Identities in the unphysical scalar sector

Although the renormalisation of this sector is not essential if one wants to arrive at finite S-matrix elements, the various two-point functions of the Goldstones and the longitudinal gauge bosons as well as their mixing are related.

To easily derive these generalised Ward-Takahashi identities that constrain the different propagators it is very useful to introduce \mathcal{L}_{GF} via the auxiliary fields as done in Eq. 3.17. The Ward-Takahashi identities are particularly easy to derive if one works with the B -fields and considers the BRS transformations on some specific Green's functions (vacuum expectation values of time ordered products). For the two-point function of any two fields ϕ_A and ϕ_B , we use the short-hand notation:

$$\langle \phi_A \phi_B \rangle = \langle 0 | (T\phi_A(x)\phi_B(y)) | 0 \rangle\tag{D.8}$$

For example, take the generic Green's function $\langle \bar{c}^i B^j \rangle$ which in fact is zero (it has a non vanishing ghost number). Subjecting it to a BRS transformation one gets:

$$\begin{aligned} \delta_{\text{BRS}} \langle \bar{c}^i B^j \rangle &= \langle (\delta_{\text{BRS}} \bar{c}^i) B^j \rangle - \langle \bar{c}^i (\delta_{\text{BRS}} B^j) \rangle = i \langle B^i B^j \rangle = 0 \\ \text{or } \langle G^i G^j \rangle &= 0 \end{aligned} \quad (\text{D.9})$$

where in the last part we have used the equation of motion for the B^i 's. The above relation leads directly to a constraint on the two-point functions of the gauge vector boson, the gauge-goldstone mixing and the goldstone two-point functions. One novelty compared to the usual linear gauge is that these identities also involve correlation functions with composite operators. Indeed if we specialise to the ZZ functions, one has with $\xi_Z = 1$

$$\begin{aligned} &\langle G_Z(x) G_Z(y) \rangle = \\ &\langle \left((\partial \cdot Z(x) + M_Z \chi_3(x) + \frac{g}{2c_W} \tilde{\epsilon} H(x) \chi_3(x) \right) \left((\partial \cdot Z(y) + M_Z \chi_3(y) + \frac{g}{2c_W} \tilde{\epsilon} H(y) \chi_3(y) \right) \rangle \\ &= \partial_x^\mu \partial_y^\nu \langle Z_\mu(x) Z_\nu(y) \rangle + 2M_Z \partial_x^\mu \langle Z_\mu(x) \chi_3(y) \rangle + M_Z^2 \langle \chi_3(x) \chi_3(y) \rangle \\ &+ \tilde{\epsilon} \frac{g}{c_W} [\partial_x^\mu \langle Z_\mu(x) (H(y) \chi_3(y)) \rangle + M_Z \langle \chi_3(x) (H(y) \chi_3(y)) \rangle] \\ &+ \left(\frac{g \tilde{\epsilon}}{2c_W} \right)^2 \langle H(x) \chi_3(x) H(y) \chi_3(y) \rangle = 0. \end{aligned} \quad (\text{D.10})$$

It is important to realise that these are the full Green's function and therefore the external legs are not *amputated*. Therefore it is crucial to note that the last two terms (in the last two lines) do not have the double pole structure.

This translates into the following identity, in momentum space,

$$\left(q^2 (\Pi_L^{ZZ} - 2M_Z \Pi^{Z\chi_3}) + M_Z^2 \Pi^{\chi_3\chi_3} \right) \equiv A_{ZZ}. \quad (\text{D.11})$$

Note that in the approach where the gauge-fixing Lagrangian is expressed in terms of renormalised quantities, Eq. D.11 also holds for the renormalised two-point function. In the linear gauge $A_{ZZ} = 0$ for any q^2 (tadpole contributions must be included here). An explicit calculation gives

$$\begin{aligned} A_{ZZ} &= \frac{\alpha \tilde{\epsilon}}{16\pi s_W^2 c_W^2} (q^2 - M_Z^2) \left\{ \tilde{\epsilon} (q^2 - 3M_Z^2) (C_{UV} - F_0(ZH)) \right. \\ &\quad \left. + 2 [q^2 (F_0(ZH) - 2F_1(ZH)) - M_H^2 (C_{UV} - F_0(ZH))] \right\}. \end{aligned} \quad (\text{D.12})$$

The functions $F_{0,1}$ are defined in Eq. G.8. We see clearly that A_{ZZ} does not vanish in the non-linear gauge, but at the Z pole. In fact the contribution A_{ZZ} can be derived directly from the last two terms of Eq. D.10. In a diagrammatic form, at one-loop, Eq. D.10 can be described as

$$\begin{aligned}
& \left(\frac{1}{q^2 - M_Z^2} \right)^2 \times \\
& \left[q_\mu q_\nu \times \begin{array}{c} Z \\ \mu \end{array} \times \begin{array}{c} Z \\ v \end{array} + 2i M_Z q_\mu \times \begin{array}{c} Z \\ \mu \end{array} \times \begin{array}{c} \chi_3 \\ \rightarrow \end{array} + M_Z^2 \times \begin{array}{c} \chi_3 \\ \rightarrow \end{array} \times \begin{array}{c} \chi_3 \\ \rightarrow \end{array} \right]_{\text{amp.}} \\
& = \left(\frac{g\tilde{\epsilon}}{2c_W} \right)^2 \left[\times \begin{array}{c} r, H \\ \rightarrow \end{array} \times \begin{array}{c} r+q, \chi_3 \\ \rightarrow \end{array} \right] + \left(\frac{g\tilde{\epsilon}}{c_W} \right) \left[iq_\mu \times \begin{array}{c} Z \\ \rightarrow \end{array} \times \begin{array}{c} H \\ \rightarrow \end{array} \chi_3 + M_Z \times \begin{array}{c} \chi_3 \\ \rightarrow \end{array} \times \begin{array}{c} H \\ \rightarrow \end{array} \chi_3 \right]_{\text{amp.}} \times \frac{1}{q^2 - M_Z^2} \tag{D.13}
\end{aligned}$$

Calculating the new graphs explicitly confirms the identity and is a check on our calculation of Π_L^{ZZ} , $\Pi^{Z\chi_3}$ and $\Pi^{\chi_3\chi_3}$. Note that for the genuine two-point functions (contributing to A_{ZZ}) the loops include all possible particles including matter fields. For the latter one gets the same contribution as in the linear gauge.

For the charged sector the identities go along the same line.

For the photon, the identities give

$$\Pi_L^{AA} = 0 \quad \text{at any } q^2. \tag{D.14}$$

For the AZ transition we get (from $\langle G_A G_Z \rangle = 0$) that

$$\Pi_L^{AZ} - M_Z \Pi^{A\chi_3} = 0. \tag{D.15}$$

This identity holds at any q^2 , but only at one-loop thanks to the fact that the vertex $AH\chi_3$ does not exist at tree-level. This can be easily checked by looking up the explicit formulae in section H.2 and section H.8.1.

E Renormalising the gauge-fixing functions

So far we have chosen to take the gauge-fixing term as being written in terms of renormalised quantities. Although this is quite practical and avoids the introduction of more counterterms for the (unphysical) parameters entering the gauge-fixing Lagrangian, it does not lead to finite Green's functions, in the general case of the non-linear gauge, even when all Feynman parameters are set to one, $\xi_{A,Z,W} = 1$. However all S-matrix elements are finite and gauge parameter independent. Therefore as we argued, this approach of taking the gauge-fixing Lagrangian as renormalised from the outset is easy to implement and at the same time acts as a good test on our system since many divergences in a few

Green's functions cancel at the level of the S-matrix. If one wants to have finite Green's functions one also needs to consider counterterms to the gauge-fixing Lagrangian Eq. 3.15. The purpose of this Appendix is to show how all two-point functions can be made finite if one also introduces counterterms for the gauge parameters, beside the renormalisation of the physical parameters (masses, electric charge) and the tadpole as well as the wavefunction renormalisation for all fields as defined in the main text, see section 4.1. For the two-point functions, the difference between this approach (taking a bare gauge fixing Lagrangian) and that of the paper (taking the gauge fixing as renormalised), only concerns the unphysical scalars (and longitudinal part of the vector bosons). Instead of Eq. 3.15 we write for the charged sector the gauge fixing terms in bare quantities,

$$\mathcal{L}_{GF,W} = -\frac{1}{\xi_W} |(\partial_\mu - ie \tilde{\alpha} \underline{A}_\mu - ig c_W \tilde{\beta} \underline{Z}_\mu) \underline{W}^{\mu+} + \xi'_W \frac{g}{2} \left((\underline{M}_W + \frac{g}{2} (\tilde{\delta} \underline{H} + i \tilde{\kappa} \underline{\chi}_3)) \underline{\chi}^+|^2 . \quad (E.1)$$

For the neutral sector one has to allow for A - Z and A - χ_3 mixing. We take ⁴

$$\begin{aligned} \mathcal{L}_{GF,(Z,A)} = & -\frac{1}{2\xi_Z} (\partial \cdot \underline{Z} + \xi'_Z (\underline{M}_Z + \frac{g}{2c_W} \tilde{\varepsilon} \underline{H}) \underline{\chi}_3)^2 - \frac{1}{2\xi_A} (\partial \cdot \underline{A} + \delta \xi'_A \underline{M}_Z \underline{\chi}_3)^2 \\ & + \delta \eta_{AZ} \partial \cdot \underline{A} \partial \cdot \underline{Z} . \end{aligned} \quad (E.2)$$

It will also be useful to introduce $\tilde{\xi}_W$ and $\tilde{\xi}_Z$ such that $\xi'_W = \sqrt{\xi_W \tilde{\xi}_W}$, $\xi'_Z = \sqrt{\xi_Z \tilde{\xi}_Z}$. At tree-level our implementation requires that $\xi_{A,Z,W} = \xi'_{Z,W} = 1$, $\delta \xi'_A = \delta \eta_{AZ} = 0$. $\delta \xi'_A$ and $\delta \eta_{AZ}$ should be considered of order $\mathcal{O}(\alpha)$ and are introduced to avoid that $\mathcal{L}_{GF,(Z,A)}$ does not induce any non diagonal photon transition. Apart from the $\delta \xi'_A$ and $\delta \eta_{AZ}$ terms, these bare gauge fixing conditions are, of course, formally the same as those we introduced in Eq. 3.15. In fact since the gauge fixing for the photon is still linear and that we are working with $\xi_A = 1$, we could still take the gauge-fixing for the photon to be renormalised. As we will see later, the two approaches lead to the same form of the two-point functions for $\hat{\Pi}_L^{AA,AZ}$ and $\hat{\Pi}^{A\chi_3}$. Since we only seek to show how finite two-point functions can be arrived at, it is sufficient to only consider the addition of the counterterms to the Feynman gauge parameters ξ and ξ' . The bare and renormalised Feynman gauge parameters are related as

$$\underline{\xi}_i = \xi_i + \delta \xi_i ; \quad \underline{\xi}'_i = \xi'_i + \delta \xi'_i ; \quad i = W, Z, A. \quad (E.3)$$

⁴ $\mathcal{L}_{GF,(Z,A)}$ be derived through the auxiliary B-field formulation and the gauge functions G^A and G^Z . One writes $\mathcal{L}_{GF,(Z,A)} = (\xi_Z/2)(\underline{B}^Z)^2 + (\xi_A/2)(\underline{B}^A)^2 + \delta \eta_{AZ} \underline{B}^A \underline{B}^Z + \underline{B}^Z \underline{G}^Z + \underline{B}^A \underline{G}^A$ with $\underline{G}^Z = \partial \cdot \underline{Z} + \xi'_Z (\underline{M}_Z + (g/2c_W) \tilde{\varepsilon} \underline{H}) \underline{\chi}_3$ and $\underline{G}^A = \partial \cdot \underline{A} + \delta \xi'_A \underline{M}_Z \underline{\chi}_3$. For the purpose of generating the counterterms for the two-point functions at the one-loop order, one makes the identification, $\delta \eta_{AZ} = \delta \tilde{\eta}_{AZ}/(\xi_A \xi_Z)$ and $\delta \xi'_A = \delta \xi_{A\chi} - (\xi'_Z/\xi_Z) \delta \tilde{\eta}_{AZ}$.

Since we will only work in the 't Hooft-Feynman gauge, it is sufficient to only consider the case with all $\xi_i = \xi'_i = 1$ apart from $\xi'_A = \delta\eta_{AZ} = 0$.

The generated counterterms for the two-point functions, allowing for the renormalisation of the gauge fixing Lagrangian, and for the approach we take in **GRACE-loop** of considering the gauge fixing Lagrangian in Eq. 3.15 renormalised, are shown below.

1. Vector-Vector

	\mathcal{L}_{GF} with renormalised quantities	\mathcal{L}_{GF} with bare quantities
WW	$\hat{\Pi}_T^W = \delta M_W^2 + 2(M_W^2 - q^2)\delta Z_W^{1/2}$	unchanged
	$\hat{\Pi}_L^W = \delta M_W^2 + 2M_W^2\delta Z_W^{1/2}$	$\hat{\Pi}_L^W = 2(M_W^2 - q^2)\delta Z_W^{1/2} + \delta M_W^2 + q^2\delta\xi_W$
ZZ	$\hat{\Pi}_T^{ZZ} = \delta M_Z^2 + 2(M_Z^2 - q^2)\delta Z_{ZZ}^{1/2}$	unchanged
	$\hat{\Pi}_L^{ZZ} = \delta M_Z^2 + 2M_Z^2\delta Z_{ZZ}^{1/2}$	$\hat{\Pi}_L^{ZZ} = 2(M_Z^2 - q^2)\delta Z_{ZZ}^{1/2} + \delta M_Z^2 + q^2\delta\xi_Z$
ZA	$\hat{\Pi}_T^{ZA} = (M_Z^2 - q^2)\delta Z_{ZA}^{1/2} - q^2\delta Z_{AZ}^{1/2}$	unchanged
	$\hat{\Pi}_L^{ZA} = M_Z^2\delta Z_{ZA}^{1/2}$	$M_Z^2\delta Z_{ZA}^{1/2} - q^2(\delta Z_{ZA}^{1/2} + \delta Z_{AZ}^{1/2} - \delta\eta_{AZ})$
AA	$\hat{\Pi}_T^{AA} = -2q^2\delta Z_{AA}^{1/2}$	unchanged
	$\hat{\Pi}_L^{AA} = 0$	$\hat{\Pi}_L^{AA} = -2q^2\delta Z_{AA}^{1/2} + q^2\delta\xi_A$

2. Scalar-Scalar

	\mathcal{L}_{GF} with renormalised quantities	\mathcal{L}_{GF} with bare quantities
HH	$\hat{\Pi}^H = 2(q^2 - M_H^2)\delta Z_H^{1/2} - \delta M_H^2 + \frac{3\delta T}{v}$	unchanged
$\chi_3\chi_3$	$\hat{\Pi}^{\chi_3} = 2q^2\delta Z_{\chi_3}^{1/2} + \frac{\delta T}{v}$	$\hat{\Pi}^{\chi_3} = 2(q^2 - M_Z^2)\delta Z_{\chi_3}^{1/2} - M_Z^2\delta\tilde{\xi}_Z$ $- \delta M_Z^2 + \frac{\delta T}{v}$
$\chi\chi$	$\hat{\Pi}^\chi = 2q^2\delta Z_\chi^{1/2} + \frac{\delta T}{v}$	$\hat{\Pi}^\chi = 2(q^2 - M_W^2)\delta Z_\chi^{1/2} - M_W^2\delta\tilde{\xi}_W$ $- \delta M_W^2 + \frac{\delta T}{v}$

3. Vector-Scalar

	\mathcal{L}_{GF} with renormalised quantities	\mathcal{L}_{GF} with bare quantities
$W\chi$	$\hat{\Pi}^{W\chi} = M_W(\delta G_W + \delta Z_W^{1/2} + \delta Z_\chi^{1/2})$	$\hat{\Pi}^{W\chi} = \frac{M_W}{2}(\delta\xi_W - \delta\tilde{\xi}_W)$
$Z\chi_3$	$\hat{\Pi}^{Z\chi_3} = M_Z(\delta G_Z + \delta Z_{ZZ}^{1/2} + \delta Z_{\chi_3}^{1/2})$	$\hat{\Pi}^{Z\chi_3} = \frac{M_Z}{2}(\delta\xi_Z - \delta\tilde{\xi}_Z)$
$A\chi_3$	$\hat{\Pi}^{A\chi_3} = M_Z\delta Z_{ZA}^{1/2}$	$\hat{\Pi}^{A\chi_3} = -M_Z\delta\xi'_A$

4. Fermion-Fermion

This remains the same in both approaches and is given by Eq. 4.6.

Note that in both approaches one has $\hat{\Pi}_L^V(0) = \hat{\Pi}_T^V(0)$ for all vectors as should be. Note also that for the 2-point functions involving photons, $\hat{\Pi}_L^{AA,ZA}$ and $\hat{\Pi}^{A\chi_3}$, $\delta\xi_A$, $\delta\xi'_A$ and $\delta\eta_{AZ}$ can be chosen so that the counterterms in both approaches are the same. In particular the Ward identities $\Pi_L^{AA} = 0$ and $\Pi_L^{AZ} - M_Z \Pi^{A\chi_3} = 0$, see Eqs. D.14-D.15, are maintained after renormalisation. Therefore we can take

$$\begin{aligned}\delta\xi_A &= 2\delta Z_{AA}^{1/2}, \quad \delta\xi'_A = -\delta Z_{ZA}^{1/2}, \\ \delta\eta_{AZ} &= \delta Z_{ZA}^{1/2} + \delta Z_{AZ}^{1/2}.\end{aligned}\quad (\text{E.4})$$

Let us turn to the charged sector (the Z transitions go along the same line). Defining

$$A_{WW}^{CT} = q^2(\hat{\Pi}_L^W - 2M_W \hat{\Pi}^{W\chi}) + M_W^2 \hat{\Pi}^{\chi\chi}, \quad (\text{E.5})$$

we find that

$$\begin{aligned}A_{WW}^{CT} &= 0 \quad \text{in our approach (as expected),} \\ &= (q^2 - M_W^2) (q^2 \delta\xi_W + M_W^2 \delta\tilde{\xi}_W + \delta M_W^2 + 2M_W^2 \delta Z_{\chi}^{1/2} - 2q^2 \delta Z_W^{1/2}) \\ &\quad \text{with } \mathcal{L}_{GF} \text{ in terms of bare fields.}\end{aligned}\quad (\text{E.6})$$

This again means that there are constraints on ξ_W and $\tilde{\xi}_W$, *i.e* they are not independent once the other wave functions have been set. Exactly the same applies for the ZZ transition. Also this means that on-shell renormalisation for the unphysical sector is possible. That is, that the scalars have poles at the same location as the physical vector bosons. For example for the W , this condition ($\tilde{\Pi}_L(M_W^2) = \tilde{\Pi}^{\chi}(M_W^2) = 0$) gives that

$$\begin{aligned}M_W^2 \delta\xi_W + \delta M_W^2 &= -\Pi_L^W(M_W^2), \\ M_W^2 \delta\tilde{\xi}_W + \delta M_W^2 &= +\Pi^{\chi}(M_W^2) + \frac{\delta T}{v}.\end{aligned}\quad (\text{E.7})$$

This shows that the renormalised $W\chi$ transition becomes finite in the non-linear gauge:

$$\tilde{\Pi}^{W\chi} = \Pi^{W\chi} + \frac{M_W}{2}(\delta\xi_W - \delta\tilde{\xi}_W) = \Pi^{W\chi} - \frac{1}{2M_W} \left(\Pi_L^W(M_W^2) + \Pi^{\chi}(M_W^2) + \frac{\delta T}{v} \right) = \text{finite}. \quad (\text{E.8})$$

This can be explicitly shown by using the full expressions for the two-point functions at one-loop given in Eqs. H.14, H.26 and H.32.

Using Eq. E.7, the renormalised $\chi\chi$ writes

$$\tilde{\Pi}^\chi = 2(q^2 - M_W^2) \left(\delta Z_\chi^{1/2} + \frac{\alpha}{16\pi s_W^2} (\tilde{\kappa} + \tilde{\delta} - (2 + 1/c_W^2)) C_{UV} + \text{finite} \right). \quad (\text{E.9})$$

In our approach we define $\delta Z_\chi^{1/2}$ so that all C_{UV} terms proportional to q^2 vanish:

$$\delta Z_\chi^{1/2} \equiv -\frac{\Pi_{C_{UV}-\text{part}}^\chi}{2q^2} = \frac{\alpha}{16\pi s_W^2} \left((2 + 1/c_W^2) - \tilde{\kappa} - \tilde{\delta} \right) C_{UV}. \quad (\text{E.10})$$

This is *exactly* the same result had we required $\tilde{\Pi}^\chi$ in Eq. E.9 to be finite. This result would have been arrived at directly had we required that the residue at the pole of the $\chi\chi$ propagator be 1. The C_{UV} part of $\delta Z_\chi^{1/2}$ would be the same, differences would appear in finite terms that have no incidence on S -matrix.

Having constrained $\delta \tilde{\xi}_W$ and $\delta Z_\chi^{1/2}$, $\delta \xi_W$ is fixed. Taking for example only the C_{UV} part of Π_L^W , from Eq. E.7, one has that

$$\delta \xi_W = -\frac{\delta M_W^2}{M_W^2} - \frac{\Pi_L^W(M_W^2)}{M_W^2} = 2\delta Z_W^{1/2} - \frac{\alpha}{4\pi s_W^2} \left(5\tilde{\alpha}^2 s_W^2 + 5\tilde{\beta}^2 c_W^2 + \frac{\tilde{\delta}^2}{4} + \frac{\tilde{\kappa}^2}{4} \right) C_{UV}. \quad (\text{E.11})$$

We indeed find, by explicit calculations, this to be verified. Similar results hold for the other combinations of two-point functions.

F A library of counterterms for the vertices

Here, we list the full counterterms to the vertices after applying the field redefinitions. Those for the ghost vertices are not shown since they are not required at one-loop. Those for the two-point functions (propagators) and the tadpole have been discussed separately for a proper definition of the renormalisation conditions.

$\langle \cdot \cdot \cdot \rangle$ will refer to the tree-level expression of the vertex defined in Sec.B but with $\tilde{\alpha} = \tilde{\beta} = \tilde{\delta} = \tilde{\varepsilon} = \tilde{\kappa} = 0$. As a result of $Z - \gamma$ mixing new vertices, denoted as (*new*), appear.

To help write our results in a compact form, we introduce, as is done, in [21] the following “correction” factors

$$\begin{aligned} \delta G_{mj} &= \frac{\delta m_j}{m_j} \\ \delta G_H &= \frac{\delta M_H^2}{M_H^2} \end{aligned}$$

$$\begin{aligned}
\delta G_W &= \frac{\delta M_W^2}{2M_W^2} \\
\delta G_Z &= \frac{\delta M_Z^2}{2M_Z^2} \\
\delta H &= \frac{\delta M_Z^2 - \delta M_W^2}{2(M_Z^2 - M_W^2)} \\
\delta G_1 &= \delta G_W - \delta H \\
\delta G_2 &= \delta G_Z - \delta H \\
\delta G_3 &= \delta G_Z - \delta G_W \\
\delta G_4 &= \frac{2\delta M_W^2 - \delta M_Z^2}{2M_W^2 - M_Z^2} - \delta G_W - \delta H
\end{aligned} \tag{F.1}$$

F.1 Vector-Vector-Vector

p_1 (μ)	p_2 (ν)	p_3 (ρ)	
W^-	W^+	A	$(\delta Y + 2\delta Z_W^{1/2} + \delta Z_{AA}^{1/2})\langle WWA \rangle + \delta Z_{ZA}^{1/2}\langle WWZ \rangle$
W^-	W^+	Z	$(\delta Y + \delta G_1 + 2\delta Z_W^{1/2} + \delta Z_{ZZ}^{1/2})\langle WWZ \rangle + \delta Z_{AZ}^{1/2}\langle WWA \rangle$

F.2 Vector-Vector-Scalar

p_1 (μ)	p_2 (ν)	p_3	
W^\pm	A	χ^\mp	$(\delta Y + \delta G_W + \delta Z_W^{1/2} + \delta Z_\chi^{1/2} + \delta Z_{AA}^{1/2})\langle WA\chi \rangle + \delta Z_{ZA}^{1/2}\langle WZ\chi \rangle$
W^\pm	Z	χ^\mp	$(\delta Y + \delta H + \delta Z_W^{1/2} + \delta Z_\chi^{1/2} + \delta Z_{ZZ}^{1/2})\langle WZ\chi \rangle + \delta Z_{AZ}^{1/2}\langle WA\chi \rangle$
W^-	W^+	H	$(\delta Y + \delta G_2 + \delta G_W + 2\delta Z_W^{1/2} + \delta Z_H^{1/2})\langle WWH \rangle$
Z	Z	H	$(\delta Y + \delta G_2 + \delta G_3 + \delta G_Z + 2\delta Z_{ZZ}^{1/2} + \delta Z_H^{1/2})\langle ZZH \rangle$
Z	A	H	$\delta Z_{ZA}^{1/2}\langle ZZH \rangle \quad (new)$

F.3 Scalar-Scalar-Vector

p_1	p_2	p_3 (μ)	
H	χ^\mp	W^\pm	$(\delta Y + \delta G_2 + \delta Z_H^{1/2} + \delta Z_\chi^{1/2} + \delta Z_W^{1/2})\langle H\chi W \rangle$
χ_3	χ^\mp	W^\pm	$(\delta Y + \delta G_2 + \delta Z_{\chi_3}^{1/2} + \delta Z_\chi^{1/2} + \delta Z_W^{1/2})\langle \chi_3\chi W \rangle$
χ^-	χ^+	A	$(\delta Y + 2\delta Z_\chi^{1/2} + \delta Z_{AA}^{1/2})\langle \chi\chi A \rangle + \delta Z_{ZA}^{1/2}\langle \chi\chi Z \rangle$
χ^-	χ^+	Z	$(\delta Y + \delta G_4 + 2\delta Z_\chi^{1/2} + \delta Z_{ZZ}^{1/2})\langle \chi\chi Z \rangle + \delta Z_{AZ}^{1/2}\langle \chi\chi A \rangle$
H	χ_3	Z	$(\delta Y + \delta G_2 + \delta G_3 + \delta Z_H^{1/2} + \delta Z_{\chi_3}^{1/2} + \delta Z_{ZZ}^{1/2})\langle H\chi_3 Z \rangle$
H	χ_3	A	$\delta Z_{ZA}^{1/2}\langle H\chi_3 Z \rangle \quad (new)$

F.4 Scalar-Scalar-Scalar

p_1	p_2	p_3	
H	H	H	$\left[(\delta Y + \delta G_2 - \delta G_W + \delta G_H + 3\delta Z_H^{1/2}) - \delta T \frac{e}{s_W M_W M_H^2} \right] \langle HHH \rangle$
H	χ^-	χ^+	$\left[(\delta Y + \delta G_2 - \delta G_W + \delta G_H + \delta Z_H^{1/2} + 2\delta Z_\chi^{1/2}) - \delta T \frac{e}{s_W M_W M_H^2} \right] \langle H\chi\chi \rangle$
H	χ_3	χ_3	$\left[(\delta Y + \delta G_2 - \delta G_W + \delta G_H + \delta Z_H^{1/2} + 2\delta Z_{\chi_3}^{1/2}) - \delta T \frac{e}{s_W M_W M_H^2} \right] \langle H\chi_3\chi_3 \rangle$

F.5 Vector-Vector-Vector-Vector

p_1 (μ)	p_2 (ν)	p_3 (ρ)	p_4 (σ)	
W^+	W^-	A	A	$(2\delta Y + 2\delta Z_W^{1/2} + 2\delta Z_{AA}^{1/2}) \langle WWAA \rangle$ $+ 2\delta Z_{ZA}^{1/2} \langle WWAZ \rangle$
W^+	W^-	A	Z	$(2\delta Y + \delta G_1 + 2\delta Z_W^{1/2} + \delta Z_{AA}^{1/2} + \delta Z_{ZZ}^{1/2}) \langle WWAZ \rangle$ $+ \delta Z_{AZ}^{1/2} \langle WWAA \rangle + \delta Z_{ZA}^{1/2} \langle WWZZ \rangle$
W^+	W^-	Z	Z	$(2\delta Y + 2\delta G_1 + 2\delta Z_W^{1/2} + 2\delta Z_{ZZ}^{1/2}) \langle WWZZ \rangle$ $+ 2\delta Z_{AZ}^{1/2} \langle WWAZ \rangle$
W^+	W^-	W^-	W^+	$(2\delta Y + 2\delta G_2 + 4\delta Z_W^{1/2}) \langle WWWW \rangle$

F.6 Vector-Vector-Scalar-Scalar

p_1 (μ)	p_2 (ν)	p_3	p_4	
A	W^\pm	H	χ^\mp	$(2\delta Y + \delta G_2 + \delta Z_{AA}^{1/2} + \delta Z_W^{1/2} + \delta Z_H^{1/2} + \delta Z_\chi^{1/2}) \langle AWH\chi \rangle$ $+ \delta Z_{ZA}^{1/2} \langle ZWH\chi \rangle$
A	W^\pm	χ_3	χ^\mp	$(2\delta Y + \delta G_2 + \delta Z_{AA}^{1/2} + \delta Z_W^{1/2} + \delta Z_{\chi_3}^{1/2} + \delta Z_\chi^{1/2}) \langle AW\chi_3\chi \rangle$ $+ \delta Z_{ZA}^{1/2} \langle ZW\chi_3\chi \rangle$
Z	W^\pm	H	χ^\mp	$(2\delta Y + \delta G_3 + \delta Z_{ZZ}^{1/2} + \delta Z_W^{1/2} + \delta Z_H^{1/2} + \delta Z_\chi^{1/2}) \langle ZWH\chi \rangle$ $+ \delta Z_{AZ}^{1/2} \langle AWH\chi \rangle$
Z	W^\pm	χ_3	χ^\mp	$(2\delta Y + \delta G_3 + \delta Z_{ZZ}^{1/2} + \delta Z_W^{1/2} + \delta Z_{\chi_3}^{1/2} + \delta Z_\chi^{1/2}) \langle ZW\chi_3\chi \rangle$ $+ \delta Z_{AZ}^{1/2} \langle AW\chi_3\chi \rangle$
A	A	χ^+	χ^-	$(2\delta Y + 2\delta Z_{AA}^{1/2} + 2\delta Z_\chi^{1/2}) \langle AA\chi\chi \rangle + 2\delta Z_{ZA}^{1/2} \langle ZA\chi\chi \rangle$
Z	A	χ^+	χ^-	$(2\delta Y + \delta G_4 + \delta Z_{ZZ}^{1/2} + \delta Z_{AA}^{1/2} + 2\delta Z_\chi^{1/2}) \langle ZA\chi\chi \rangle$ $+ \delta Z_{ZA}^{1/2} \langle ZZ\chi\chi \rangle + \delta Z_{AZ}^{1/2} \langle AA\chi\chi \rangle$
Z	Z	χ^+	χ^-	$(2\delta Y + 2\delta G_4 + 2\delta Z_{ZZ}^{1/2} + 2\delta Z_\chi^{1/2}) \langle ZZ\chi\chi \rangle$ $+ 2\delta Z_{AZ}^{1/2} \langle ZA\chi\chi \rangle$
W^+	W^-	H	H	$(2\delta Y + 2\delta G_2 + 2\delta Z_W^{1/2} + 2\delta Z_H^{1/2}) \langle WWHH \rangle$
W^+	W^-	χ_3	χ_3	$(2\delta Y + 2\delta G_2 + 2\delta Z_W^{1/2} + 2\delta Z_{\chi_3}^{1/2}) \langle WW\chi_3\chi_3 \rangle$
W^+	W^-	χ^-	χ^+	$(2\delta Y + 2\delta G_2 + 2\delta Z_W^{1/2} + 2\delta Z_\chi^{1/2}) \langle WW\chi\chi \rangle$
Z	Z	H	H	$(2\delta Y + 2\delta G_2 + 2\delta G_3 + 2\delta Z_{ZZ}^{1/2} + 2\delta Z_H^{1/2}) \langle ZZHH \rangle$
Z	Z	χ_3	χ_3	$(2\delta Y + 2\delta G_2 + 2\delta G_3 + 2\delta Z_{ZZ}^{1/2} + 2\delta Z_{\chi_3}^{1/2}) \langle ZZ\chi_3\chi_3 \rangle$
Z	A	H	H	$\delta Z_{ZA}^{1/2} \langle ZZHH \rangle$ (new)
Z	A	χ_3	χ_3	$\delta Z_{ZA}^{1/2} \langle ZZ\chi_3\chi_3 \rangle$ (new)

F.7 Scalar-Scalar-Scalar-Scalar

p_1	p_2	p_3	p_4	
H	H	H	H	$\left[(2\delta Y + 2\delta G_2 - 2\delta G_W + \delta G_H + 4\delta Z_H^{1/2}) - \delta T \frac{e}{s_W M_W M_H^2} \right] \langle HHHH \rangle$
χ_3	χ_3	χ_3	χ_3	$\left[(2\delta Y + 2\delta G_2 - 2\delta G_W + \delta G_H + 4\delta Z_{\chi_3}^{1/2}) - \delta T \frac{e}{s_W M_W M_H^2} \right] \langle \chi_3 \chi_3 \chi_3 \chi_3 \rangle$
χ^\pm	χ^\mp	χ^\mp	χ^\pm	$\left[(2\delta Y + 2\delta G_2 - 2\delta G_W + \delta G_H + 4\delta Z_\chi^{1/2}) - \delta T \frac{e}{s_W M_W M_H^2} \right] \langle \chi \chi \chi \chi \rangle$
H	H	χ_3	χ_3	$\left[(2\delta Y + 2\delta G_2 - 2\delta G_W + \delta G_H + 2\delta Z_H^{1/2} + 2\delta Z_{\chi_3}^{1/2}) - \delta T \frac{e}{s_W M_W M_H^2} \right] \langle HH \chi_3 \chi_3 \rangle$
H	H	χ^+	χ^-	$\left[(2\delta Y + 2\delta G_2 - 2\delta G_W + \delta G_H + 2\delta Z_H^{1/2} + 2\delta Z_\chi^{1/2}) - \delta T \frac{e}{s_W M_W M_H^2} \right] \langle HH \chi \chi \rangle$
χ^+	χ^-	χ_3	χ_3	$\left[(2\delta Y + 2\delta G_2 - 2\delta G_W + \delta G_H + 2\delta Z_\chi^{1/2} + 2\delta Z_{\chi_3}^{1/2}) - \delta T \frac{e}{s_W M_W M_H^2} \right] \langle \chi \chi \chi_3 \chi_3 \rangle$

F.8 Fermion-Fermion-Vector

We define $L, R = (1 \mp \gamma_5)/2$.

p_1	p_2	p_3	(μ)	
\bar{f}	f	A		$(\delta Y + \delta Z_{AA}^{1/2} + 2\delta Z_{fL}^{1/2}) e Q_f \gamma^\mu L + (\delta Y + \delta Z_{AA}^{1/2} + 2\delta Z_{fR}^{1/2}) e Q_f \gamma^\mu R + \delta Z_{ZA}^{1/2} \frac{e}{2s_W c_W} (2I_3 \gamma^\mu L - 2s_W^2 Q_f \gamma^\mu (L + R))$
\bar{f}	f	Z		$(\delta Y + \delta G_2 + \delta G_3 + \delta Z_{ZZ}^{1/2} + 2\delta Z_{fL}^{1/2}) \frac{e}{2s_W c_W} 2I_3 \gamma^\mu L + (\delta Y - \delta G_2 + \delta G_3 + \delta Z_{ZZ}^{1/2} + 2\delta Z_{fL}^{1/2}) \frac{e}{2s_W c_W} (-2s_W^2 Q_f \gamma^\mu L) + (\delta Y - \delta G_2 + \delta G_3 + \delta Z_{ZZ}^{1/2} + 2\delta Z_{fR}^{1/2}) \frac{e}{2s_W c_W} (-2s_W^2 Q_f \gamma^\mu R) + \delta Z_{AZ}^{1/2} e Q_f \gamma^\mu (L + R)$
\bar{U}/\bar{D}	D/U	W^+/W^-		$(\delta Y + \delta G_2 + \delta Z_{(U/D)L}^{1/2} + \delta Z_{(D/U)L}^{1/2} + \delta Z_W^{1/2}) \frac{e}{\sqrt{2}s_W} \gamma^\mu L$

F.9 Fermion-Fermion-Scalar

$$L, R = (1 \mp \gamma_5)/2$$

p_1	p_2	p_3
\bar{f}	f	H
		$(\delta Y + \delta G_2 + \delta G_{mf} - \delta G_W + \delta Z_{fR}^{1/2} + \delta Z_{fL}^{1/2} + \delta Z_H^{1/2}) \left(-\frac{e}{2s_W} \frac{m_f}{M_W} \right) L$
		$+ (\delta Y + \delta G_2 + \delta G_{mf} - \delta G_W + \delta Z_{fL}^{1/2} + \delta Z_{fR}^{1/2} + \delta Z_H^{1/2}) \left(-\frac{e}{2s_W} \frac{m_f}{M_W} \right) R$
\bar{U}/\bar{D}	U/D	χ_3
		$(\delta Y + \delta G_2 + \delta G_{mf} - \delta G_W + \delta Z_{(U/D)R}^{1/2} + \delta Z_{(U/D)L}^{1/2} + \delta Z_{\chi_3}^{1/2}) \left((-/+) \frac{ie}{2s_W} \frac{m_f}{M_W} \right) (-L)$
		$+ (\delta Y + \delta G_2 + \delta G_{mf} - \delta G_W + \delta Z_{(U/D)L}^{1/2} + \delta Z_{(U/D)R}^{1/2} + \delta Z_{\chi_3}^{1/2}) \left((-/+) \frac{ie}{2s_W} \frac{m_f}{M_W} \right) R$
\bar{U}	D	χ^+
		$(\delta Y + \delta G_2 + \delta G_{mU} - \delta G_W + \delta Z_{UR}^{1/2} + \delta Z_{DL}^{1/2} + \delta Z_{\chi}^{1/2}) \frac{-ie}{\sqrt{2}s_W} \frac{m_U}{M_W} (-L)$
		$+ (\delta Y + \delta G_2 + \delta G_{mD} - \delta G_W + \delta Z_{UL}^{1/2} + \delta Z_{DR}^{1/2} + \delta Z_{\chi}^{1/2}) \frac{-ie}{\sqrt{2}s_W} \frac{m_D}{M_W} R$
\bar{D}	U	χ^-
		$(\delta Y + \delta G_2 + \delta G_{mD} - \delta G_W + \delta Z_{DR}^{1/2} + \delta Z_{UL}^{1/2} + \delta Z_{\chi}^{1/2}) \frac{-ie}{\sqrt{2}s_W} \frac{m_D}{M_W} (-L)$
		$+ (\delta Y + \delta G_2 + \delta G_{mU} - \delta G_W + \delta Z_{DL}^{1/2} + \delta Z_{UR}^{1/2} + \delta Z_{\chi}^{1/2}) \frac{-ie}{\sqrt{2}s_W} \frac{m_U}{M_W} R$

G Properties of two-point functions

As mentioned earlier loop integrals are calculated using dimensional regularisation. In the following l will be the loop momentum. Since one-point and two-point functions (tadpoles and self-energies) are essential in the derivation of the counterterms, we list here the properties of these functions.

For the one-point function, which corresponds for example to the diagram shown in Fig.3-(a), we have the well known result:

$$\int \frac{d^n \ell}{i(2\pi)^n} \frac{1}{\ell^2 - m_A^2} = \frac{1}{16\pi^2} m_A^2 \left(C_{UV} - \log m_A^2 + 1 \right) \quad (\text{G.1})$$

where C_{UV} is defined in Eq. 4.25.

A typical two-point function refers to a diagram as shown in Fig.3.

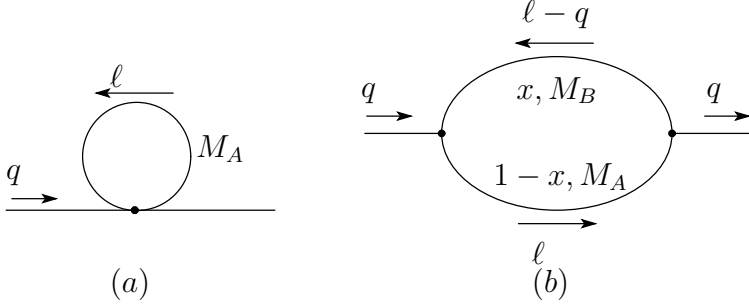


Figure 3: Diagrams for the one-point (a) and two-point functions (b)

This leads to the calculation of

$$\begin{aligned} & \int \frac{d^n \ell}{i(2\pi)^n} \frac{N(\ell)}{(\ell^2 - M_A^2)((\ell - q)^2 - M_B^2)} \\ &= \int \frac{d^n \ell}{i(2\pi)^n} \int_0^1 dx \frac{N}{[(1-x)(\ell^2 - M_A^2) + x((\ell - q)^2 - M_B^2)]^2}. \end{aligned} \quad (\text{G.2})$$

where $N(\ell)$ depends, in general, on the momenta ℓ, q and the masses. Defining D_2 as

$$D_2 = (1-x)M_A^2 + xM_B^2 - x(1-x)s, \quad (s = q^2) \quad (\text{G.3})$$

we usually need to compute

$$\int \frac{d^n \ell}{i(2\pi)^n} \frac{1}{(\ell^2 - D_2)^2} = \frac{1}{16\pi^2} (C_{UV} - \log D_2) \quad (\text{G.4})$$

$$\int \frac{d^n \ell}{i(2\pi)^n} \frac{\ell^2}{(\ell^2 - D_2)^2} = \frac{1}{16\pi^2} 2D_2 \left(C_{UV} + \frac{1}{2} - \log D_2 \right) \quad (\text{G.5})$$

$$\int \frac{d^n \ell}{i(2\pi)^n} \frac{\ell^\mu \ell^\nu}{(\ell^2 - D_2)^2} = \frac{1}{16\pi^2} \frac{D_2}{2} (C_{UV} + 1 - \log D_2) g^{\mu\nu} \quad (\text{G.6})$$

Then the integral over the parameter x gives

$$\int_0^1 dx D_2 = \frac{1}{2}(M_A^2 + M_B^2) - \frac{1}{6}s \quad (\text{G.7})$$

$$F_n(A, B) = \int_0^1 dx x^n \log D_2 = \int_0^1 dx x^n \log \left[(1-x)M_A^2 + xM_B^2 - x(1-x)s \right] \quad (\text{G.8})$$

We do not show the explicit form of F_n in terms of elementary functions (the result is well known). We only encounter $n = 0, 1, 2$.

The notation $F(A, B) = F_1(A, B) - F_2(A, B) = F(B, A)$ is sometimes used.

$$\begin{aligned}\tilde{F}(A, B) &= \int_0^1 dx D_2 \log D_2 \\ &= M_A^2 (F_0(A, B) - F_1(A, B)) + M_B^2 F_1(A, B) - s F(A, B)\end{aligned}\tag{G.9}$$

We have several relations for the F_n functions as shown below. All F_n can be reduced into F_0 .

Exchange of A and B

$$\begin{aligned}F_0(B, A) &= F_0(A, B) \\ F_1(B, A) &= F_0(A, B) - F_1(A, B) \\ F_2(B, A) &= F_0(A, B) - 2F_1(A, B) + F_2(A, B)\end{aligned}\tag{G.10}$$

Reduction into F_0 , $A \neq B$

$$F_1(A, B) = \frac{1}{2} \left(1 + \frac{M_A^2 - M_B^2}{s} \right) F_0(A, B) + \frac{1}{2s} \left(M_B^2 \log M_B^2 - M_A^2 \log M_A^2 - M_B^2 + M_A^2 \right)\tag{G.11}$$

$$\begin{aligned}F_2(A, B) &= \frac{2}{3} \left(1 + \frac{M_A^2 - M_B^2}{s} \right) F_1(A, B) - \frac{M_A^2}{3s} F_0(A, B) \\ &\quad + \frac{1}{3s} \left(M_B^2 \log M_B^2 + \frac{1}{2}(M_A^2 - M_B^2) \right) - \frac{1}{18}\end{aligned}\tag{G.12}$$

Reduction into F_0 , $A = B$

$$F_1(A, A) = \frac{1}{2} F_0(A, A)\tag{G.13}$$

$$F_2(A, A) = \frac{1}{3} \left(1 - \frac{M_A^2}{s} \right) F_0(A, A) + \frac{M_A^2}{3s} \log M_A^2 - \frac{1}{18}\tag{G.14}$$

G functions (Derivative of F)

$$G_n(A, B) = \frac{d}{ds} F_n(A, B) = \int_0^1 dx \frac{-x^n \cdot x(1-x)}{D_2}\tag{G.15}$$

F and G at special energy

$$\begin{aligned} F_n(A, B; C) &= F_n(A, B)|_{s=M_C^2} \\ F_n(A, B; 0) &= F_n(A, B)|_{s=0} \\ G_n(A, B; C) &= G_n(A, B)|_{s=M_C^2} \\ G_n(A, B; 0) &= G_n(A, B)|_{s=0} \end{aligned} \tag{G.16}$$

F_0 for $s = 0$

$$F_0(A, B, 0) = \begin{cases} \log M_A^2 & (A = B) \\ \frac{M_B^2 \log M_B^2 - M_A^2 \log M_A^2}{M_B^2 - M_A^2} - 1 & (A \neq B) \end{cases} \tag{G.17}$$

H Results for the one-loop corrections to the propagators

We here give the details on the calculation of the loop corrections to the various propagators and mixings. For the vector bosons we present both the transverse and longitudinal part as defined in Section 4.3. We also show the various contributions by classifying them according to the diagrams of Fig. 3. Therefore for each propagator we show a table containing the two types of diagrams. The fermion contributions are summed over all fermion species in the case of the neutral sector and over all doublets in the charged sector. In both cases summing over colour for quarks is implied. Before presenting the results for the two-point function, we first start by presenting the one-loop contribution to the tadpole. Although we will require this contribution to vanish against the tadpole counterterm we give its full expression for completeness. Also, the latter is needed for the Ward identities.

H.1 The tadpole

The tadpole contribution T^{loop} only receives contributions from diagrams of the type shown in Fig. 3-(a) where $A = W, Z, \chi, \chi_3, H, c, c^Z, f$. The result is as follows:

$$\begin{aligned}
T^{loop} = & \frac{e}{16\pi^2 s_W M_W} \left[M_W^2 \left((C_{UV} - \log M_W^2 + 1)(3M_W^2 + \frac{1}{2}M_H^2) - 2M_W^2 \right) \right. \\
& + M_Z^2 \left((C_{UV} - \log M_Z^2 + 1)(\frac{3}{2}M_Z^2 + \frac{1}{4}M_H^2) - M_Z^2 \right) \\
& + \frac{3}{4}M_H^4 (C_{UV} - \log M_H^2 + 1) \\
& \left. - \sum_f 2m_f^4 (C_{UV} - \log m_f^2 + 1) \right]. \tag{H.1}
\end{aligned}$$

It is important to note that all dependence on the non-linear gauge parameters (namely $\tilde{\varepsilon}$ and $\tilde{\delta}$) vanishes among all diagrams and is therefore the same as in the usual linear gauge. This can be considered as a check on the calculation, since the tadpole T can be considered as a basic parameter of the theory.

From this expression we immediately derive the tadpole counterterm:

$$\delta T = -T^{loop}. \tag{H.2}$$

H.2 $A - A$

For all the two-point functions we will list, as done in the table below, the contributing diagrams where (a) corresponds to the type shown in Fig. 3-(a) and (b) to Fig. 3-(b)

(b)	$(A, B) = (W, W), (W, \chi), (\chi, W), (\chi, \chi), (c^+, c^+), (c^-, c^-), (f, f)$
(a)	$A = W, \chi, c^+, c^-$

$$\begin{aligned}
\Pi_T^{AA}(q^2) = & \frac{\alpha}{4\pi} q^2 \left[7C_{UV} - 5F_0(W, W) - 12F(W, W) + \frac{2}{3} - 4(1 - \tilde{\alpha})(C_{UV} - F_0(W, W)) \right. \\
& \left. - 8 \sum_f Q_f^2 \left(\frac{1}{6}C_{UV} - F(f, f) \right) \right]. \tag{H.3}
\end{aligned}$$

Note that independently of the gauge parameter $\Pi_T^{AA}(0) = 0$. This is just a remnant of the QED gauge invariance which is explicit at one-loop. This also gives $\Pi_L^{AA}(q^2) = 0$ which we explicitly verify. More generally we will also check explicitly that in both the linear and non-linear gauges $\Pi_T(0) = \Pi_L(0)$ for all vector-vector transitions. This is another check on the calculation and encodes the property that there is no spurious pole in the propagators essential for the Goldstone mechanism.

H.3 $Z - A$

(b)	$(A, B) = (W, W), (W, \chi), (\chi, W), (\chi, \chi), (c^+, c^+), (c^-, c^-), (f, f)$
(a)	$A = W, \chi, c^+, c^-$

$$\Pi_T^{ZA} = \frac{\alpha}{4\pi} \frac{c_W}{s_W} \left\{ \begin{array}{l} q^2 \left[C_{UV} \left(7 + \frac{1}{6c_W^2} \right) - 4 \left(3 - \frac{1}{2c_W^2} \right) F(W, W) + \frac{2}{3} - \left(5 + \frac{1}{2c_W^2} \right) F_0(W, W) \right. \\ - 2(1 - \tilde{\beta}) (C_{UV} - F_0(W, W)) \\ - \frac{2}{c_W^2} \sum_f |Q_f| \left(1 - 4|Q_f|s_W^2 \right) \left(\frac{1}{6} C_{UV} - F(f, f) \right) \left. \right] \\ - 2(1 - \tilde{\alpha})(q^2 - M_Z^2) (C_{UV} - F_0(W, W)) \end{array} \right\}, \quad (\text{H.4})$$

$$\Pi_L^{ZA} = \frac{\alpha}{2\pi} \frac{c_W}{s_W} (1 - \tilde{\alpha}) M_Z^2 (C_{UV} - F_0(W, W)). \quad (\text{H.5})$$

Note that we do get as a check that $\Pi_T^{ZA}(0) = \Pi_L^{ZA}(0)$. Moreover for $\tilde{\alpha} = 1$ this condition is even stronger since we get $\Pi_T^{ZA}(0) = \Pi_L^{ZA} = 0$. This is due to the fact that for this particular choice of the parameter, the gauge-fixing in the charged sector which contributes here (note that fermions do not contribute to Π_L^{ZA}), there is an additional $U(1)_{\text{QED}}$ gauge invariance. This choice is therefore very useful. As we will see this is also responsible for the vanishing of the induced $A - \chi_3$ transition, see section H.8.1. It is also important to remark that at the Z -pole the $\tilde{\alpha}$ dependence vanishes. This is also responsible for the fact that the counterterms needed for the mass definitions do not depend on the gauge fixing.

H.4 $Z - Z$

(b)	$(A, B) = (W, W), (W, \chi), (\chi, W), (\chi, \chi), (H, \chi), (H, Z), (c^+, c^+), (c^-, c^-), (f, f)$
(a)	$A = W, H, \chi_3, \chi, c^+, c^-$

$$\Pi_T^{ZZ} = \frac{\alpha}{4\pi s_W^2 c_W^2} \left(T_b^{ZZ} + T_f^{ZZ} + (1 - \tilde{\beta}) (q^2 - M_Z^2) \Delta T^{ZZ} \right), \quad (\text{H.6})$$

$$\begin{aligned} T_b^{ZZ} &= C_{UV} \left[q^2 \left(7c_W^4 - \frac{1 - 2c_W^2}{6} \right) - 2M_W^2 - M_Z^2 \right] + \frac{2}{3} q^2 c_W^4 - \frac{q^2}{12} \\ &\quad - 8q^2 c_W^4 F_0(W, W) + q^2 (F_0(W, W) - 4F(W, W)) \left(3c_W^4 + \frac{1 - 4c_W^2}{4} \right) \end{aligned}$$

$$\begin{aligned}
& + 2M_W^2 F_0(W, W) + \frac{q^2}{2} F(H, Z) - \frac{M_H^2}{2} F_0(H, Z) - \frac{M_Z^2 - M_H^2}{2} F_1(H, Z) \\
& + M_Z^2 F_0(H, Z) + \frac{1}{4} (M_H^2 \log M_H^2 + M_Z^2 \log M_Z^2), \\
T_f^{ZZ} & = -\frac{1}{2} \sum_f \left[\left((1 - 4|Q_f|s_W^2)^2 + 1 \right) \left(\frac{1}{6} C_{UV} - F(f, f) \right) q^2 - m_f^2 (C_{UV} - F_0(f, f)) \right], \tag{H.7}
\end{aligned}$$

$$\Delta T^{ZZ} = -4c_W^4 (C_{UV} - F_0(W, W)). \tag{H.8}$$

We have,

$$\Pi_{\text{NonLinear}}^T(M_Z^2) = \Pi_{\text{Linear}}^T(M_Z^2).$$

$$\begin{aligned}
\Pi_L^{ZZ} & = \frac{\alpha}{16\pi s_W^2 c_W^2} \left\{ q^2 \left[C_{UV} \tilde{\epsilon}^2 - \frac{1}{3} + 2F(H, Z) - (1 - \tilde{\epsilon})^2 F_0(H, Z) - 4F_2(H, Z) \right. \right. \\
& \quad \left. \left. + 4(1 - \tilde{\epsilon}) F_1(H, Z) \right] \right. \\
& - 4M_Z^2 (C_{UV} - F_0(H, Z)) - 2M_H^2 F_0(H, Z) - 2(M_Z^2 - M_H^2) F_1(H, Z) \\
& + (M_H^2 \log M_H^2 + M_Z^2 \log M_Z^2) - 8M_W^2 (C_{UV} - F_0(W, W)) (1 - 2c_W^2(1 - \tilde{\beta})) \\
& \left. + 2 \sum_f m_f^2 (C_{UV} - F_0(f, f)) \right\}. \tag{H.9}
\end{aligned}$$

It is easy to see that, for any choice of the gauge parameters, $\Pi_L^{ZZ}(0) = \Pi_T^{ZZ}(0)$ which is a check on the calculation. Also note that the $\tilde{\epsilon}$ dependence is proportional to q^2 .

H.5 $W - W$

(b)	$(A, B) = (Z, W), (Z, \chi), (A, W), (A, \chi), (H, \chi), (H, W), (\chi_3, \chi),$ $(c^Z, c^+), (c^Z, c^-), (c^A, c^+), (c^A, c^-), (f, f')$
(a)	$A = A, Z, W, H, \chi_3, \chi, c^+, c^-$

$$\Pi_T^{WW} = \frac{\alpha}{4\pi s_W^2} \left(T_b^{WW} + T_f^{WW} + (q^2 - M_W^2) \Delta T_{\tilde{\alpha}, \tilde{\beta}}^{WW} \right), \tag{H.10}$$

$$T_b^{WW} = C_{UV} \left(\frac{19}{6} q^2 + 2M_W^2 - M_Z^2 \right) - \frac{q^2}{6}$$

$$\begin{aligned}
& +4s_W^2 \left[q^2(F(A, W) - F_0(A, W)) - M_W^2 F_1(A, W) \right] \\
& +c_W^2 \left[4q^2(F(Z, W) - F_0(Z, W)) - 4(M_W^2 - M_Z^2)F_1(Z, W) \right. \\
& \left. + \left(-7M_Z^2 + \frac{M_Z^2}{c_W^2} \right) F_0(Z, W) \right] + \frac{q^2}{2} (F(H, W) + F(Z, W)) + M_W^2 F_0(H, W) \\
& -\frac{1}{2} \left[M_H^2 F_0(H, W) + M_Z^2 F_0(Z, W) + (M_W^2 - M_H^2) F_1(H, W) \right. \\
& \left. + (M_W^2 - M_Z^2) F_1(Z, W) \right] \\
& + \frac{5M_W^2}{2} \log M_W^2 + \frac{M_Z^2}{4} \log M_Z^2 + \frac{M_H^2}{4} \log M_H^2 + 2M_W^2 \log M_Z^2, \tag{H.11}
\end{aligned}$$

$$\begin{aligned}
T_f^{WW} = & -\frac{1}{2} \sum_{doublet} \left\{ 4 \left(\frac{1}{6} C_{UV} - F(f, f') \right) q^2 - (m_f^2 + m_f'^2) C_{UV} + 2m_f^2 F_1(f', f) \right. \\
& \left. + 2m_f'^2 F_1(f, f') \right\}, \tag{H.12}
\end{aligned}$$

$$\Delta T_{\tilde{\alpha}, \tilde{\beta}}^{WW} = -2 \left(s_W^2 \tilde{\alpha} (C_{UV} - F_0(A, W)) + c_W^2 \tilde{\beta} (C_{UV} - F_0(Z, W)) \right). \tag{H.13}$$

Here also we check that ,

$$\Pi_{\text{NonLinear}}^T(M_W^2) = \Pi_{\text{Linear}}^T(M_W^2).$$

$$\begin{aligned}
\Pi_L^{WW} = & \frac{\alpha}{4\pi s_W^2} \left\{ C_{UV} \left(2M_W^2 - M_Z^2 \right) - \frac{5}{6} q^2 \right. \\
& + 2s_W^2 \left[q^2(6F(A, W) - F_0(A, W)) - 2M_W^2 F_1(A, W) \right] \\
& + c_W^2 \left[2q^2(6F(Z, W) - F_0(Z, W)) - 4(M_W^2 - M_Z^2)F_1(Z, W) \right. \\
& \left. + \left(\frac{M_Z^2}{c_W^2} - 7M_Z^2 \right) F_0(Z, W) \right] \\
& + \frac{1}{2} \left[q^2 \left(3F(H, W) - \frac{F_0(H, W)}{2} \right) + 2M_W^2 F_0(H, W) - M_H^2 F_0(H, W) \right. \\
& \left. - (M_W^2 - M_H^2) F_1(H, W) \right] \\
& + \frac{1}{2} \left[q^2 \left(3F(Z, W) - \frac{F_0(Z, W)}{2} \right) - M_Z^2 F_0(Z, W) - (M_W^2 - M_Z^2) F_1(Z, W) \right] \\
& + \frac{5M_W^2}{2} \log M_W^2 + \frac{M_Z^2}{4} \log M_Z^2 + \frac{M_H^2}{4} \log M_H^2 + 2M_W^2 \log M_Z^2 \\
& + 2s_W^2 \tilde{\alpha} \left[3q^2(F_0(A, W) - 2F_1(A, W)) + M_W^2(C_{UV} - F_0(A, W)) \right] \\
& + 2c_W^2 \tilde{\beta} \left[3q^2(F_0(Z, W) - 2F_1(Z, W)) + M_W^2(C_{UV} - F_0(Z, W)) \right]
\end{aligned}$$

$$\begin{aligned}
& + s_W^2 \tilde{\alpha}^2 q^2 (5C_{UV} - 6F_0(A, W) + 2F_1(A, W) - 2) \\
& + c_W^2 \tilde{\beta}^2 q^2 (5C_{UV} - 6F_0(Z, W) + 2F_1(Z, W) - 2) \\
& + \frac{\tilde{\delta}}{2} q^2 (F_0(H, W) - 2F_1(H, W)) + \frac{\tilde{\kappa}}{2} q^2 (F_0(Z, W) - 2F_1(Z, W)) \\
& + \frac{\tilde{\delta}^2}{4} q^2 (C_{UV} - F_0(H, W)) + \frac{\tilde{\kappa}^2}{4} q^2 (C_{UV} - F_0(Z, W)) \\
& + \frac{1}{2} \sum_{doublet} \left\{ (m_f^2 + m_f'^2) C_{UV} - 2m_f^2 F_1(f', f) - 2m_f'^2 F_1(f, f') \right\} . \tag{H.14}
\end{aligned}$$

We again have that, for any choice of the gauge parameters, $\Pi_L^{WW}(0) = \Pi_T^{WW}(0)$ which is a check on the calculation. Also note that the $\tilde{\delta}, \tilde{\kappa}$ dependence is proportional to q^2 , as is any dependence quadratic in $\tilde{\alpha}, \tilde{\beta}$. All these dependencies will be present in the propagators/mixings of the Goldstones.

Note that for both the WW and ZZ transition the tadpole contribution is not included as it will be canceled against that of the tadpole counterterms. Moreover note that such contribution do not depend on the gauge parameter. On the other hand the inclusion of the tadpole one-loop correction is needed for the Ward identities relating the bosonic two-point functions.

H.6 $H - H$

(b)	$(A, B) = (W, W), (W, \chi), (\chi, W), (\chi, \chi), (Z, \chi_3), (\chi_3, \chi_3), (Z, Z), (H, H), (c^+, c^+), (c^-, c^-), (c^Z, c^Z), (f, f)$
(a)	$A = W, Z, H, \chi, \chi_3, c^+, c^-, c^Z$

Here we explicitly add the tadpole contribution.

$$\Pi^H(q^2) + \frac{3\delta T}{v} = \frac{\alpha}{4\pi s_W^2} \left(\Pi_b^H + \Pi_f^H + (q^2 - M_H^2) \Pi_{\tilde{\delta}, \tilde{\epsilon}}^H \right) , \tag{H.15}$$

with

$$\begin{aligned}
\Pi_b^H &= C_{UV} \left[- \left(q^2 + \frac{M_H^2}{2} \right) \left(1 + \frac{1}{2c_W^2} \right) + \frac{3M_H^4}{4M_W^2} \right] - \frac{9M_H^4}{8M_W^2} F_0(H, H) \\
&\quad - F_0(W, W) \left(-q^2 + 3M_W^2 + \frac{M_H^4}{4M_W^2} \right) - \frac{F_0(Z, Z)}{2c_W^2} \left(-q^2 + 3M_Z^2 + \frac{M_H^4}{4M_Z^2} \right) \\
&\quad - \left(\frac{M_H^2}{2} + 3M_W^2 \right) (1 - \log M_W^2) - \frac{1}{2c_W^2} \left(\frac{M_H^2}{2} + 3M_Z^2 \right) (1 - \log M_Z^2)
\end{aligned}$$

$$-\frac{3M_H^4}{4M_W^2}(1 - \log M_H^2), \quad (\text{H.16})$$

$$\Pi_f^H = \sum_f \frac{m_f^2}{M_W^2} \left\{ \frac{q^2}{2} (C_{UV} - F_0(f, f)) + 2m_f^2 (1 - \log m_f^2 + F_0(f, f)) \right\}, \quad (\text{H.17})$$

$$\Pi_{\tilde{\delta}, \tilde{\epsilon}}^H = (-C_{UV} + F_0(W, W)) \tilde{\delta} + (-C_{UV} + F_0(Z, Z)) \frac{\tilde{\epsilon}}{2c_W^2}. \quad (\text{H.18})$$

Again at $q^2 = M_H^2$ the self-energy is independent of the gauge parameter, which means that the shift in the Higgs mass will also not depend on the gauge parameters.

H.7 $f - f$

At one-loop the result is the same as in the linear gauge, but we give here the full result that includes mass effects as well as the contribution of the Goldstones. We have neglected all fermion mixing. The K_j^f have been introduced in section 4 and correspond to the different Lorentz structures of the fermion propagator. Since we are neglecting mixing and assuming \mathcal{CP} -invariance $K_5^f = 0$ holds. We have also found it convenient to express each of these Lorentz coefficient in a basis that corresponds to the various contributions to the self energy (photon exchange, W-exchange, etc...).

(b)	$(A, B) = (f, A), (f, Z), (f', W), (f, H), (f, \chi_3), (f', \chi)$
(a)	None

$$K_j^f(s) = \frac{\alpha}{4\pi} \left[Q_f^2 K_j^A + \frac{1}{c_W^2} Q_f^2 s_W^2 K_j^{Z(1)} - \frac{1}{2c_W^2} |Q_f| K_j^{Z(2)} + \frac{1}{8s_W^2 c_W^2} K_j^{Z(3)} \right. \quad (\text{H.19})$$

$$\left. + \frac{1}{4s_W^2} K_j^W + \frac{1}{4s_W^2 c_W^2} \frac{m_f^2}{M_Z^2} K_j^S \right] \quad (j = 1, \gamma, 5\gamma),$$

$$K_1^A = m_f [-4C_{UV} + 2 + 4F_0(f, A)],$$

$$K_\gamma^A = C_{UV} - 1 - 2F_1(f, A), \quad (\text{H.20})$$

$$K_{5\gamma}^A = 0,$$

$$K_1^{Z(1)} = m_f [-4C_{UV} + 2 + 4F_0(f, Z)], \quad K_1^{Z(2)} = K_1^{Z(1)}, \quad K_1^{Z(3)} = 0,$$

$$K_\gamma^{Z(1)} = C_{UV} - 1 - 2F_1(f, Z), \quad K_\gamma^{Z(2)} = K_\gamma^{Z(1)}, \quad K_\gamma^{Z(3)} = K_\gamma^{Z(1)}, \quad (\text{H.21})$$

$$K_{5\gamma}^{Z(1)} = 0, \quad K_{5\gamma}^{Z(2)} = -K_\gamma^{Z(1)}, \quad K_{5\gamma}^{Z(3)} = -K_\gamma^{Z(1)},$$

$$\begin{aligned}
K_1^W &= 0, \\
K_\gamma^W &= C_{UV} - 1 - 2F_1(f', W), \\
K_{5\gamma}^W &= -K_\gamma^W,
\end{aligned} \tag{H.22}$$

$$\begin{aligned}
K_1^S &= m_f \left[-F_0(f, H) + F_0(f, Z) - 2 \frac{m_f'^2}{m_f^2} (C_{UV} - F_0(f', W)) \right], \\
K_\gamma^S &= C_{UV} - F_1(f, H) - F_1(f, Z) + \frac{1}{2} \left(1 + \frac{m_f'^2}{m_f^2} \right) (C_{UV} - 2F_1(f', W)), \\
K_{5\gamma}^S &= +\frac{1}{2} \left(1 - \frac{m_f'^2}{m_f^2} \right) (C_{UV} - 2F_1(f', W)).
\end{aligned} \tag{H.23}$$

H.8 The Goldstone sector

We do not need to be explicit about the renormalisation of this sector in order to arrive at finite S-matrix elements. Nonetheless we list all the vector-Goldstone mixings and Goldstone propagators.

H.8.1 $A - \chi_3$

(b)	$(A, B) = (W, \chi), (\chi, W), (c^+, c^+), (c^-, c^-), (f, f)$
(a)	None

There is no fermionic contribution.

$$\Pi^{A\chi_3}(q^2) = \frac{\alpha M_W}{2\pi s_W} (1 - \tilde{\alpha}) (C_{UV} - F_0(W, W)) . \tag{H.24}$$

As expected this does vanish for $\tilde{\alpha} = 1$ and is a remnant of the $U(1)_{\text{QED}}$ gauge invariance for this value of the parameter.

H.8.2 $Z - \chi_3$

(b)	$(A, B) = (W, \chi), (\chi, W), (H, \chi_3), (H, Z), (c^+, c^+), (c^-, c^-), (f, f)$
(a)	None

$$\begin{aligned}
\Pi_{Z\chi_3} &= \frac{\alpha M_Z}{8\pi s_W^2 c_W^2} \left\{ c_W^2 (-3 + 4c_W^2(1 - \tilde{\beta}) - \tilde{\kappa}) (C_{UV} - F_0(W, W)) \right. \\
&+ \frac{M_H^2}{2M_Z^2} [F_0(H, Z) - 2F_1(H, Z)] - \left[\frac{3C_{UV}}{2} - F_1(H, Z) - F_0(H, Z) \right] \\
&+ \tilde{\epsilon} \left[\frac{C_{UV}}{2} - F_1(H, Z) + \frac{M_H^2}{2M_Z^2} (C_{UV} - F_0(H, Z)) \right] \\
&+ \tilde{\epsilon}^2 (C_{UV} - F_0(H, Z)) \\
&\left. + \sum_f \frac{m_f^2}{M_Z^2} (C_{UV} - F_0(f, f)) \right\}. \tag{H.25}
\end{aligned}$$

H.8.3 $W - \chi$

(b)	$(A, B) = (H, W), (H, \chi), (Z, \chi), (Z, W), (A, \chi), (A, W), (c^A, c), (c^Z, c^+), (c^Z, c^-), (f, f')$
(a)	None

$$\begin{aligned}
\Pi_{W\chi_+} &= \frac{\alpha M_W}{16\pi s_W^2} \left\{ C_{UV} \left(2 - \frac{3}{c_W^2} \right) \right. \\
&+ C_{UV} \left(\frac{M_H^2}{M_W^2} \tilde{\delta} + \tilde{\kappa} + \tilde{\delta} + 2\tilde{\delta}^2 + s_W^2 (18\tilde{\alpha}^2 - 12\tilde{\alpha}) + 4\tilde{\beta}(4 - 3c_W^2) + 18c_W^2\tilde{\beta}^2 \right) \\
&+ 4s_W^2 (4F_1(A, W) - F_0(A, W)) \\
&+ 4s_W^2 \tilde{\alpha} (-6F_1(A, W) + 6F_0(A, W) - 5\tilde{\alpha}F_0(A, W) + \tilde{\alpha}F_1(A, W)) \\
&+ F_1(Z, W) \left(s_W^2 \left(-16 - \frac{2}{c_W^2} \right) - 2\tilde{\kappa} - 24c_W^2\tilde{\beta} + 4c_W^2\tilde{\beta}^2 \right) \\
&+ F_0(Z, W) \left(2 - 4c_W^2 + 4\frac{s_W^2}{c_W^2} - 16\tilde{\beta} + 24c_W^2\tilde{\beta} - 20c_W^2\tilde{\beta}^2 \right) \\
&+ \frac{M_H^2}{M_W^2} (2F_1(W, H) - F_0(W, H)(1 + \tilde{\delta})) + 2(2F_0(W, H) - F_1(W, H)) \\
&+ 2\tilde{\delta} (F_1(W, H) - F_0(W, H)(1 + \tilde{\delta})) \\
&+ 8\tilde{\alpha}s_W^2(1 - \tilde{\alpha}) - 8\tilde{\beta} (1 - c_W^2(1 - \tilde{\beta})) \\
&\left. + 4 \sum_{doublet} \frac{1}{M_W^2} \left[\frac{m_f^2 + m_f'^2}{2} C_{UV} - (m_f'^2 F_0(f', f) + m_f'^2 F_1(f, f')) \right] \right\}. \tag{H.26}
\end{aligned}$$

H.8.4 $\chi_3 - \chi_3$

(b)	$(A, B) = (W, \chi), (\chi, W), (H, Z), (H, \chi_3), (c^+, c^+), (c^-, c^-), (f, f)$
(a)	$A = W, Z, \chi_3, \chi, H, c^+, c^-, c^Z$

The second line of Π^{χ_3} shows the fermionic contributions. Since the tadpole contribution appears with Π^{χ_3} , we present the formula for the sum. We note that C^{χ_3} , the coefficient for the divergent part, is proportional to s in the linear gauge.

$$\begin{aligned} \Pi^{\chi_3}(q^2) + \frac{\delta T}{v} = & \frac{\alpha}{16\pi s_W^2} \left[C^{\chi_3} C_{UV} + d_{WW}^{\chi_3} F_0(W, W) + d_{HZ}^{\chi_3} F_0(H, Z) + d_0^{\chi_3} \right. \\ & \left. + 2q^2 \sum_f \frac{m_f^2}{M_W^2} (C_{UV} - F_0(f, f)) \right], \end{aligned} \quad (\text{H.27})$$

$$C^{\chi_3} = - \left(\frac{2}{c_W^2} + 4 \right) q^2 + \tilde{\varepsilon} \frac{2}{c_W^2} (M_H^2 + q^2) + \tilde{\varepsilon}^2 \frac{3}{c_W^2} M_Z^2 - 4\tilde{\kappa} q^2, \quad (\text{H.28})$$

$$d_{WW}^{\chi_3} = 4q^2(1 + \tilde{\kappa}), \quad (\text{H.29})$$

$$d_{HZ}^{\chi_3} = \frac{1}{c_W^2} \left(2M_H^2 - M_Z^2 + 2q^2 - \frac{(M_H^2)^2}{M_Z^2} - 2\tilde{\varepsilon}(M_H^2 + q^2) - 3\tilde{\varepsilon}^2 M_Z^2 \right), \quad (\text{H.30})$$

$$d_0^{\chi_3} = \frac{1}{c_W^2} \left[\left(\frac{(M_H^2)^2}{M_Z^2} - M_H^2 \right) \log M_H^2 + \left(M_Z^2 - M_H^2 \right) \log M_Z^2 - \frac{(M_H^2)^2}{M_Z^2} + 2M_H^2 - M_Z^2 \right]. \quad (\text{H.31})$$

H.8.5 $\chi - \chi$

(b)	$(A, B) = (H, W), (H, \chi), (\chi_3, W), (Z, \chi), (Z, W), (A, \chi), (A, W), (c^Z, c^+), (c^Z, c^-), (f, f')$
(a)	$A = A, Z, W, H, \chi_3, \chi, c^+, c^-$

The second line of Π^χ shows the fermionic contribution. Since the tadpole contribution appears with Π^χ , we present the formula for the sum. We note that C^χ , the coefficient for the divergent part, is proportional to s in the linear gauge.

$$\begin{aligned} \Pi^\chi(q^2) + \frac{\delta T}{v} = & \frac{\alpha}{16\pi s_W^2} \left[C^\chi C_{UV} + d_{ZW}^\chi F_0(Z, W) + d_{HW}^\chi F_0(H, W) + d_{AW}^\chi F_0(A, W) + d_0^\chi \right. \\ & \left. + 2q^2 \sum_f \frac{m_f^2}{M_W^2} (C_{UV} - 2F_1(f', f)) \right], \end{aligned} \quad (\text{H.32})$$

$$\begin{aligned} C^\chi = & - \left(\frac{2}{c_W^2} + 4 \right) q^2 - 32\tilde{\alpha} s_W^2 M_W^2 + 32\tilde{\beta} s_W^2 M_W^2 + 16\tilde{\alpha}^2 s_W^2 M_W^2 + 16\tilde{\beta}^2 c_W^2 M_W^2 \\ & + 2\tilde{\delta}(q^2 + M_H^2) + 3\tilde{\delta}^2 M_W^2 + 2\tilde{\kappa}q^2 - \tilde{\kappa}^2 M_W^2, \end{aligned} \quad (\text{H.33})$$

$$\begin{aligned} d_{ZW}^\chi = & \left(2 - 8s_W^2 + \frac{2}{c_W^2} \right) q^2 - 16c_W^2 M_W^2 - \frac{6}{c_W^2} M_W^2 - \frac{1}{c_W^2} M_Z^2 - 8s_W^2 M_W^2 + 23M_W^2 \\ & - 32\tilde{\beta} s_W^2 M_W^2 - 16\tilde{\beta}^2 c_W^2 M_W^2 - 2\tilde{\kappa}q^2 + \tilde{\kappa}^2 M_W^2, \end{aligned} \quad (\text{H.34})$$

$$d_{HW}^\chi = 2q^2 - M_W^2 + 2M_H^2 - \frac{(M_H^2)^2}{M_W^2} - 2\tilde{\delta}(s + M_H^2) - 3\tilde{\delta}^2 M_W^2, \quad (\text{H.35})$$

$$d_{AW}^\chi = 8s_W^2(s - M_W^2) + 32\tilde{\alpha} s_W^2 M_W^2 - 16\tilde{\alpha}^2 s_W^2 M_W^2, \quad (\text{H.36})$$

$$\begin{aligned} d_0^\chi = & \log M_W^2 \left(-M_H^2 + 2M_W^2 - M_Z^2 \right) + \log M_H^2 \left(\frac{(M_H^2)^2}{M_W^2} - M_H^2 \right) \\ & + \log M_Z^2 \left(\frac{M_Z^2}{c_W^2} + 8s_W^2 M_Z^2 - M_Z^2 \right) - \frac{(M_H^2)^2}{M_W^2} + 2M_H^2 + 6M_W^2 - \frac{M_Z^2}{c_W^2} - 6M_Z^2 \\ & + 16\tilde{\alpha} s_W^2 M_W^2 - 16\tilde{\beta} s_W^2 M_W^2 - 8\tilde{\alpha}^2 s_W^2 M_W^2 - 8\tilde{\beta}^2 c_W^2 M_W^2. \end{aligned} \quad (\text{H.37})$$

I Direct determination of the charge counterterm

A direct derivation of δY necessitates the calculation of the vertex eeA with on-shell electrons and in the Thomson limit where the photon momentum $q \rightarrow 0$, $\Gamma_e^\mu(0)$. In this limit one can relate the vertex to the electron self-energy as depicted Fig.4 (p is the electron momentum and l is the integration momentum). Due to the identities

$$\frac{\partial}{\partial p_\mu} \left(\frac{-1}{\not{p} + \not{\ell} - m} \right) = \frac{-1}{\not{p} + \not{\ell} - m} \gamma^\mu \frac{-1}{\not{p} + \not{\ell} - m}, \quad (\text{I.1})$$

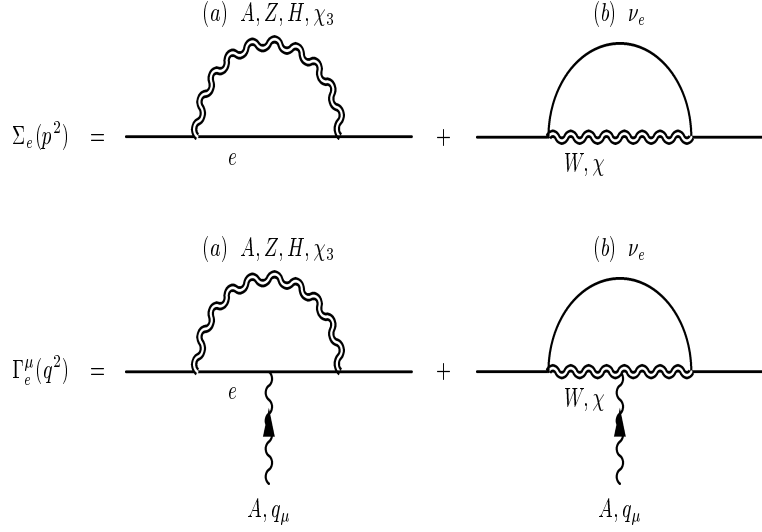


Figure 4: Electron self energy and eeA vertex

and

$$\frac{\partial}{\partial p_\mu} \left(\frac{1}{(p + \ell)^2 - M^2} \right) = \frac{-2(p + \ell)^\mu}{((p + \ell)^2 - M^2)^2}, \quad (\text{I.2})$$

The major part of $\Gamma_e^\mu(0)$ can be calculated by the corresponding fermion self energy. Using the notation in Fig.4,

$$(a) \ A, Z, H, \chi_3 \quad \Gamma_e^\mu(0) = (-e) \left. \frac{\partial}{\partial p_\mu} \Sigma(p^2) \right|_{p=m}, \quad (\text{I.3})$$

$$(b) \ W, \chi \quad \Gamma_e^\mu(0) = (-e) \left. \frac{\partial}{\partial p_\mu} \Sigma(p^2) \right|_{p=m} + G_e^\mu. \quad (\text{I.4})$$

It is only G_e^μ which is gauge parameter dependent, in fact it only depends on $\tilde{\alpha}$ and vanishes for $\tilde{\alpha} = 1$.

$$G_e^\mu = -\frac{\alpha}{4\pi} \frac{e}{s_W^2} (1 - \tilde{\alpha}) (C_{UV} - \log M_W^2) \gamma^\mu L. \quad (\text{I.5})$$

We note that for this particular value of the gauge parameter there is a residual $U(1)_{\text{QED}}$ symmetry and therefore no wonder that the naive Ward identity is verified in this case in Eq. I.4.

The gauge-parameter independent part of $\Gamma_\mu(0)$ is derived from the (on-shell) electron self-energy . We obtain

$$\begin{aligned}
\frac{\partial}{\partial p_\mu} \Sigma(p^2) \Big|_{p=m} &= (2m_e K'_1(m_e^2) + 2m_e^2 K'_\gamma(m_e^2) + K_\gamma(m_e^2)) \gamma^\mu + K_{5\gamma}(m_e^2) \gamma^\mu \gamma_5 \\
&= -2\delta Z_{eL}^{1/2} \gamma^\mu L - 2\delta Z_{eR}^{1/2} \gamma^\mu R.
\end{aligned} \tag{I.6}$$

Here Eq.4.20 is used.

The counterterm for eeA vertex, $\Gamma_e^\mu(0)$, is defined in Sec.F.8. Adding this to the loop calculation we get

$$\begin{aligned}
\tilde{\Gamma}_e^\mu(0) &= \Gamma_e^\mu(0) + \hat{\Gamma}_e^\mu(0) \\
&= (-e\gamma^\mu) \left(\delta Y + \delta Z_{AA}^{1/2} - \frac{s_W}{c_W} \delta Z_{ZA}^{1/2} \right) + \left[-\frac{e}{2s_W c_W} \delta Z_{ZA}^{1/2} \gamma^\mu L + G_e^\mu \right].
\end{aligned} \tag{I.7}$$

The second term (within square brackets) vanishes identically. Imposing the renormalisation condition (Eq.4.21) $\tilde{\Gamma}_e^\mu(0) = 0$,

$$\delta Y = -\delta Z_{AA}^{1/2} + \frac{s_W}{c_W} \delta Z_{ZA}^{1/2}. \tag{I.8}$$

and we find the linear gauge result

$$\delta Y = \frac{\alpha}{4\pi} \left\{ -\frac{7}{2}(C_{UV} - \log M_W^2) - \frac{1}{3} + \frac{2}{3} \sum_f Q_f^2 (C_{UV} - \log m_f^2) \right\}. \tag{I.9}$$

References

- [1] G. Bélanger, F. Boudjema, J. Fujimoto, T. Ishikawa, T. Kaneko, K. Kato and Y. Shimizu, Nucl.Phys. (Proc. Suppl.) **116** (2003) 353; hep-ph/0211268.
- [2] G. Bélanger, F. Boudjema, J. Fujimoto, T. Ishikawa, T. Kaneko, K. Kato and Y. Shimizu, Phys. Lett. **B559** (2003) 252; hep-ph/0212261.
- [3] A. Denner, S. Dittmaier, M. Roth and M. M. Weber, Phys.Lett. **B560** (2003) 196; hep-ph/0301189 and Nucl.Phys. **B660** (2003) 289; hep-ph/0302198.
- [4] For a review of some of these techniques and achievements, see Z. Bern, Nucl.Phys. (Proc. Suppl.) **117** (2003); hep-ph/0212406.
- [5] For a review see, R. Harlander and M. Steinhauser, Prog.Part.Nucl.Phys. **43** (1999) 167; hep-ph/9812357.

- [6] T. Ishikawa, T. Kaneko, K. Kato, S. Kawabata, Y. Shimizu and H. Tanaka, KEK Report 92-19, 1993, GRACE manual Ver. 1.0.
- [7] F. Yuasa, Y. Kurihara and S. Kawabata, Phys. Lett. **414** (1997) 178.
- [8] S. Tsuno *et al.*, Comput.Phys.Commun. **151** (2003) 216; hep-ph/0204222.
- [9] J. Fujimoto, T. Ishikawa, Y. Shimizu, K. Kato, N. Nakazawa and T. Kaneko, Acta Phys. Polonica **B28** (1997) 945.
- [10] G. Bélanger *et al.*, Proceedings of AIHENP 99, Heraklion, Crete, Greece; hep-ph/9907406.
- [11] G. Bélanger, F. Boudjema, J. Fujimoto, T. Ishikawa, T. Kaneko, K. Kato, Y. Shimizu and Y. Yasui, Phys.Lett. **B** in Press; hep-ph/0307029.
- [12] For a description of the program see for example M. Jimbo and H. Tanaka and T. Kaneko and T. Kon, hep-ph/9503363.
J. Fujimoto *et al.*, Comp. Phys. Commun. **111** (1998) 185 and J. Fujimoto *et al.*, Comput.Phys.Commun. **153** (2003) 106.
- [13] For some of these issues as well as a comprehensive review of radiative correction in the electroweak theory see, D. Y. Bardin and G. Passarino, *The standard model in the making: precision study of the electroweak interactions*, Clarendon Press, Oxford, U.K. (1999).
- [14] K. Fujikawa, Phys. Rev. **D7** (1973) 393
M. Base and N.D. Hari Dass, Ann. Phys. **94** (1975) 349
M.B. Gavela, G. Girardi, C. Malleville and P. Sorba, Nucl. Phys. **B193** (1981) 257
N.G. Deshpande and M. Nazerimonfared, Nucl. Phys. **B213** (1983) 390
F. Boudjema, Phys. Lett. **B187** (1987) 362.
M. Baillargeon and F. Boudjema, Phys. Lett. **B272** (1991) 158, *ibid* **B317** (1993) 371.
- [15] F. Boudjema and E. Chopin, Z.Phys. **C73** (1996) 85.
- [16] H. Tanaka, Comput. Phys. Commun. **58** (1990) 153.
- [17] A.C. Hearn: *REDUCE User's Manual*, version 3.7, Rand. Corp. 1999.
- [18] J. A. M. Vermaasen: *New Features of FORM*; math-ph/0010025.
- [19] S. Kawabata, Comp. Phys. Commun. **41** (1986) 127; *ibid.*, **88** (1995) 309.
- [20] F. Yuasa *et al.*, Proceedings AIHENP 99, hep-ph/0006268. F. Yuasa, D. Perret-Gallix, S. Kawabata and T. Ishikawa, Nucl.Instrum.Meth. **A389** (1997) 77.

- [21] K. Aoki, Z. Hioki, R. Kawabe, M. Konuma and T. Muta, *Suppl. Prog. Theor. Phys.* **73** (1982) 1.
- [22] M. Bohm, H. Spiesberger and W. Hollik, *Fortsch.Phys.* **34** (1986) 687.
- [23] A. Denner, J. Küblbeck, R. Mertig and M. Böhm, *Z. Phys. C* **56** (1992) 261.
B.A. Kniehl, *Z. Phys. C* **55** (1992) 605.
See also, J. Fleischer and F. Jegerlehner, *Nucl. Phys. B* **216** (1983) 469.
- [24] T. Bhattacharya and S. Willenbrock, *Phys. Rev. D* **47** (1993) 469.
K. Melnikov, M. Spira and O. Yakovlev, *Z. Phys. C* **64** (1994) 401.
B. A. Kniehl, C.P. Palisoc and A. Sirlin, *Nucl. Phys. B* **591** (2000) 296.
- [25] G. Passarino and M. Veltman, *Nucl. Phys.* **160** (1979) 151.
- [26] L.M. Brown and R.P. Feynman, *Phys. Rev.* **85** (1952) 231.
- [27] Z. Bern, L. Dixon and D.A. Kosower, *Phys.Lett. B* **302** (1993) 299; *Erratum-ibid. B* **318** (1993) 649.
- [28] G. J. van Oldenborgh, *Comput. Phys. Commun.* **58** (1991) 1.
- [29] J. Fujimoto, Y. Shimizu, K. Kato and Y. Oyanagi, *Prog. Theor. Phys.* **87** (1992) 1233.
- [30] J. Fujimoto, M. Igarashi, N. Nakazawa, Y. Shimizu and K. Tobimatsu, *Suppl. Prog. Theor. Phys.* **100** (1990) 1.
- [31] W. Beenakker and A. Denner, *Nucl. Phys. B* **338** (1990) 349.
Phys. Lett. B **282** (1992) 185.
- [32] <http://minami-home.kek.jp/jf/nlg.html>.
- [33] F. Bloch and A. Nordsieck, *Phys. Rev.* **52** (1937) 54.
D.R. Yennie, S.C. Frautchi and H. Suura, *Ann. of Phys.* **13** (1961) 379.
- [34] G. 't Hooft and M. Veltman, *Nucl. Phys. B* **153** (1979) 365.
- [35] Y. Kurihara, J. Fujimoto, T. Munehisa and Y. Shimizu, *Prog.Theor.Phys.* **96** (1996) 1223.
T. Munehisa, J. Fujimoto, Y. Kurihara and Y. Shimizu, *Prog.Theor.Phys.* **95** (1996) 375.
- [36] J. Fleischer, A. Leike, T. Riemann, and A. Werthenbach, hep-ph/0302259.
- [37] J. Fujimoto and Y. Shimizu, *Mod. Phys. Lett. A* **3** (1988) 581.

- [38] W. Beenakker, S. van der Marck, and W. Hollik, *Nucl. Phys.* **B365** (1991) 24–78.
- [39] J. Fleischer, J. Fujimoto, T. Ishikawa, A. Leike, T. Riemann, Y. Shimizu, and A. Werthenbach, in *Second Symposium on Computational Particle Physics* (CPP, Tokyo, 28–30 Nov 2001), KEK Proceedings 2002-11 (2002) (Y. Kurihara, ed.), pp. 153–162, hep-ph/0203220.
- [40] J. Fleischer, T. Hahn, W. Hollik, T. Riemann, C. Schappacher, and A. Werthenbach, contribution to the second workshop of the extended ECFA/DESY study *Physics and Detectors for a 90 to 800 GeV Linear Collider*, 12-15 April 2002, Saint-Malo, France, hep-ph/0202109.
- [41] For a nice review on the radiative corrections to $e^+e^- \rightarrow W^+W^-$ and related issues, see W. Beenakker and A. Denner, *Int. J. Mod. Phys.* **A9** (1994) 4837.
- [42] M. Lemoine and M. Veltman, *Nucl. Phys.* **B164** (1980) 445.
M. Böhm, A. Denner, T. Sack, W. Beenakker, F.A. Berends and H. Kuijf, *Nucl. Phys.* **B304** (1988) 463.
J. Fleischer, F. Jegerlehner and M. Zrałek, *Z. Phys.* **C42** 1989 409.
- [43] A. Denner, J. Küblbeck, R. Mertig and M. Böhm, *Z. Phys.* **C56** (1992) 261.
- [44] A. Denner, S. Dittmaier and M. Strobel, *Phys.Rev.* **D53** (1996) 44.
- [45] A. Denner and S. Dittmaier and R. Schuster, *Nucl. Phys.* **B452** (1995) 80.
- [46] G. Jikia, *Nucl. Phys.* **B494** (1997) 19.
- [47] A. Denner and S. Dittmaier, *Nucl.Phys.* **B398** (1993) 239.
- [48] A. Denner and S. Dittmaier, *Nucl.Phys.* **B398** (1993) 265.
- [49] A. Denner and T. Hahn, *Nucl.Phys.* **B525** (1998) 27; hep-ph/9711302.
- [50] A. Denner, S. Dittmaier, M. Roth and M.M. Weber, hep-ph/0307193.

